KU LEUVEN

ARENBERG DOCTORAL SCHOOL
Faculty of Engineering Science

Optimization of Network Support by Distributed Energy Resources

Sam Weckx

Dissertation presented in partial fulfillment of the requirements for the degree of Doctor in Engineering Science

July 2015

Optimization of Network Support by Distributed Energy Resources

Sam WECKX

Examination committee:
Prof. dr. ir. P. Sas, chair
Prof. dr. ir. J. Driesen, supervisor
Prof. dr. ir. G. Deconinck
Prof. dr. ir. J. Poortmans
Dr. ir. R. D'hulst
Dr. ir. T. De Rybel
Prof. dr. ir. R. Iravani
(University of Toronto, Canada)
Prof. dr. ir. D. Montesinos i Miracle
(Universitat Politècnica de Catalunya, Spain)

Dissertation presented in partial fulfillment of the requirements for the degree of Doctor in Engineering Science

July 2015

Abstract

The integration of intermittent renewable energy sources in the distribution network is a challenge for the network operators. In the past, the operation of the low voltage network needed limited attention from the operators. They could guarantee a sufficient voltage quality with a limited effort. The introduction of solar panels has created new network situations. Energy can flow from the low voltage network towards the medium voltage network during a period of low consumption and high solar production. This reverse power flow can lead to an unacceptable rise in the grid voltage. Moreover, a significant increase in the number of electric vehicles can be expected. Inconsiderate charging of this fleet of cars could cause an increase in the evening load peak. Therefore, larger voltage deviations from the nominal voltage are expected in the future. These voltage deviations are limited by standards to protect the consumer. It is the task of the network operator to comply with these terms. This work will analyse different, advanced algorithms to control the network state.

At first, European distribution networks are analysed. The effect of solar generation on the distribution network is evaluated. However, accurate, digital information of the grid topology is often missing due to the low requirements for distribution networks in the past. Exact information concerning the cable lengths, or the phase of connection, might be lacking. Analysing or controlling the network, based on this limited information, can therefore be hard or even impossible. To resolve this problem, a method has been developed to train a model based on historical smart meter data. No information concerning the network topology is required a priori. All control algorithms that will be developed in this work can cope with this trained model, or with a model based on accurate grid topology data from the system operator.

Subsequently, different control strategies for solar panels and electric vehicles with a single- or three-phase connection to the network are analysed and compared. They can support the network by injecting or absorbing reactive power. If necessary, solar units can inject less energy into the network and

electric vehicles can charge at a lower rate. Solar panels and electric vehicles with a three-phase connection to the network can be modified to transfer power from low loaded phases to severely loaded phases. The different control strategies are divided into two categories. First of all, there are the local control strategies, that try to support the network based on locally-measured information only. Secondly, there are the central control strategies, that first collect all of the available information and then make a decision. A combined implementation, where local controllers are tuned by a central controller is investigated.

After that, two demand response algorithms, more specifically real-time pricing and an auction-based strategy, will be extended with network support. With demand response algorithms consumption patterns of electricity can be modified and, therefore, it is gaining a lot of attention. Network constraints will have to be taken into account when implementing these algorithms. In case of real-time pricing, the network operator can define different grid tariffs in an iterative way. These tariffs are an incentive for both flexible demand and solar panels to support the network. Also, the auction-based strategy can be modified to provide grid support. By transforming the bids made to the market, grid conditions can be controlled.

Finally, frequency support by controlling residential demand is investigated. The frequency can be supported at crucial moments by intelligently steering the demand. The decrease of consumer comfort will be minimized by the algorithm.

Beknopte samenvatting

De integratie van hernieuwbare energiebronnen in het distributienetwerk vormt een uitdaging voor de netwerkoperatoren. Vroeger vergde de operatie van het laagspanningsnetwerk weinig aandacht van de operatoren. Zij konden zonder al te veel moeite de spanningskwaliteit garanderen. De introductie van zonnepanelen heeft er echter voor gezorgd dat er nieuwe situaties ontstaan. Tijdens een periode van laag verbruik en grote zonneproductie kan er energie van het laagspanningsnetwerk naar het middenspanningsnetwerk vloeien. Deze omgekeerde energiestroom kan leiden tot een onaanvaardbare stijging van de netspanning. Daarbovenop valt dan nog een toename van het aantal elektrische wagens te verwachten. Het ondoordacht laden van deze wagens zou de lastpiek tijdens de avond kunnen vergroten, met een grotere belasting van het netwerk tot gevolg. In de toekomst worden er dan ook grotere spanningsdeviaties verwacht van de nominale spanning. Ter bescherming van de verbruiker zijn deze spanningsdeviaties gelimiteerd door standaarden. Het is de taak van de netbeheerder om te voldoen aan deze eisen. Dit werk zal verschillende, geavanceerde algoritmes onderzoeken voor de controle van de netwerktoestand.

In eerste instantie worden Europese distributienetwerken geanalyseerd. De invloed van zonnepanelen op het distributienet wordt onderzocht. Door de lage eisen die vroeger aan het distributienet werden gesteld ontbreekt meestal grondige digitale informatie over de exacte topologie van deze netwerken. Zo kan informatie over de exacte kabellengtes of de fase van aansluiting van elke verbruiker ontbreken. Het netwerk analyseren en controleren gebaseerd op de gelimiteerde beschikbare data van de topologie bij de netbeheerder is daarom soms moeilijk tot zelfs onmogelijk. Om dit probleem te omzeilen is er een methode ontwikkelt die toelaat om een model op te stellen van het netwerk gebaseerd op historische slimme meter data. Geen enkele a priori informatie over de netwerktopologie is vereist. Dit model laat toe om het netwerk te controleren. Alle controlealgoritmes die vervolgens zijn ontwikkeld kunnen overweg met zowel een model gebaseerd op accurate netwerkdata van de netbeheerder als met het model dat wordt bekomen aan de hand van historische slimme meter data.

Vervolgens worden verschillende controle strategieën voor zonnepanelen en elektrische wagens met zowel een enkelfasige als driefasige aansluiting geanalyseerd en vergeleken. Zij kunnen het netwerk ondersteunen door het absorberen of injecteren van reactief vermogen. Indien nodig kunnen zonnepanelen tijdelijk minder energie op het net plaatsen en elektrische wagens tijdelijk minder energie consumeren. Indien ze over een driefasige aansluiting beschikken kan ook energie van licht belaste fases getransfereerd worden naar zwaar belaste fases ter ondersteuning van het net. De controlestrategieën worden onderverdeeld in twee categorieën. Er zijn de lokale controlestrategieën, die enkel op basis van lokaal meetbare informatie het net proberen te ondersteunen en de centrale controlestrategieën, die alle informatie verzamelen en op basis hiervan beslissingen nemen. Een gecombineerde implementatie, waarbij lokale controllers door een centrale instantie worden aangepast, wordt geëxploreerd.

Daarna worden twee vormen van actieve vraagsturing, met name real-time prijssturing en een veiling-gebaseerde strategie, uitgebreid met netwerkondersteunende diensten. Actieve vraagsturing komt steeds meer onder de aandacht. Tijdens actieve vraagsturing zal moeten rekening gehouden worden met de verschillende netwerkbeperkingen. In geval van real-time prijssturing kan de netwerkbeheerder op een iteratieve manier verschillende netwerktarieven bepalen. Deze netwerktarieven vormen een incentive voor zowel flexibele lasten als zonnepanelen om het net te ondersteunen. Bij de veiling-gebaseerde strategie zullen de biedingen zo worden aangepast opdat ze alle beperkingen van het netwerk respecteren.

Tot slot wordt ook nog frequentieondersteuning aan de hand van residentiele vraagsturing onderzocht. Het intelligent aansturen van deze vraag laat toe om op cruciale momenten de frequentie te ondersteunen. De verbruikers boeten hierbij minimaal in aan comfort.

Voorwoord

Een doctoraat is vergelijkbaar met een grondige renovatie van een huis. Je denkt bij de start goed te weten wat er komt en de motivatie is eindeloos. Zo moeilijk kan dat toch allemaal niet zijn? Je vliegt er in. Al snel ondervind je dat sommige aspecten toch iets gecompliceerder zijn, dat dingen veel langer duren dan gedacht en je beseft dat je hier en daar toch wat over het hoofd hebt gezien. Je stelt je plannen bij. Nu en dan vraag je je af waar je toch aan begonnen bent. Had ik niets beter kunnen doen met mijn tijd? Gelukkig pak je zo een project niet alleen aan. Van alle kanten komt er advies, steun en een helpende hand. Je zet door en dankzij die hulp staat er uiteindelijk iets waar je trots op kan zijn. Je bent tevreden met het eindresultaat, maar denkt toch: dit nooit meer. Voor een verbouwing geldt alvast dat dit gevoel na enkele maanden weer omslaat en dan besef je pas hoe leuk het eigenlijk was. Ik denk dat net hetzelfde geldt voor een doctoraat.

Vooreerst wens ik mijn promotor prof. Johan Driesen te bedanken voor de kans die hij mij heeft gegeven om te starten aan dit doctoraat. Hij heeft me door dit doctoraat geleid. Hij gaf me de vrijheid en het vertrouwen om mezelf te verdiepen in verschillende domeinen die hebben bijgedragen in dit doctoraat.

I would also like to thank the members of my examination committee (prof. Deconinck, prof. Poortmans, prof. Iravani, prof. Montesinos, Dr. De Rybel and Dr. D'hulst) for thoroughly reviewing my text. Thanks to the discussion we had during the preliminary defense, I could further improve my text.

Meer specifiek moet ik Dr. Tom De Rybel bedanken voor de begeleiding tijdens het eerste jaar van mijn doctoraat. Hij had de soms ondankbare taak om een groep startende doctoraatsstudenten te sturen in een bij momenten hectisch werkpakket van Linear. Ik heb hier zeer veel uit bijgeleerd en er zijn zelfs verschillende onderwerpen uit dit doctoraat voortgevloeid uit dit werkpakket, iets wat ik op dat ogenblik waarschijnlijk niet besefte.

De jaren daarop werd ik uitstekend begeleid door Dr. Reinhilde D'hulst. Met

al mijn vragen kon ik bij haar terecht. Zij stuurde mij vanaf het begin een zeer interessante richting op en weet als geen ander welke facetten van het domein mij het meeste boeien. Hierbij werd ze vaak geholpen door Dr. Bert Claessens, die ik daarom ook graag wens te bedanken.

Een woord van dank gaat ook uit aan de mensen van het Labo, zowel dat op Electa als dat op VITO. Steeds kon ik snel rekenen op de hulp van Roland, Johan, Luc, Guy, Marcel en Filip. Veel dank gaat ook uit naar het Electa-secretariaat: Katleen, Veerle, Nathalie, Diane en Nele. Het is zeer aangenaam dat quasi alle praktische en administratieve problemen voor ons worden opgelost en dit bovendien zeer snel.

Dit onderzoek werd mede mogelijk gemaakt door een beurs van het FWO Vlaanderen en VITO. Hen wil ik bedanken voor de financiële en praktische ondersteuning gedurende de laatste vier jaar van mijn doctoraat.

De collega's van Electa maakten werken aangenaam. De vele pauzes en (sport)activiteiten zorgden voor voldoende afwisseling en afleiding. Speciale dank ook voor Jeroen Tant, van wie ik veel heb bijgeleerd en wiens code ik meermaals zeer nuttig kon gebruiken. Ook de collega's van Mechanica en Fysica wil ik bedanken voor de wekelijkse voetbalmatchkes. Hoewel we soms bleven spelen tot niemand meer kon, gaven ze me steeds terug energie om weer in mijn doctoraat te vliegen.

Mijn vrienden van de KLJ en mijn oud-klasgenoten wisten mij gelukkig vaak meer te boeien dan mijn doctoraat met hun verhalen, gezamenlijke activiteiten, reizen en avonturen. Die afwisseling was absoluut nodig. Hetzelfde geldt voor mijn oud-kotgenoten uit de Sint-Annastraat en Koen, Ruben en Hans die mij Leuven zullen doen herinneren als een plaats waar wij vanalles hebben beleefd en niet als de plaats waar ik heb gewerkt.

Een woordje van dank is ook zeker op zijn plaats voor alle steun van mijn ouders en zussen. Ook de rest van mijn familie en schoonfamilie wil ik hiervoor bedanken.

En tot slot Nathalie, jou kan ik niet genoeg bedanken voor alle hulp, entertainment, steun en zoveel meer. Danku om er altijd voor mij te zijn.

Sam Weckx,
Juli 2015

Abbreviations and Symbols

Abbreviations

Abbreviation	Description
AC	Alternating Current
ACE	Area Control Error
ADMM	Alternating Direction Method of Multipliers
CDF	Cumulative Distribution Function
DC	Direct Current
DG	Distributed Generation
DSM	Demand Side Management
DSO	Distribution System Operator
EV	Electric Vehicle
FCR	Frequency Containment Reserves
FRR	Frequency Restoration Reserves
LS	Least Squares
LV	Low Voltage
PDF	Probability Density Function
PHEV	Plug-in Hybrid Electric Vehicles
PV	Photovoltaic Generation
RMS	Root Mean Square
RMSE	Root Mean Square Error
RR	Replacement Reserves
SOC	State Of Charge
TSO	Transmission System Operator
VUF	Voltage Unbalance Factor

Symbols

Symbol	Description
c^{+}_{imb}	Expected positive imbalance price
c^{-}_{imb}	Expected negative imbalance price
C	Stored energy in an EV
D	Load damping constant
E^{max}	Upper flexibility bound of a cluster of loads
E^{min}	Lower flexibility bound of a cluster of loads
$F_{HP}T_{RH}$	Turbine time constant
G	Total generated power
M	Double of the system inertia constant
P	Active power consumption
$\mathbf{P}$	Vector with active power consumption of all households
P^{curt}	Curtailed active power
P^{DA}	Planned day-ahead cluster consumption
P^{EV}	Active power consumption by an EV
P^{flex}	Active power consumption by a flexible load
P^{load}	Power consumption by a household, excluding its EV
$P^{\mathbf{Load}}$	Total planned power consumption by a cluster of loads
$P^{\text{On/Off}}$	Power consumption when a device is turned on
P^{PV}	Active power production by a PV panel
Q	Reactive power consumption
$\mathbf{Q}$	Vector with reactive power consumption of all households
$R^{1,+}$	Activated upward primary reserves
$R^{2,+}$	Activated upward secondary reserves
$R^{1,-}$	Activated downward primary reserves
$R^{2,-}$	Activated downward secondary reserves
S	Inverter rating
$T_{\triangle\omega}$	Frequency detection time constant
T_{CH}	Turbine time constant
T_{RH}	Turbine time constant
T_G	Governor time constant

Symbol	Description
U	Utility function
V^0	Voltage magnitude at the distribution transformer
$V^{\min}$	Minimum allowed voltage
$V^{\max}$	Maximum allowed voltage
W	Welfare function
p_r	Corner price bid function
x	Binary variable that defines if an EV is charging
w	Weighting factor
$\triangle E_{dep}^{EV}$	Required energy by the time of departure
$\triangle t_{dep}^{EV}$	Time till departure
β	Parameter characterizing customer types
η	Three phase droop constant
δ	Step size
λ	Lagrange multiplier
ω	Parameter characterizing customer types
ψ	Charging efficiency
ε	Slack variable
ς	Ratio between active and reactive power
ϱ	Weighting factor
γ	Priority of charging parameter

Indices

Subscript

Symbol	Description
h	Customer index
i	Phase index
k	Substation index
p	Knot number
t	Time step

Contents

List of Figures

List of Tables

Chapter 1

Introduction

1.1 Context and Motivation

The electricity grid is going through a transition phase. The large amount of investments in distributed generation and the liberalization of the electricity market have drastically changed the way the electricity grid is operated. Distributed generation is intermittent and hard to predict. The amount is still rising, which will have to be handled by the system operators. The upcoming electrification of the transportation system will further challenge the system operators during the next decades. The electricity grid will therefore need to evolve into a smart grid. The smart grid should enable the efficient use of distributed generation and cope with the increasing demand for electricity by the transportation system.

Distributed generation (DG) is currently widespread in the electrical grid. It can be defined as electric power generation within distribution networks, or on the customer side of the network [1]. Often, this power generation is based on renewable sources. The most commonly used technologies in Belgium are solar power and wind power. To fight against climate change, the European Union has set the 20-20-20 targets: by 2020, the aim is to reduce the emissions of greenhouse gases by 20% compared to the 1990 level, increase the energy efficiency by 20% and reach 20% of renewables in the total energy consumption in the EU. These targets accelerate the integration of distributed generation, as these are an important part of the solution in reaching these goals.

In Belgium, the installed capacity of solar power is more than twice the installed capacity of wind power [2]. Due to government incentives, there

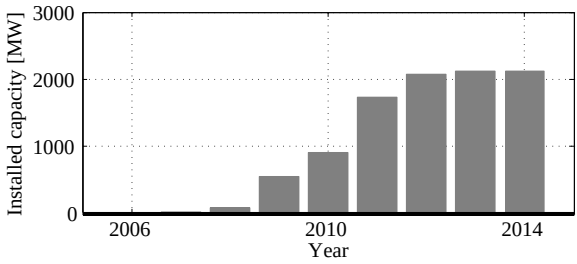

Figure 1.1: Evolution of the installed solar capacity in Flanders.

was a spectacular rise of the number of photovoltaic installations over the last 10 years. Fig. 1.1 presents the evolution of the solar capacity in Flanders approved by the VREG [3]. The current amounts of installed solar power can not be neglected by the system operators any more. They change the operation and management of both the transmission and the distribution network.

The current number of Plug-in Hybrid Electric Vehicles (PHEV) and Electric Vehicles (EV) in Belgium is negligible. However, they are considered as part of the future solution for the fossil fuels scarcity, as well as to the environmental problems associated with their wide usage [4]. Furthermore, the absence of tailpipe emissions reduces local concentrations of pollutant emissions, resulting in a positive impact on public health [5]. Besides that, there is also a possible reduction of CO_2-emitting transportation fuels. In Belgium, the average consumption of an EV is of the same magnitude as the yearly electric energy consumption of an average household. Therefore, EVs will become a considerable extra load for the network.

The increasing share of renewables in the electricity production and the on-going electrification of the transport system requires new strategies for the operation and management of the electricity grid in order to maintain, or even to improve, the power-supply reliability, quality and cost [6]. In addition, the liberalization of the grid leads to new management structures, where trading of energy and power is becoming important. Controlling distributed generation and electric demand will be crucial in the future operation of the electric grid. A smart grid infrastructure should enable this control and help to create a more efficient and sustainable energy system.

The smart grid can be defined as an electric system that uses information, two-way, cyber-secure communication technologies, and computational intelligence in an integrated fashion across electricity generation, transmission, substations, distribution and consumption to achieve a system that is clean, safe, secure, reliable, resilient, efficient, and sustainable [7]. The roll-out of a metering and

communication infrastructure will make it possible to develop and implement new operation strategies for the electricity network.

The smart grid will have to be reliable, flexible and scalable. Scalability is the ability of a control structure to cope efficiently with a system that is increasing in size. In this case the increasing amount of distributed energy resources has to be handled. Centralizing all information to define an optimal control strategy will be impossible, as computational limits and memory limits will be violated. Besides that, the underlying infrastructure will constrain the amount of communication. The suggested control approaches of this work will efficiently handle an increasing amount of participating parties. They will require limited computational power at device level. Besides cost, this is also beneficial for the installation and maintenance of the device software.

1.2 Grid Integration of Distributed Generation and Electric Vehicles

The electricity grid is typically divided into a transmission grid and a distribution grid. Electricity is transported via the transmission network from the big power plants to industrial customers and the distribution network. This occurs at a high voltage. Distribution system operators distribute the electricity to small-size enterprises and families. This takes place at a lower voltage. Transmission system operators and distribution system operators have different responsibilities. Therefore, the increasing amount of distributed generation poses different challenges for them.

1.2.1 Integration into the Distribution Network

A high penetration of distributed photovoltaic generators (PV) in low voltage (LV) distribution networks may lead to power quality problems. The distribution grid was originally developed for a unidirectional power flow, but due to the integration of distributed generators, power flows have become bidirectional during periods of high production and low consumption of energy, like on a sunny afternoon.

Distribution cables typically have a R/X ratio bigger than 1. The reverse, active power flow during a sunny afternoon will result in a voltage rise over the cable impedance. To avoid equipment damage, distribution network voltages have a fixed permissible voltage range. However, this voltage range might

be exceeded for high penetration levels of PV. This voltage rise is the most important limiting factor for more PV capacity [8–10].

In many parts of the world (including Australia, Asia, Europe, and Africa), distribution networks are of the three-phase, four-wire type [11]. Often, the majority of the residential customers is connected to a single phase. In these three-phase, four-wire grids with single-phase loads, or PV units, a special effect, called the neutral point shifting [12], occurs. When active or reactive power is consumed or produced by a single-phase load, or PV unit, a current will flow through the neutral conductor. This, in turn, results in a voltage drop over the impedance of the neutral conductor and the neutral voltage experienced by all of the customers will shift. Therefore, due to this neutral point shift, there is a coupling between the different phases. Moreover, this also means that we cannot simplify a three-phase, four-wire grid with single-phase loads by a single-phase grid. Future chapters will elaborate on this phenomenon.

Single-phase PV units are often not equally spread across the three phases of the distribution network [13, 14]. This can result in exceeding the voltage unbalance limits, especially at the end of the feeder [13, 14]. A similar reasoning goes for single-phase EV chargers [15]. Unbalanced voltages can result in negative effects on network and consumer equipment. An equal loading of all the phases will reduce the system losses and the voltage rise. In a balanced system, the maximum, or minimum, voltage limit will be reached at the three phases at the same time, where in an unbalanced system one phase will be out of limits faster.

A high penetration of EVs can lead to similar problems. EVs are charged through the electricity system. A typical driving pattern will result in a charging of the EV during the residential peak load in the evening. This extra load can result in overloading of the distribution transformer, or the distribution lines. Another problem that can occur is the severe voltage drop caused by the increased load. Most EVs are parked longer than needed to charge completely. The moments of charging, therefore, can be shifted in time to reduce the impact of EVs on the network.

Harmonics and DC current injection from inverters are generally not a problem, since modern inverters have to comply with strict standards [9]. Voltage fluctuations from passing clouds are also not problematic, because of slow ramps and an averaging effect over large areas [9].

Therefore, the major technical challenge for the distribution system operator will be to control the grid voltage. Besides that, attention will have to be paid to unbalance in the grid and the increased loading of the different grid components.

Voltage parameters	EN 50160
Voltage Variations	**95% of the time:** ± 10% based on 10 min mean RMS values **100% of the time:** +10%/-15% based on 10 min mean RMS values
Voltage Unbalance	**95% of the time:** < 2% based on 10 min mean RMS values

Table 1.1: EN 50160 limits for voltage variations and voltage unbalance.

Voltage Control in Distribution Networks

The distribution system operator must design and operate the system to keep the voltage characteristics within preassigned limits. The main document providing adequate network conditions for user equipment is standard EN 50160: 'Voltage characteristic of electricity supplied by public electricity networks' [16]. EN 50160 gives the main voltage parameters and their permissible deviation ranges at the point of common coupling in public distribution networks, under normal operating conditions. The permissible ranges for the voltage variations and the voltage unbalance, on which this work focusses, are shown in Table 1.1. The voltage unbalance is defined as the ratio of the negative-sequence voltage component to the positive-sequence voltage component. Some regulators have introduced voltage quality standards that are more strict than those indicated in EN 50160 [17].

Different solutions have been discussed in literature to comply with the applicable voltage quality standards. These can be divided into the following categories:

- Reinforcement of the distribution network
- On-load transformer tap changer
- Network reconfiguration
- Active power curtailment
- Reactive power control
- Battery energy storage
- Demand response

The most straightforward solution is to reinforce the network by increasing the section of the distribution feeders, lowering the impedance of the network.

Due to the lower impedance, voltage deviations will be limited. In many cases, reinforcing the networks will be expensive and more sophisticated mitigation methods will be investigated.

A tap changer on the distribution transformer can increase or decrease the input voltage of the distribution network by changing the position of a mechanical or electronic device. Different control methods have been presented to define the best moments of changing the tap position [18, 19]. An on-load tap changer will avoid voltage problems, but will not make the network operation more efficient. Another disadvantage of using an on-load transformer tap changer is that distribution transformers, or distribution cables, can still be overloaded. Solely off-load tap changers are momentarily used in the LV distribution network of Flanders, due to economic reasons.

By changing the open/closed states of sectionalizers and tie switches, the topological structure of distribution networks can be altered [20]. This structure can be optimized to avoid voltage problems. This type of voltage control is discussed in [21]. Most of the time, European LV distribution networks are not equipped with these sectionalizers and often it will be impossible to install them, due to the geographical topology of the distribution network.

Active power curtailment consists of reducing the output power of the PV panel, or reducing the charging power of an EV. This will reduce the voltage rise/drop over the feeder resistance. The current regulation for distributed generation is a special form of active power curtailment. PV installations have to automatically disconnect when a maximum voltage is reached. Such disconnections have a considerable cost for the owners of the PV installations. Households located at the end of the distribution feeder experience a higher voltage rise and will therefore disconnect more often. More advanced control strategies are needed, with or without additional reactive power control.

Reactive power control, on the other hand, consists of injecting, or absorbing, an extra amount of reactive power to control the voltage. The maximum reactive power that can be injected, or generated, is limited by the rated apparent power of the inverter or charger. Fig. 1.2 presents the different operating regions of a PV inverter with a production of P^{PV}, in case of active power curtailment (on the left) and reactive power control (in the middle). However, both active and reactive power can be controlled at the same time, and, when combined, there is a wide region of possible operating points available, shown in the right of Fig. 1.2. Only applying active power curtailment can lead to a high amount of curtailed green energy, whereas reactive power control can sometimes be insufficient to control the voltage. Therefore, the whole range of operating points will be considered in this work, in contrast to the active power curtailment methods of [22–24] and the reactive power control methods of [8, 25, 26].

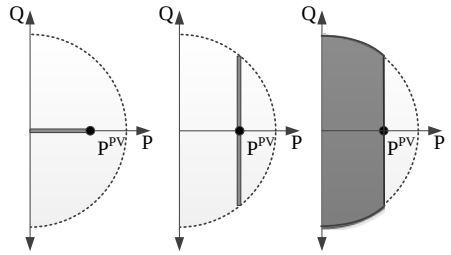

Figure 1.2: Operating regions of three control strategies for PV inverters: Active power curtailment (left), Reactive power control (middle), Active and reactive power control (right)

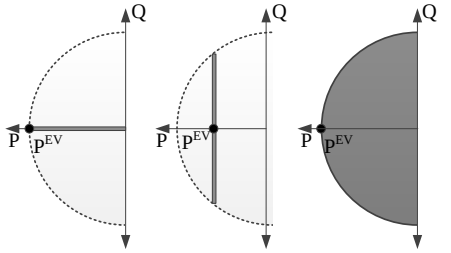

Figure 1.3: Operating regions of three control strategies for loads with a power electronics interface, such as an EV: Active power curtailment (left), Reactive power control (middle), Active and reactive power control (right)

For EVs, the charging power is not defined by the meteorological conditions, in contrast to PV. In case of an uncoordinated charging strategy, EVs would immediately charge at their maximal capacity. Active power curtailment consists of reducing the charging power to support the grid voltage. In this work, we will not consider the ability of EVs to inject power into the grid. For reactive power control, on the other hand, the standard charging power of the EV needs to be reduced to have sufficient margin to inject or absorb the required amount of reactive power. A more advanced control will make use of the whole range of operating points available when adapting both the active and reactive power [27]. These concepts are not limited to EVs, but can be applied to all loads with a power electronic interface, such as heat pumps. Fig. 1.3 presents the different operating regions for loads with a power electronic interface.

The effectiveness of these control algorithms depends on the R/X ratio of the network. Besides that, it is also important to take into account the neutral point shifting effect in three-phase, four-wire grids. For reactive power control,

special care is required as it might worsen the system losses and increase the loading of the distribution transformer and cables.

Battery energy storage systems can be used to avoid active power curtailment, by storing the excess of energy. Battery energy storage systems can be combined with reactive voltage control. In case of a variable electricity price, they can postpone injection to times of the highest electricity price. A detailed analysis has been made in [28].

Finally, demand response for voltage control consists of encouraging the consumer to consume more power during a period of high PV production and to avoid extra consumption during peak consumption periods. Demand response is defined as all of the intentional modifications to consumption patterns of electricity that are intended to alter the timing, level of instantaneous demand, or the total electricity consumption [29]. Not all of the potential benefits are exploited when flexible demand is only used to avoid local network limitations. Demand response can also be applied to a central, economic objective. I.e. a retailer can reduce the production cost of electricity by reducing peak demand. The purpose of a demand response algorithm should be to control the electric demand with both of the previously mentioned objectives combined. On the one hand, a global economic objective should be optimized and, on the other hand, network limitations should be respected at all times and, if necessary, the demand should be controlled to support the network.

1.2.2 Integration into the Transmission Network

The Transmission System Operator (TSO) faces other challenges when integrating distributed generation into the network. In a power system the imbalance between generation and demand should be minimized as much as possible to ensure frequency stability and to avoid blackouts. The TSO is responsible for ensuring frequency stability at all times. To maintain the balance of injection and intake, the TSO has a balancing mechanism. An Access Responsible Party is responsible for maintaining the quarter-hourly balance between total injections and total offtakes of the grid users for which it has been designated as their Access Responsible Party [30]. When there is an imbalance in the customer portfolio of an Access Responsible Party, an imbalance tariff is used by the TSO to calculate the reimbursement, or penalty, the Access Responsible Party receives.

If a system imbalance persists, the TSO itself will take the necessary steps to balance the control area. The TSO, therefore, will contract operating reserves from balance providers and use these to control the imbalance. Three levels of control are generally used by the TSO to maintain the balance between

supply and demand. In Europe, ENTSO-e has defined these as the Frequency Containment Reserves (FCR), the Frequency Restoration Reserves (FRR) and the Replacement Reserves (RR). However, the traditional nomenclature is still widely used by system operators, dividing operating reserves into primary, secondary and tertiary reserves. The control by FCR is a local automatic control that adjusts the active power generation and consumption to quickly restore the balance between load and generation [31]. It is a joint action of all the TSOs of the Synchronous Area [32]. FRR have an activation time less than 15 minutes and are used to restore the area control error of the control block to zero in case of an imbalance in the block [32]. The FRR consists of an automatic and a manual part. The response time of each type of control is different. FCR react very quickly within the first few seconds after a disturbance. The FRR can be activated in 30 seconds to 15 minutes. RR are optional reserves with an activation lead time exceeding 15 minutes [32].

The increasing amount of distributed generation aggravates the system imbalances and results in a higher demand for reserves [33,34]. It is characterised by fluctuating power generation, which is difficult to predict. Especially in small, isolated systems without transmission interconnections, the wind power variability can be important, due to the absence of cross-border flexible capacity. In small- or medium-sized areas, wind power variations and prediction errors are likely to be correlated [35]. Due to the introduction of wind and solar energy, the amount of dispatchable power generation is reduced. Conventional power plants provide most reserves, together with pumped hydro installations and industrial consumers. The reserve requirements can result in must-run obligation costs for conventional power plants and reduced efficiency costs, due to partial loading. Applying dynamic reserves, where the amount of reserves depend on the predicted wind output, can reduce costs. Wind power can also actively participate in the provision of frequency reserves, but this will require the curtailment of wind energy.

The installation of a communication infrastructure for smart metering offers new possibilities to provide reserves. Distributed generation and (residential) demand can support the frequency when they are properly controlled. Residential devices, like fridges, freezers, water heaters and EVs, can make a significant contribution to primary frequency reserves [36]. The major challenge that remains is how to guarantee the availability of these reserves provided by residential demand, while taking into account the customer comfort settings.

1.3 Scope of the Work

A high penetration of controllable power electronics that interface photovoltaic panels and electric vehicles with the distribution network should not be a limitation for the power quality, but an opportunity. Most of the photovoltaic systems provide their rated, or maximum, power during just a small fraction of the time so that the remaining power capacity available in the inverter can be used to implement other functions. Electric vehicles are often parked longer than required to charge completely, resulting in a significant amount of flexible consumption if the charging power of EVs can be controlled. Extra grid supporting features can be added to the charger when the EV does not charge at maximum power. These extra services are called ancillary services. EURELECTRIC defines ancillary services as follows [37]:

> *Ancillary services are all services required by the transmission or distribution system operator to enable them to maintain the integrity and stability of the transmission or distribution system as well as the power quality*

There is a wide variety of ancillary services. This work focusses on voltage control and frequency control.

PV panels and EVs have the technical possibilities to support the network. However, providing ancillary services has to be done in a well-considered way. Curtailing active power produced by PV panels will result in a reduced income of the owner. Decreasing the charging power of an EV will extend the charging time of its battery. Customer comfort settings have to be respected when implementing an algorithm, otherwise the algorithm might not be socially accepted. Reactive power should be used with special care, as a thoughtless implementation might otherwise increase grid losses and component loading.

The scope of this work is to analyse how voltage and frequency control can be provided in an optimal way, under different circumstances. The application of an active and reactive voltage control strategy by PV panels will be explored. Practical considerations, such as data communication limits, or privacy concerns, can make it difficult to implement this optimal strategy. Therefore, simpler implementations are also analysed and are compared to the optimal solution. It is also possible that demand is already actively controlled by a demand response algorithm. Control algorithms to support the network will have to cooperate with this demand response algorithm, instead of counteracting it. Two types of demand response algorithms will be extended to be able to provide voltage control. Finally, one of these demand response algorithms will be used

to provide frequency reserves with residential demand. Special care will be given to the reliability of these reserves.

1.4 Outline and Main Contributions

This section gives the structure and main contributions of each chapter.

First of all, **Chapter 2** analyses the effect of active and reactive power consumption on the voltage in unbalanced, three-phase, four-wire distribution grids. The dependency between the power consumption and the grid voltage is called the voltage sensitivity. A new method to extract voltage sensitivity factors, based on historical smart meter data only, is introduced. Many of the newly proposed voltage control algorithms rely on these voltage sensitivity factors, which are the linearised dependencies between the voltage magnitude and the active and reactive power consumption. These linearised dependencies are normally obtained by algorithms which rely on accurate grid topology information. Due to the traditionally passive operation of low voltage distribution networks, this information is typically missing, incomplete or inaccurate. Thanks to the proposed method, a large amount of voltage control algorithms can be applied, even under these conditions. Data of a practical laboratory setup is used to validate the proposed method under real-life conditions.

Subsequently, **Chapter 3** discusses a new method, combining both central and local active and reactive power control for PV units. The local control functions of the PV units are defined as piecewise linear functions. The parameters of all the local control functions are regularly reoptimized. This results in an optimal use of reactive power and a minimum amount of curtailed active power, while respecting network limitations. This method makes use of voltage sensitivity factors, which can be obtained by applying the algorithm developed in Chapter 2. Using the model based on the voltage sensitivity factors will speed-up the optimization of the local control functions.

While Chapter 3 is limited to single-phase PV inverters, **Chapter 4** investigates the possibilities of three-phase, balancing inverters. In this chapter, three-phase PV inverters and off-board three-phase EV chargers are used to reduce the losses and the voltage unbalance in three-phase, four-wire distribution grids. This is done by injecting the majority of the produced power into the phase with the highest power consumption, or by transferring power from highly loaded to less loaded phases. The improvements made by using EV chargers and PV inverters that can balance the network are investigated. Several simulations show a positive effect on the system losses, the grid voltage and voltage unbalance.

Finally a local controller is proposed to control the balancing between the phases when a real-time communication channel is not available. The method could be easily extended to other loads with a power electronic interface, such as heat pumps.

Chapters 3 and 4 describe different strategies for the control of single-phase PV inverters and three-phase PV inverters. In these strategies, either a central control unit directly controlled the PV inverters, or they are controlled based on local information. Another possibility to control the network state is to give real-time monetary incentives to curtail active power, or to provide reactive power. Therefore, in **Chapter 5**, a locational marginal pricing algorithm is proposed to control the voltage in unbalanced distribution grids. With locational network prices, the distribution system operator can steer the reactive power consumption and active power curtailment of PV panels to guarantee a safe network operation. Flexible loads also respond to these prices. The locational prices will be defined in real-time by an algorithm which relies on Dual Decomposition. The locational prices are a natural extension of a classic, real-time pricing demand response strategy, where the total price consists of a real-time energy price and a network price. The locational network prices can differ between the three phases in unbalanced grids. This can be due to a higher consumption, or production, in one of the phases, compared to the other phases. It will be shown that the locational prices are an effective way to control the grid voltage. The price setting will be carefully analysed. In this chapter, we also make use of voltage sensitivity factors, which can be obtained by applying the algorithm developed in Chapter 2.

Chapter 6 introduces a market-based, multi-agent control mechanism that incorporates distribution transformer and voltage constraints for the charging of a fleet of EVs. The algorithm solves an utility maximization problem in a distributed way, assigning most charging power to the EVs with the highest need for energy. The remaining capacity of each of the EV chargers is used for reactive voltage control. The optimal solution is found after the exchange of just one single message, in contrast to the method described in Chapter 5 which requires more communication. Also, this control mechanism uses the voltage sensitivity factors of Chapter 2. The algorithm has been tested in a practical laboratory setup.

Finally, in **Chapter 7**, the multi-agent demand control system, which was discussed in Chapter 6, is extended to provide spinning reserves. With the proposed control framework, an aggregator of dynamic demand is able to control the consumption and the response on frequency changes of a cluster of loads. The primary frequency support by the cluster of loads can emulate the primary control of a conventional generator. The total customer welfare remains maximal during the frequency support by applying utility functions for each device.

Chapter 2

Voltage Sensitivity Analysis of Distribution Grids

Voltage Sensitivity Analysis of a Laboratory Distribution Grid with Incomplete Data

Sam Weckx, Reinhilde D'hulst, Johan Driesen

Published in IEEE Transactions on Smart Grid, vol.6, no.3, pp.1271-1280, May 2015

2.1 Introduction

A high penetration of distributed generators and electric vehicles in Low Voltage (LV) distribution network challenges the future grid operation. More intelligent methods should be used for a better utilization of the distribution network, in order to maintain, or even to improve, the power-supply reliability and quality. Voltage rise is normally the main limiting factor to prevent the increase of photovoltaic (PV) generation in LV networks [10], while a high penetration

The first author is the main author of the article. The contributions of the first author include the literature study, the development of the model and the analysis of the simulation results. The practical validation was done in cooperation with Filip Leemans, Marcel Stevens and Johan De Winter.

of electric vehicles (EVs) can result in significant voltage drops. Therefore, Distribution System Operators (DSOs) are discovering a need to develop and validate new voltage management strategies [38].

The development of voltage management strategies is a challenging task due to the non-linear relationship between the network load and the grid voltage. Many of the developed voltage management strategies use a linearised model that describes the dependency of the voltage magnitude as a function of the power injections [22, 39–58]. These linearised models are usually based on a voltage sensitivity analysis.

Sensitivity analysis at the transmission level is a routine task, where the sensitivity factors are typically obtained from the Jacobian matrix derived from the Newton Raphson load-flow method [59]. However, obtaining the Jacobian matrix for distribution networks is less practical, as load-flow calculations need to be performed for every change in operating conditions. The relatively high R/X ratio of LV distribution grids makes the Newton Raphson load-flow method less suitable for solving the load-flow problem [60]. A specific method to calculate the grid voltages in distribution grids is the backward-forward sweep method [61], which makes no use of the Jacobian matrix.

A popular alternative to obtain the voltage sensitivity factors is the 'perturb-and-observe' method, which consists of making small modifications and measuring the impact on the voltage magnitude[38]. This method is significantly less efficient, due to the need to recompute the entire network state for a change on each bus. In order to increase the computational efficiency of the voltage sensitivity calculation in distribution grids of the previously mentioned methods, different alternatives have been proposed [59, 60, 62–65]. These methods still require information about grid topology and cable parameters to obtain the voltage sensitivity coefficients.

LV grids are the most unknown and manually controlled elements of the electricity grid [66]. Grid topology information is often not available in an easily accessible, digital structure. The information that utilities have about the LV electricity grid is usually limited to which meter is connected to which LV substation [66]. Exact lengths between houses, or of the connecting cable between the smart meter and the distribution feeder are often not available. Moreover, the phase to which each household with a single-phase connection is connected is often unknown [67–69]. This information is crucial for the previously mentioned algorithms. To overcome these problems, a computational-intensive grid topology identification method has been developed which can only be applied under several assumptions [70]. However, for most voltage management strategies, having the voltage sensitivity coefficients, or a linear power flow model, is sufficient.

In this chapter, an algorithm with low complexity is proposed that can obtain the voltage sensitivity factors and a linear load-flow model based on historical smart meter data. No information about the grid topology is required. The proposed algorithm assumes that, at every customer, both active and reactive power are measured by a smart meter. The voltage magnitudes of nodes that are interesting for a DSO are measured by the smart meters. These nodes will be called the control nodes. The DSO can access this data, which might be stored at a database. The low voltage network considered is an unbalanced, three-phase, four-wire, radial system. Only radial operated distribution networks are considered, as these are the majority for the connection of residential customers to the grid. The network topology is considered to be fixed. In case the network gets reconfigured, new data will have to be collected to obtain the voltage sensitivity factors.

In the first part of this chapter, the algorithm is tested on an unbalanced distribution grid simulated in Matlab. In the last part, actual data of a small laboratory grid is used to validate the algorithm in real-life conditions. This chapter is structured as follows: the distribution grid used in the simulation results is described in Section 2.2. In Section 2.3, the algorithm that extracts the voltage sensitivity information from historical smart meter data is presented. It will be shown that the phase of connection of a single-phase household can be extracted from the sign of these voltage sensitivity factors. The obtained, linear voltage model will be compared to the exact results in Section 2.4. It will be shown that the obtained, linear voltage model makes errors of the same size as the non-linear system of load-flow equations when there are realistic uncertainties on the applied load and grid models. Finally, Section 2.5 discusses the practical laboratory grid where the algorithm is tested. The obtained voltage sensitivity factors of the laboratory grid are used to implement a voltage management strategy.

2.2 Simulated Network

The network used in the simulations is an existing, three-phase, four-wire, radial distribution system with a TT earthing arrangement in Belgium. The network consists of 62 customers and is depicted in Fig. 2.1. This network is a semi-urban reference network in the LINEAR project [71]. It is a weak network, vulnerable to voltage problems [14].

All main feeder cables are of type EAXVB 1 kV $4\times150mm^2$, except for the cable between node A and node B, which is of type EAXVB 1 kV $4\times95mm^2$. Cable properties are defined in table 2.1. The impedance values are calculated

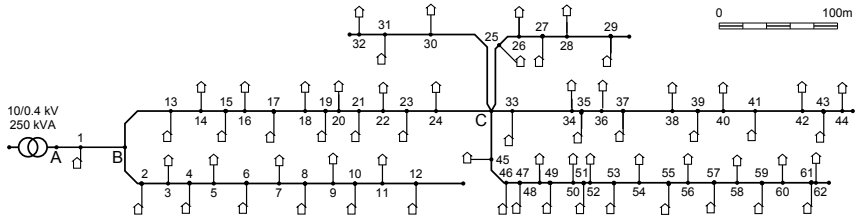

Figure 2.1: The network used in the simulations. All lengths are drawn to scale.

according to design specifications in the Belgian standard for underground distribution cables NBN C33-322 [72], with an assumed operating temperature of 45 °C. All households have a single-phase connection with a nominal line-to-neutral voltage of 230 V and are equally spread across the three phases. Statistically representative, residential load profiles are available to perform load-flow simulations. Generation of these load profiles is described in [73]. In [73], the privacy problem of data provided by electrical companies is bypassed by transforming a large dataset of residential load profiles into a model that is able to create a set of synthetic, non-aggregated load profiles. This model was trained based on a large database of measured residential load profiles provided by the DSOs in Flanders. A constant power load model was assumed for 80% of this load, while a constant impedance load model was assumed for 20% of this load. This division between different load models generally varies in time for individual consumers [74], but in this work these are kept constant. All households with an odd number are equipped with a PV-installation with a nominal power of 3 kW. The PV is modelled as a constant power load. The voltage at the secondary side of the transformer is considered to be 230 V during no load.

Table 2.1: Properties of the simulated network.

Properties	**Value**	**Unit**
Total feeder length	1657	[m]
Impedance of EAXVB 1 kV 4 × 95 mm^2	0.352+0.078j	[Ω/km]
Impedance of EAXVB 1 kV 4 × 150 mm^2	0.227+0.078j	[Ω/km]

2.3 Grid Identification

If distribution grid parameters, load profiles and load models are available, the voltages in all of the nodes of the grid can be calculated with a load-flow algorithm. A non-linear set of equations describes the relation between the voltages in the grid and the power profiles:

$$V_{h,t} = f\left(V_t^0, \mathbf{P}_t, \mathbf{Q}_t\right) \tag{2.1}$$

where

- $V_{h,t}$ is the voltage magnitude of customer h at timestep t
- V_t^0 is the voltage magnitude at the distribution transformer at timestep t
- $\mathbf{P}_t$ is a vector with the active power consumption of all customers at timestep t
- $\mathbf{Q}_t$ is a vector with the reactive power consumption of all customers at timestep t

For radial distribution networks, the backward-forward sweep method can be applied [61] to solve this non-linear system of equations that describes the relation between the complex powers of all customers and the voltage magnitude.

The non-linear load-flow models are difficult to handle in optimization formulations due to their non-convexity. Besides that, the effect of changes in one part of the network on other parts of the network cannot be easily quantified due to the complexity of the model. Therefore, the non-linear load-flow models are sometimes approximated by a linear model, which can depend on the network loading [38, 43].

2.3.1 A Constant Linear Voltage Model

A first, simple approximation consists of assuming a constant linear model:

$$V_{h,t} \approx V_t^0 + \sum_{\tilde{h}=1}^{N} \mu_{h,\tilde{h}}^P P_{\tilde{h},t} + \sum_{\tilde{h}=1}^{N} \mu_{h,\tilde{h}}^Q Q_{\tilde{h},t}, \tag{2.2}$$

where

- $P_{\tilde{h},t}$ is the active power of customer $\tilde{h}$ at timestep t

- $Q_{\tilde{h},t}$ is the reactive power of customer $\tilde{h}$ at timestep t
- $\mu^P_{h,\tilde{h}}$ is the influence of active power of customer $\tilde{h}$ on the voltage magnitude of house h
- $\mu^Q_{h,\tilde{h}}$ is the influence of reactive power of customer $\tilde{h}$ on the voltage magnitude of house h

The parameters of interest of this model, $\mu_{h,\tilde{h}}$ and $\mu_{h,\tilde{h}}$, can be obtained based on historical smart meter data. We assume that smart meters measure active and reactive power, as well as the voltage magnitude. In case a house has a three-phase connection to the grid, voltage and power are measured in each phase separately. Also, the voltage magnitude at the distribution transformer is assumed to be measured. This data is stored in a database. If multiple time steps are available, a least squares problem (LS) can be recognised in (2.2) with $\mu^P_{h,\tilde{h}}$ and $\mu^Q_{h,\tilde{h}}$ as unknowns. If the influence on the voltage of house h needs to be defined, one can solve the following problem:

$$\min_{\mu^P,\mu^Q} \quad \sum_{t=1}^{n_t} \|V_{h,t} - V_t^0 - \sum_{\tilde{h}=1}^{N} \mu^P_{h,\tilde{h}} P_{\tilde{h},t} - \sum_{\tilde{h}=1}^{N} \mu^Q_{h,\tilde{h}} Q_{\tilde{h},t}\|_2^2, \tag{2.3}$$

where n_t is the total amount of time steps available for least squares.

This linear least squares problem does not require any information about the grid. Nor the location or the order of the customers matters. Historic data is used to define the approximated voltage sensitivity factors $\mu^P_{h,\tilde{h}}$ and $\mu^Q_{h,\tilde{h}}$. It is assumed that there is no electricity theft in the LV grid. This can be verified by comparing the sum of the measured power of all smart meters with the measurements at the substation transformer. If the measurements are sensitive to outliers, the 1-norm can be applied in (2.3) instead of the 2-norm. When prior knowledge of the grid is available, this can be included by adding constraints to the LS problem (2.3) and making it a convex optimization problem [75] which can be efficiently solved [76].

An advantage is that the approximated voltage sensitivity factors are calculated off-line. Calculating the actual sensitivity factors in real-time is often too computationally intensive and requires a real-time communication of the load profiles of the different customers. Therefore, some applications use already approximated sensitivity factors, based on off-line load-flow calculations that are sometimes updated depending on the network operation, e.g., heavy or light loading conditions [22, 46, 47]. By regularly updating the voltage control signals, small errors made by using approximated sensitivity factors can also be compensated [46].

The constant linear model will be a linearization of the average loads occurring in the grid. It therefore describes the nonlinear load-flow equations best when the load is average, but it will make larger errors if there is a very large load or a high reverse power flow. The linearization errors made by the model of (2.3) will depend on the grid topology, the load models and the load profiles. Due to the fact that many parameters influence the linearization error, it is hard to define exact limits for the validity of the model.

2.3.2 A Piecewise-Linear Voltage Model

In (2.2), the approximated sensitivity factors $\mu^P_{h,\tilde{h}}$ and $\mu^Q_{h,\tilde{h}}$ are assumed to be constant. However, in [59] is shown that the actual sensitivity factors vary depending on the loading of the network. The approximated sensitivity factors $\mu^P_{h,\tilde{h}}$ and $\mu^Q_{h,\tilde{h}}$ can also be made dependent on the network operation. The different, captured time steps of the historical smart meter data are divided into different categories, e.g., heavy loading time periods, light loading periods and reverse power flow periods due to distributed generation. These categories can be found by summing-up all the load profiles.

For each category of points a linear model will be formed that approximates the non-linear load-flow equation (2.1) for this category. The more categories, the more accurate the approximation of the non-linear load-flow equation, however, it is important that sufficient data points are part of each category to obtain an overdetermined system and to train an accurate linear model for each category. When more points are part of a category, the training of a model will be less sensitive to measurement noise or outliers. Besides that, more points will better describe the average operating conditions. Using three or four categories is also more intuitive for operators and tends to give a good approximation, as will be shown later on in this chapter. Therefore, it is suggested to divide the total number of points into three different categories with an equal amount of points in each category, so that each category has an overdetermined system of the same size.

The least squares problem (2.2) can then be solved for only those time steps of each category, e.g. for the low loading period $T^{\mathbf{Low}}$:

$$\min_{\mu^P,\mu^Q} \quad \sum_{t\in T^{\mathbf{Low}}} \|V_{h,t} - V^0_t - \sum_{\tilde{h}=1}^{N} \mu^P_{h,\tilde{h}} P_{\tilde{h},t} - \sum_{\tilde{h}=1}^{N} \mu^Q_{h,\tilde{h}} Q_{\tilde{h},t}\|_2^2, \tag{2.4}$$

The solution of this least squares problem provides a set of approximated sensitivity factors for different levels of network loading. This model will therefore be called the piecewise-linear model, whereas the one with the constant

sensitivity factors will be called the constant linear model. The historical load and voltage profiles on which the model is based will be called the training data.

With the trained linear load-flow model, the voltages at the customers nodes can be computed by evaluating (2.2) without any knowledge of the cable lengths. An important task for DSOs is to evaluate the impact on the grid voltage with an increasing amount of PV generation, or an increasing usage of heat pumps and electric vehicles. The linear load-flow model can be used to calculate the according voltage rise or drop when grid topology data is missing.

A disadvantage of the linear and piecewise-linear load-flow model is that it does not provide an estimate of the grid losses. It can only be used to define the voltage sensitivity factors, not the loss sensitivity factors. Therefore, the main applications of these models is in voltage calculations and voltage control strategies of grids with missing or inaccurate grid data.

2.3.3 Practical Implementation

To solve (2.4), the DSO needs to collect the load profiles of all households and the corresponding voltage profiles in which the DSO is interested. Smart meters can communicate their profiles to a database, where the DSO can access this data. Preferably, the DSO will also check if there was any energy theft during this period.

By adding-up the load profiles, the system operator can divide the data into periods of different loading. The voltage sensitivity factors are now obtained by solving (2.4) for each period. There will be a set of different voltage sensitivity factors for each load category. Fig. 2.2 presents a flowchart of this procedure. Yearly, (2.4) can be solved with the load and voltage profiles of the year before to check if the model still accurately describes the network behavior.

When the LV network gets reconfigured, (2.4) needs to be solved again with load and voltage profiles that occurred during the new reconfiguration. However, reconfiguration rarely occurs in European LV networks.

In Section 2.4, the distribution grid of Fig. 2.1 is simulated and the load profiles and voltage profiles are obtained from this simulation environment. In Section 2.5, actual grid data of a laboratory distribution grid is accessed from a database and is used to calculate the voltage sensitivity factors.

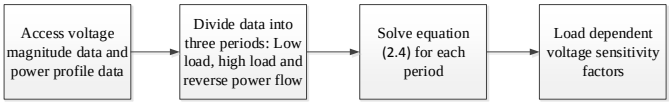

Figure 2.2: Flowchart to obtain the load-dependent voltage sensitivity factors based on historical smart meter data.

2.4 Simulation Results

The algorithm was tested on the network of Fig. 2.1. A piecewise-linear model was calculated, based on historic data of the previous month. This model was used to obtain the voltages in phase V of node 62 of a new day of which the measured load profiles were available. Fig. 2.3 compares the voltage obtained by an exact solution of the non-linear system of equations and the voltage obtained by the trained, linear model. The non-linear system of equations was solved by the backward-forward sweep method [61]. Both the backward-forward sweep method and the training of the piecewise-linear model was implemented in Matlab [77]. The errors of the piecewise-linear model are clearly small.

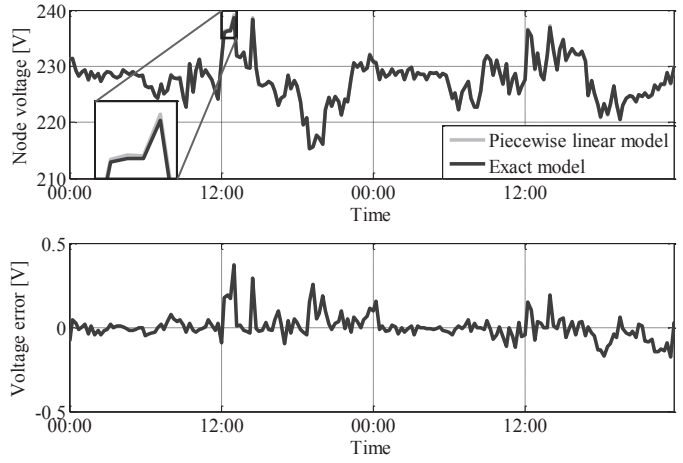

Figure 2.3: At the top the voltage of node 62 for the exact load-flow and by a trained piecewise-linear model. At the bottom the error of the piecewise-linear model compared to the exact load-flow.

In a second simulation, the grid voltages for one month will be computed, based on the available load profiles. An exact load-flow with perfect knowledge of all cable parameters and load models does not make any errors when computing the grid voltages. However, accurate grid or load data is rare. Different models can be made, with realistic errors on the cable lengths or load models. These models can be compared with the exact load-flow model and with the trained models, based on historical data. Four different load-flow models will be compared to the exact load-flow model.:

Inaccurate Cable Length

This load-flow model consists of the non-linear load-flow equations (2.1) of the grid in Fig. 2.1, but assumes a cable between node A and B which is 10% longer than the actual length. Therefore, the solution of this set of non-linear equations will make errors compared to the exact load-flow model.

Inaccurate Load Models

The second load-flow model consists of the non-linear load-flow equations (2.1) of the grid in Fig. 2.1. However, the load models are assumed to be 100% constant power models, whereas the actual load models were chosen to be a power load model for 80% of this load and a constant impedance load model for 20% of the load. Therefore, the solution of this set of non-linear equations will make errors, compared to the exact load-flow model.

Constant Linear Model

The third load-flow model is obtained by solving (2.3), based on historical load and voltage profiles of the previous month. No data about the grid topology or of the phase of connection of each customer, was needed. This model will make errors, due to the linearisation, compared to the exact load-flow model.

Piecewise-Linear Model

The fourth load-flow model is obtained by solving (2.4), based on historical load and voltage profiles of the previous month. No data about the grid topology or of the phase of connection of each customer was needed. This model will make errors due to the linearisation, compared to the exact load-flow model. This model can adapt to different loading conditions in the network.

Table 2.2: Estimation errors of different load-flow models.

Load flow model	**RMSE [V]**	**MaxAE [V]**
Non-linear model with inaccurate cable length	0.089	0.42
Non-linear model with inaccurate load models	0.054	0.69
Trained linear model based on historical data	0.06	0.94
Trained piecewise-linear model based on historical data	0.043	0.69

Fig. 2.4 plots the probability density function (PDF) of the voltage error compared to the exact model of three representative nodes of the network for the four load-flow models that were previously described. One of the nodes is located at the beginning of the feeder, one in the middle and one at the end. It can be seen that the errors are similar and that they slightly increase for nodes located at the end of the feeder. Note that these errors are small and will be in the range of the measurement noise. Using another grid and other load profiles will result in different errors made by the different load-flow models. 62 Statistically representative, residential load profiles were used. In [73], the privacy problem of data provided by electrical companies is bypassed by transforming a large dataset of residential load profiles into a model that is able to create a set of synthetic, non-aggregated load profiles. This model was trained based on a large database of measured residential load profiles provided by the DSOs in Flanders. The grid is an existing Belgian distribution grid

Table 2.2 shows the Root Mean Square voltage Error (RMSE) and the Maximum Absolute voltage Error (MaxAE) of the four load-flow models. It can be concluded from Fig. 2.4 and Table 2.2 that the models that were trained based on historical data make small errors, but these are in the same range as when realistic errors are included in cable lengths or load models. Moreover, when the trained piecewise-linear model is applied, errors can even be slightly smaller than in case of a load-flow model with inaccurate grid or load data. So, even with small realistic uncertainties on the cable lengths or load models, the trained linear or piecewise-linear models become valid alternatives to the set of non-linear equations (2.1). Note that, when there is no information about the phase of connection of each household, an exact solution of the non-linear system of equations can easily make errors of several Volts, especially when the PV generation is unequally distributed across the three phases.

The approximated sensitivities obtained by solving the least squares problem

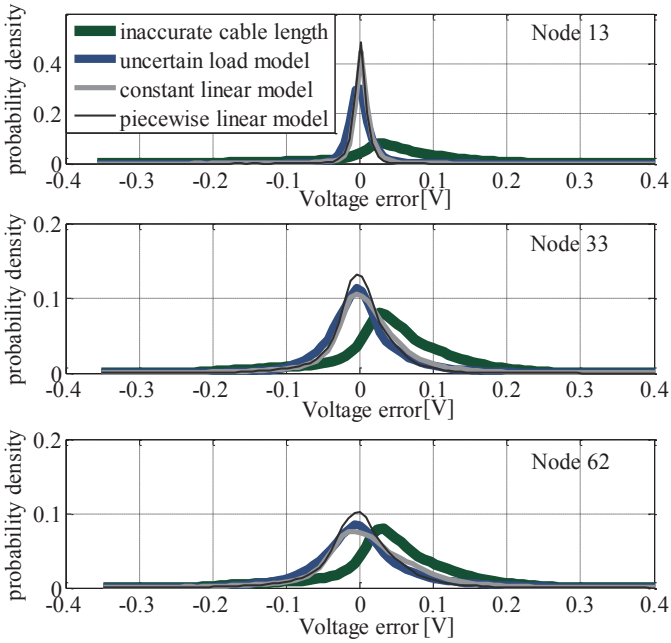

Figure 2.4: Probability density function of the voltage error in three nodes for four different load-flow models: 1) An exact load-flow with inaccurate cable length information 2) An exact load-flow with inaccurate assumptions regarding load models 3) A trained constant linear model 4) A trained piecewise-linear model.

can be compared with the actual sensitivities. As was discussed earlier, the actual sensitivity factors vary depending on the loading of the network. In Fig. 2.5, the actual sensitivity factors are compared to the approximated sensitivities, where the influence of consumption of node 55 on the phase voltages of node 62 is presented. The actual sensitivity factors are calculated by the 'perturb-and-observe' method [38]. All households had an equal load, which ranged from -1 kW up to 1.5 kW, to obtain the voltage sensitivity factors for different grid loading levels. The piecewise-linear model gives a better approximation of the actual sensitivity factor. The available, historical data was divided into three parts, each with the same amount of time steps, to obtain the piecewise-linear model. As can be seen in Fig. 2.5, increasing the consumption of node 55 will reduce the voltage in phase U at node 62, whereas it will increase the voltages of phase V and W. This is due to the neutral point shift [12, 14]. Due to the resistive and inductive voltage drop across the neutral conductor, a load or PV

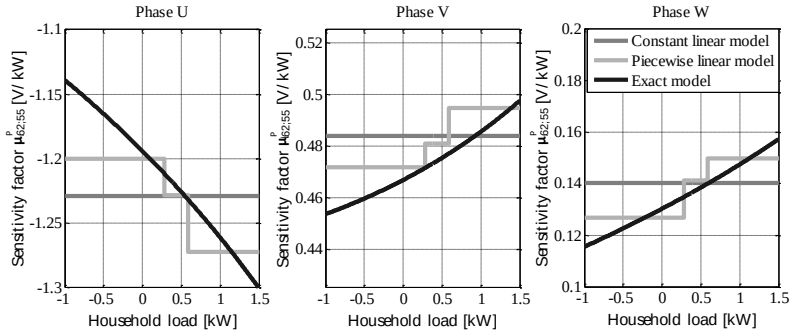

Figure 2.5: The actual and the approximated voltage sensitivities of the phase voltages of node 62 due to active power consumption of household 55 for different levels of household loading.

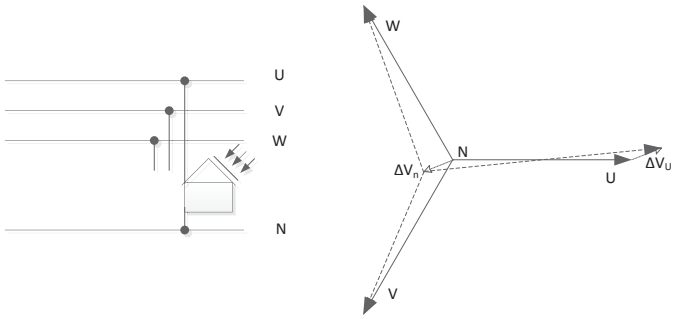

Figure 2.6: The neutral displacement due to the injection of a single-phase PV unit.

unit connected to one phase will affect the phase voltages of the other phases. PV generation in one phase will increase the voltage of that phase, whereas the other two phase voltages decrease, as shown in Fig. 2.6. Therefore, it can be concluded that the load in node 55 is connected to phase U.

Due to the neutral point displacement, the constants $\mu^P_{h,\tilde{h}}$ and $\mu^Q_{h,\tilde{h}}$ obtained by the least squares method will give a measure of the location throughout the grid and the phase to which the household is connected. If the smart meter that measured the voltage V^h is connected to the same phase as the household $\tilde{h}$, the constant $\mu^P_{h,\tilde{h}}$ will be negative, because the active power consumption has created a voltage drop. On the other hand, when the household is connected to another phase, $\mu^P_{h,\tilde{h}}$ will have a small positive value, due to the neutral point

shift [12]. This allows all of the loads that are connected at the same phase to be grouped, based on the constants $\mu^P_{h,\tilde{h}}$ and $\mu^Q_{h,\tilde{h}}$. Fig. 2.7 shows the influence of loads of all houses on the phase voltage of house 44, when all households are connected by a single phase to the network. This is obtained by applying the least squares method, using historic data of one month. Obviously, the consumption of node 44 has the biggest influence on the voltage of node 44. All nodes with a negative sensitivity factor are connected to the same phase as household 44. Node 42 and 43 are connected to another phase, and, therefore, extra consumption in these nodes will increase the voltage of household 44. In this case, there was an alternating sequence of U, V, W, U, V, W,... for the phase of connection of each household.

This method of phase identification is less computationally intensive than [68], where a mixed-integer program is formed to identify the phase of connection of customers. [69] solves a combinatorial optimization problem by a Tabu search method. The phase of connection can also be identified by a unique signal injection, as proposed by [78]. This would require adapting the smart meter, which might be costly.

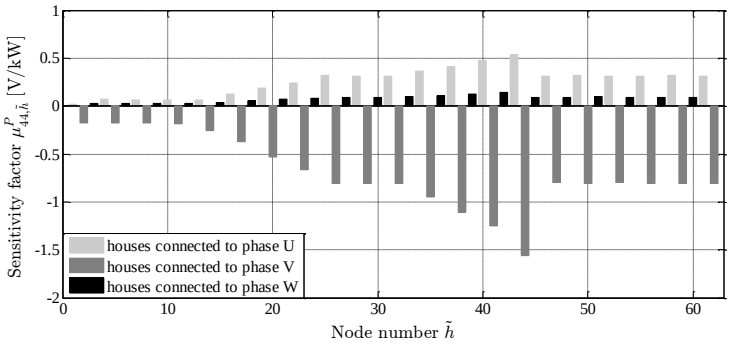

Figure 2.7: The influence of active power of all houses $\tilde{h}$ on the phase voltage of house 44.

2.5 Practical Evaluation

The methods described in section 2.3 are tested in the VITO HomeLab. The HomeLab is a Smart Grid research and test facility for domestic energy management and demand response. The smart grid test infrastructure consists of roughly 300 m EAXVB $4\times16mm^2$ cable, to which different white good appliances can be connected, as shown in Fig. 2.8. The consumption of four

electric heaters can be managed by a solid-state relay, controlled by an Arduino unit. Five households can be simulated. A household is simulated by one white good appliance and an electric heater. The active and reactive power of each household are measured every 10 s, as well as the phase voltage magnitude. The data is automatically saved in a SQL database.

Forming an exact load-flow model that perfectly matches the measured voltages with the calculated voltages is a hard task, even for a small grid like this one. It requires several, iterative adaptations of the non-linear system of equations, to cope with slight errors in cable parameters, cable lengths, or load models. Moreover, it is very difficult to identify the exact cause of the errors made by the exact model, which makes it a difficult task to adapt the correct parameters to improve the load-flow model. Therefore, the techniques described in Section 2.3 are applied to obtain a load-flow model based on measured data, without knowledge of the grid data. Obviously, when an exact model is available, this model should be preferred to obtain the voltage sensitivity factors.

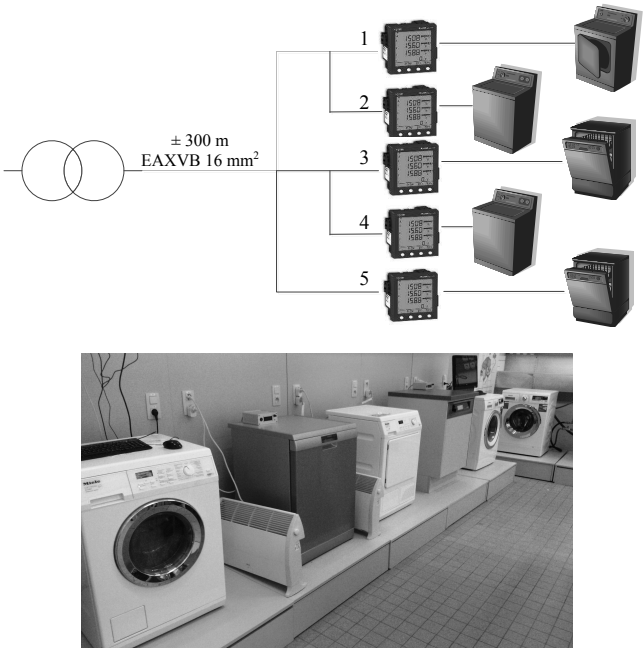

Figure 2.8: The laboratory distribution network topology.

2.5.1 Grid Identification

During seven hours, different devices were turned on and off. The data of the first four hours was used as a training set to obtain the voltage sensitivity factors by solving (2.3). A constant linear model is trained. Due to the absence of distributed generation in the test grid, there are no significantly different operating points that require the use of the piecewise-linear model of (2.4). The data of the last three hours is used as a validation set. Fig. 2.9 shows the measured voltage of this period in three nodes of the network and the voltages that are calculated, based on the trained, linear voltage model. The linear voltage model clearly resembles the measured voltages, without having any information on the grid topology, the load models, or the phase of connection of each of the households. The errors made during this validation period are shown in Fig. 2.10, for each of the nodes in the network. For more than 95% of the time, the errors made by the constant linear model are less than 1 V. The RMSE of this model equals 0.421 V, while the MaxAE equals 2.06 V.

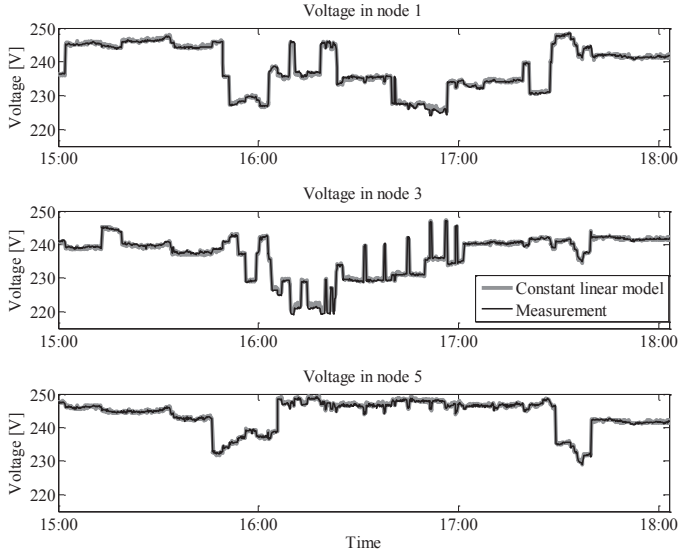

Figure 2.9: The measured voltage and the voltage obtained by a linear model for three nodes of the test grid.

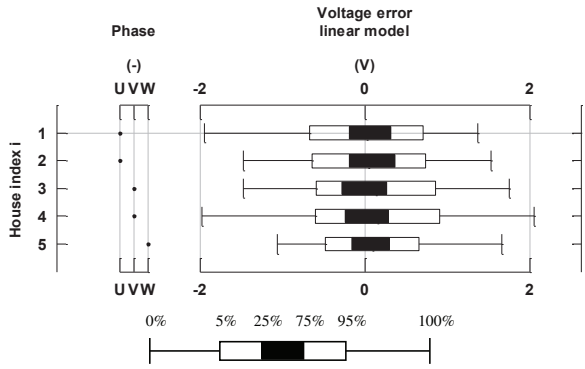

Figure 2.10: The voltage estimation error by a constant linear model and the phase of connection of each of the loads.

The phase of connection of each household is also depicted in Fig. 2.10. The voltage sensitivity factors that express the influence of active power consumption on the voltages in node 1, 3 and 5 are presented in Fig. 2.11. It can be seen that nodes 1 and 2 are connected to the same phase, and nodes 3 and 4 are connected to another phase. When the phase of connection is extracted from the voltage sensitivity factors, the loading in each phase can be computed.

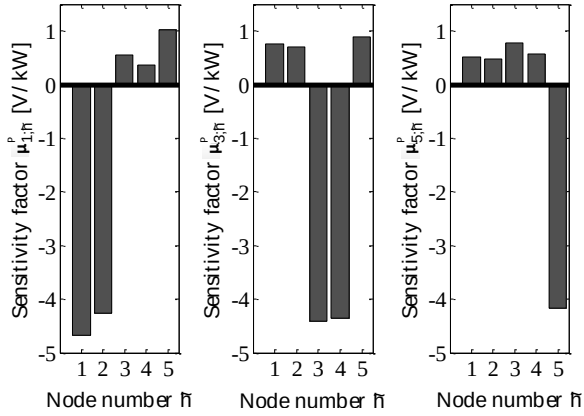

Figure 2.11: The influence of active power consumption of all houses $\tilde{h}$ on the phase voltage of house 1 (left), house 3 (middle) and house 5 (right).

It can be concluded that a simple and effective constant linear load-flow model can be computed, based on measured grid data. This linear model can be used

in a voltage control strategy.

2.5.2 Voltage Control

In the laboratory test grid, voltage control strategies can be tested. These strategies can rely on the linear voltage model obtained in Section 2.5.1. Here, a voltage control strategy is proposed that makes use of one central control unit. This central unit receives from each EV a request to charge at a specified charging power. Each EV also defines the urgency of charging by one number, called the priority γ. Besides the information of the EVs, the central unit also reads-out the voltage of the nodes vulnerable to voltage problems.

With the sensitivity factors $\mu^P_{h,\tilde{h}}$ from the trained model, the control unit can calculate what the voltage would be if no EV was charging during the previous time step (V_h^{noEV}):

$$V_h^{noEV} \approx V_{h,t-1} - \sum_{i=1}^{N_{EVs}} \mu^P_{h,\tilde{h}} P^{EV}_{\tilde{h}} x_{\tilde{h},t-1} \tag{2.5}$$

where

- $V_{h,t-1}$ is the measured voltage of node h
- $x_{\tilde{h},t-1}$ binary variable that defines if EV $\tilde{h}$ was charging during the previous timestep $t-1$
- $P^{EV}_{\tilde{h},t-1}$ was the requested charging power by EV $\tilde{h}$ at the previous timestep $t-1$

Now, the central control unit can check if all EVs can charge at the same time without causing voltage problems. By making use of the sensitivity factors obtained in Section 2.5.1, the expected voltage when all EVs would charge during the next timestep can be computed:

$$V_{h,t} \approx V_h^{noEV} + \sum_{\tilde{h}=1}^{N_{EVs}} \mu^P_{h,\tilde{h}} P^{EV}_{\tilde{h},t} \tag{2.6}$$

where

- $P^{EV}_{\tilde{h},t}$ is the requested charging power by EV i at timestep t

This expected voltage should be compared with the allowed voltage limits. The central control unit can give permission to all EVs to charge if this expected voltage is higher than the minimum allowed voltage. Otherwise, if all EVs can not charge all at the same time, the central unit will solve an optimization problem that tries to maximize the amount of EVs that can charge, weighted by their priority:

$$\begin{aligned} \max_{x_{\tilde{h},t},\varepsilon} \quad & \sum_{\tilde{h}=1}^{N_{EVs}} \gamma_{\tilde{h}} x_{\tilde{h},t} - \varrho\varepsilon \\ \text{subject to} \quad & x \in \{0,1\} \\ & V_{h,t} = V_h^{noEV} + \sum_{i=1}^{N_{EVs}} \mu_{h,\tilde{h}}^{P} P_{\tilde{h},t}^{EV} x_{\tilde{h},t} \\ & V_{h,t} \geq V^{min} - \varepsilon \\ & \varepsilon \geq 0 \end{aligned} \tag{2.7}$$

where

- $x_{\tilde{h},t}$ binary variable that defines if EV $\tilde{h}$ can charge or not at timestep t
- ε is a slack variable to keep the problem feasible
- ϱ is a weighting factor of the slack variable
- V^{min} is the minimum voltage allowed in the grid

The priority of charging γ should depend on the time left before departure and the required energy by the time of departure. EVs with a limited time before departure and still a high need for energy will have a high priority. Examples of how EVs can define their priority of charging can be found in [79–81]. The slack variable ε is applied to guarantee a feasible problem [46]. Due to a high, uncontrollable load, it can become impossible to keep the voltage within limits at some moments. The slack variable keeps the problem feasible and makes sure that the algorithm tries to bring the voltage as close to the limits as possible if this occurs. The weighting factor of the slack variable is chosen ten times higher than the maximum possible priority.

The minimum voltage allowed in the grid, V^{min}, depends on the applied voltage standard of the region of operation. In the laboratory setup, the minimum voltage is set at 227 V, so that it will quickly go out of limits if the EV charging is not controlled.

The control signals $x_{\tilde{h},t}$ can be send to all EVs when this optimization problem is solved. The control actions will give rise to a voltage which will be approximately equal to V_h. This procedure is shown in Fig. 2.12. The communication from the EVs to the central control unit can be made event-based. Only when the EV adapts its priority, or charging power, it has to inform the central unit, otherwise the central unit can use the last-sent values. The actions defined by the central control unit are independent from history, so there is no possible accumulation of errors.

This voltage control strategy is tested in the VITO HomeLab. Fig. 2.13 presents the practical implementation of the central control unit. The central control unit is implemented in Matlab. The central unit communicates via a database with the Arduino load control units. Each Arduino control unit can switch a solid-state relay to turn on or off an electric heater. The four available, controllable electric heaters are used to emulate four EVs that charge at a rate of 1.6 kW. One electric heater is connected to node 1, one to node 2, one to node 3 and one to node 4.

It is assumed that the emulated EVs connected to node 1 and 3 have a high need for the requested energy, while the emulated EVs connected to node 2 and 4 have a low need for the requested energy. Therefore, the priority γ of EVs 1 and 3 is higher than the priority of EVs 2 and 4. The different priorities are given in Table 2.3. For the ease of presentation, the priorities are kept constant during the test. The central control unit checks the network conditions every 10 s and solves optimization problem (2.7) if necessary.

The total load in each phase during this test is plotted in Fig. 2.14, while the voltage is shown in Fig. 2.15. It is clear from the plotted, total load that the EVs can charge when the total load is low in their phase, and have to stop charging when the uncontrollable load by the households is high. When an EV charges and the uncontrollable load suddenly rises, the voltage drops. The control unit quickly corrects the voltage drop by stopping the charging of the EV in this phase. I.e. at 12:30, it quickly stops the charging of the EVs connected to phase V after a sudden increase of the uncontrollable load. This way, the voltage drops only for a short period of time below the acceptable limits.

Two EVs are connected to phase U and two to phase V. At some moments, the total, uncontrollable load is high in one phase, and only one of the two EVs connected to a phase can charge to comply with the voltage limits. In this case, the optimization control problem lets the EV with the highest priority charge, while the other EV has to stop charging. In Fig. 2.14, it can be seen that at 13:00, EV 1 can charge, but EV 2 has to stop charging because, otherwise, the voltage will drop to an unacceptable level.

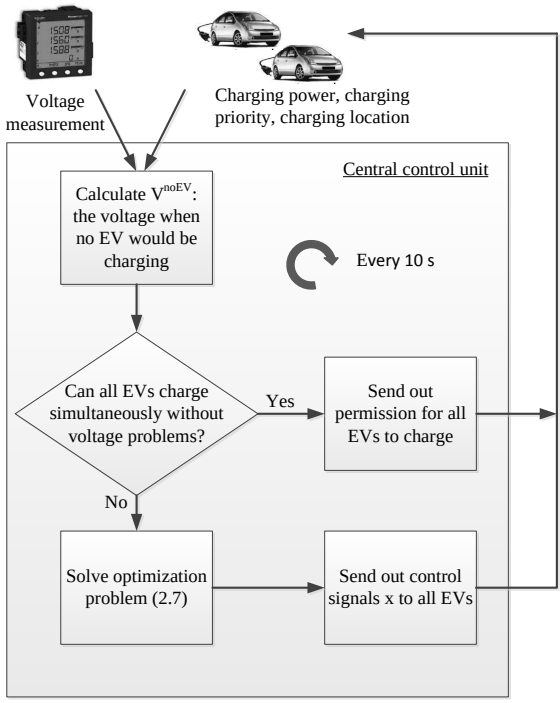

Figure 2.12: Flowchart of the voltage control strategy for EVs executed by the central control unit.

Table 2.3: The used priorities of the four EVs in the practical setup.

	EV 1	EV 2	EV 3	EV 4
Priority	0.8	0.6	0.75	0.5

Problem (2.7) can be extended with constraints that limit the total load in each phase. Future work focusses on testing and validating different voltage management strategies with the obtained voltage sensitivity factors.

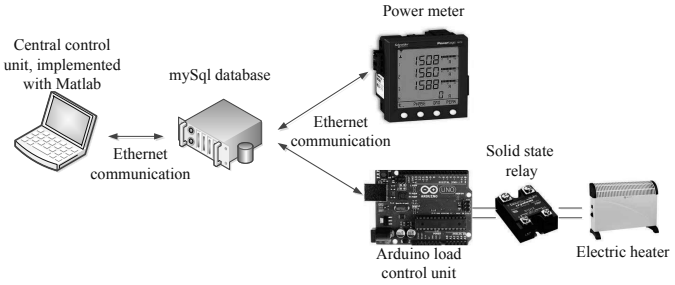

Figure 2.13: Practical implementation of the voltage control strategy.

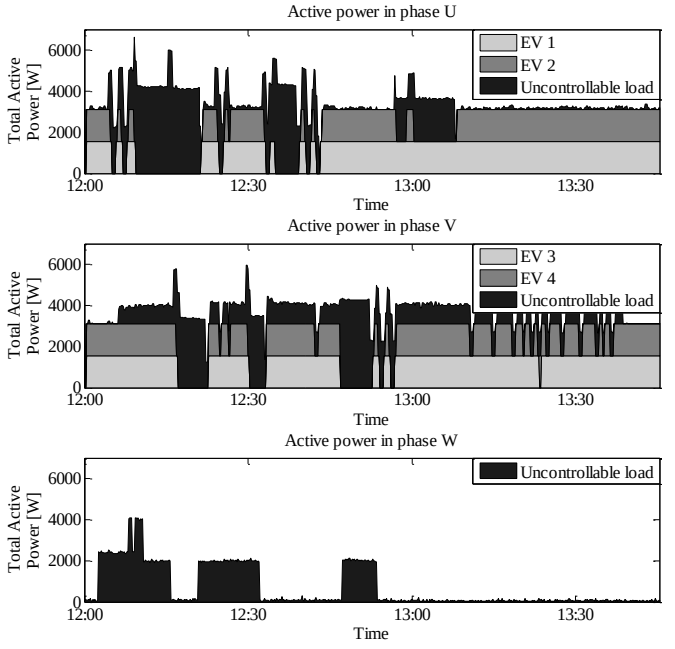

Figure 2.14: The total, active power consumption in phase U, V and W during the test of the implemented voltage management strategy. The loads are stacked on each other in this plot.

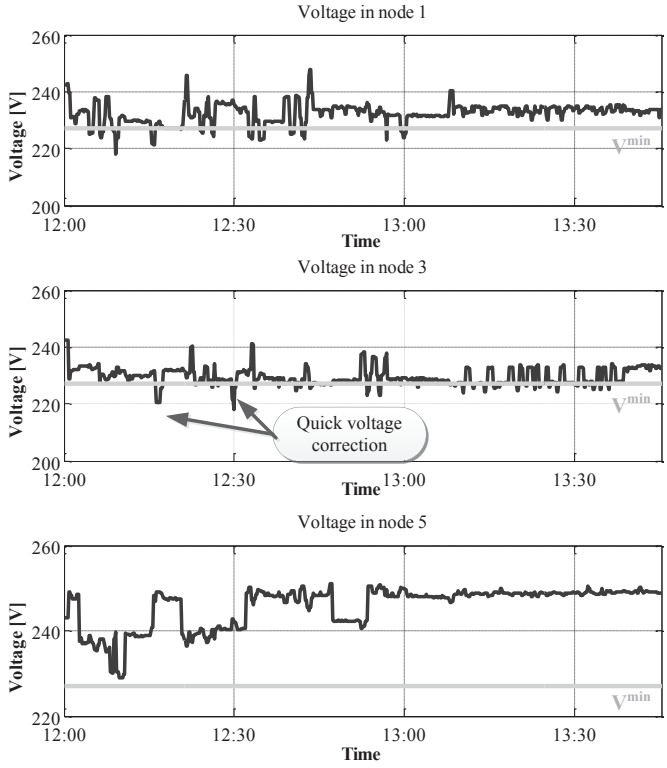

Figure 2.15: The voltages of nodes connected to phase U (node 1), V (node 3) and W (node 5) during the test of the implemented voltage management strategy.

2.6 Conclusion

A linearised load-flow model is identified by means of historical smart meter data for radial distribution grids with incomplete or inaccurate data. This model depends on the loading of the network and could be obtained by solving a least squares problem. No information concerning grid topology, load models, or the phase of connection was required. It was shown that the voltage sensitivities obtained, based on historical smart meter data, are accurate approximations of the actual voltage sensitivities. The approximated voltage sensitivities provide information about both the location and the phase of each customer. These voltage sensitivities are crucial for many voltage management strategies.

The algorithm has been verified in a practical laboratory environment. A validation set of data was used to compare the output of a trained, linearised load-flow model with actual data, which were shown to match accurately. The algorithm could also correctly identify the phase to which each household was connected. As an example of the many applications, the voltage sensitivities were used in a voltage control strategy. A central control unit evaluates if the requested power of an EV can be consumed without harming the grid. When the voltage dropped below the allowed limits, the control unit could quickly correct the voltage to an acceptable level.

Chapter 3

Voltage Control with PV Inverters

Combined Central and Local Active and Reactive Power Control of PV Inverters

Sam Weckx, Carlos Gonzalez de Miguel, Johan Driesen

Published in IEEE Transactions on Sustainable Energy, vol.5, no.3, pp.776-784, July 2014

3.1 Introduction

The increasing penetration of photovoltaic (PV) panels challenges the future grid operation. During periods of low demand, the high active power injection by the PV inverters can result in transformer overloading, or a rise of the grid voltage to critical levels. Voltage rise is normally the main limiting factor to prevent the increase of PV generation in Low Voltage (LV) networks [10]. PV inverters provide their nominal, or maximum power, during just a small fraction

The first author is the main author of the article. The contributions of the first author include the development of the model, the optimization framework and the analysis of the simulation results. The second author contributed with the development of the model and the analysis of the results.

of the time so that the remaining power capacity available in the inverter can be used for voltage control. Voltage control by reactive power control and active power curtailment is shown to be an economically interesting solution [82].

Different local reactive power control methods are proposed. These include methods based on local voltage measurements [10, 25, 26, 83], local power production measurements [10, 25, 26, 84], or a combination of both [25, 26]. In [85], local measurements are used to define the voltage reference for a reactive voltage controller. These local control methods can result in a significant amount of unnecessary reactive power consumption, or insufficient voltage support, when local parameters are not tuned to the structure of the grid. Most of these local controllers are characterised by only one parameter, making it impossible to be optimal for different states of the system. Besides that, local controllers cannot avoid transformer overloading.

The installation of a communication infrastructure for smart metering offers new possibilities for voltage control. Intelligence can be added to a substation, or another, local agent responsible for network control. An optimization of reactive power consumption results in the most efficient reactive power support to avoid overvoltage, or to remain in a specified voltage band. This optimization can be performed at a central unit [46, 86, 87], or by an iterative communication procedure between intelligent, neighbouring PV inverters [10, 88, 89]. However, system conditions in a grid with a high penetration of PV generation can rapidly change due to the movement of clouds. It is therefore important that the reactive control can adapt to changing system conditions [90]. Reactive power support, as planned by an optimization unit, can therefore become insufficient, or excessive when no real-time optimization is performed. Computational and communicational burdens might hinder this real-time implementation. Local controllers are not vulnerable to these changing conditions.

The amount of reactive power that can be supplied is limited. At time steps of high active power production, the part of the inverter capacity remaining for reactive power might not be sufficient to keep the voltage at acceptable levels. Moreover, due to the high R/X values in LV networks, the effect of reactive power is limited. Active power curtailment is then required to avoid a violation of the upper voltage limit. Local active power curtailment methods are proposed in [10, 22, 91]. This curtailment is a direct cost to the owner of the PV panels, due to the reduction of generated energy. It is therefore recommended to make optimal use of the available reactive power to minimize the amount of active power curtailment.

In this work, a centralized optimization algorithm optimizes the parameters of the local controllers every 15 minutes. The local controllers are optimized to obtain near-optimal performance, even when the PV production changes due to

cloud movement in this 15-minute time period.

In [92], a centralized optimization algorithm tunes one parameter of each local reactive power controller reacting on local measurements of the voltage. In this work, both curtailed active and reactive power are controlled, based on a local measurement of the produced PV power. The local control methods are defined by multiple parameters, resulting in a more optimal behaviour. The corresponding optimization problem is a convex optimization problem which can be solved efficiently.

This chapter is structured as follows: In Section 3.2, the effectiveness of reactive voltage control in three-phase, four-wire, unbalanced, radial distribution networks is studied. In Section 3.3, the convex optimization problem that results in the tuning of the local control parameters is presented. The test system is described in Section 3.4. Finally, Section 3.5 discusses the obtained results and compares them with different local control methods.

3.2 Effectiveness of Reactive Power in Three-Phase Four-Wire LV Networks

Distribution networks are characterised by low X/R values. It is well described in the literature that, for a single-phase line with mainly resistive line impedance, reactive power has a limited effect on the voltage [25, 93]. European LV distribution networks are, however, often of the three-phase, four-wire type. The connection of single-phase loads and PV units to three-phase, four-wire LV networks will not only alter the voltage profile in the connected phase, but also the two other phase voltages due to a neutral point shift [12]. The neutral-point shift originates from the return current through the neutral conductor. Consider a three-phase four-wire cable with $R = 3X$, with a PV unit connected at one side and a delta-grounded wye (Dyn) transformer with a perfectly balanced network at the other side. Fig. 3.1 presents the phase voltages before and after reactive power absorption of a PV unit connected to phase U. The phase voltages are considered to be balanced before reactive power absorption by the PV panel. The full line is the phase voltage before the absorption of reactive power, the dashed line is the phase voltage after the absorption.

Reactive power absorption in phase U significantly increases the phase voltage of phase W and decreases the phase voltage of phase V. Therefore, in grids with low X/R values, decreasing the voltage in one phase can be done with less reactive power injection in another phase than by absorbing reactive power in the specific phase itself. This effect is important for reactive power control in

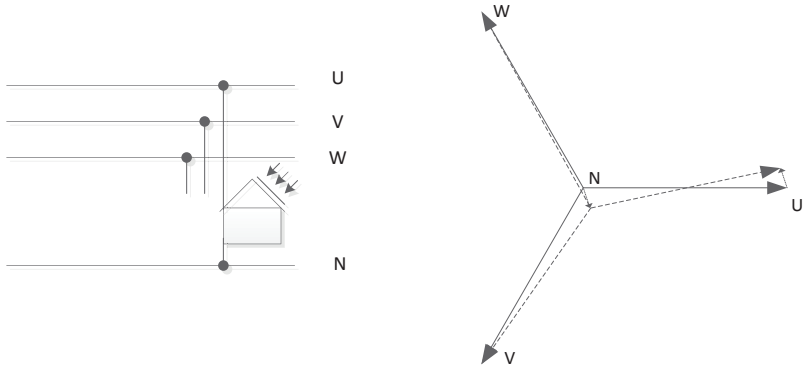

(a) Single-phase PV inverter connected to phase U.

(b) Phase voltages before and after absorption of reactive power in phase U.

Figure 3.1: Neutral point shifting due to the absorption of reactive power in phase U.

grids where PV panels are not equally spread across the three phases. When the voltage rises to critical levels in the phase with the highest PV production, local reactive controllers of PV panels connected to the other phases could respond as well. These panels can make their reactive power support dependent on their PV production, as a high PV production can be a good indication of overvoltage in the phase with the highest PV production. A central optimization of all the local control parameters, which is regularly repeated, can take this into account.

Neutral-point shifting also occurs with active power injection. As shown in [12], active power injection in one phase increases the voltage of that phase, but decreases the voltage in the other two phases. Therefore, grids where the PV installations are unequally distributed across the three phases are significantly more vulnerable to overvoltage [14]. PV generation in a distribution grid is rarely spread equally across the three phases, resulting in phases that can be more vulnerable to severe voltage rises than others.

Four different, local voltage control methods are presented in Fig. 3.2 [25, 26]. The first three controllers react to the local voltage measurement, whereas the fourth controller reacts on a local measurement of the produced PV power. The first two local control methods only use reactive power. Reactive voltage control alone can sometimes be insufficient and active power also needs to be curtailed to avoid excessively high voltages. The third local control method

combines reactive voltage support with active power curtailment. Reactive power is absorbed starting from a voltage of 1.08 p.u. Active power curtailment starts from a voltage of 1.09 p.u. with a total reduction of the produced power at 1.11 p.u. The reactive power contribution from the inverters that are nearest to the transformer will be negligible, since the measured voltage levels at these inverters will be lower, and therefore can result in a weaker voltage support [26]. If the reactive power capabilities of inverters close to the transformer are to be exploited, the droop parameters have to be made location dependent [22].

Inverters equipped with the fourth local control method react to a local measurement of the produced PV power. Inverters close to the transformer will participate in voltage control, but have no feedback about the actual voltage. Time periods with a large amount of PV generation often do not coincide with the moments of peak power demand. This results in a rise of the grid voltage. A controller based on a local measurement of the produced power can help to avoid voltage limit violations by absorbing reactive power during peak production. This fourth local control method requires the inverter to have a higher rating than the maximum produced PV power. It is assumed that each inverter can still inject or absorb reactive power to obtain a $\cos(\varphi)$ of 0.95 at maximal PV production.

The local control methods of Fig. 3.2 will not result in a minimum use of reactive power while avoiding voltage problems. However, note that these local control methods are robust, reliable and easy to implement. Besides that, no grid model is needed to implement these control approaches. Therefore, when no grid model and communication infrastructure is available, these control methods can be applied. This chapter assumes that a grid model and a communication infrastructure are available, and, therefore, implementing the proposed central controller comes at limited or no extra cost. The local control methods of Fig. 3.2 can then be used as a back-up system.

In this work, local control parameters are centrally optimized to guarantee a minimum us of reactive power while avoiding voltage problems. The optimized local controllers react to their PV output power, like local control method four. The control functions are first-order splines. A first-order spline is a piecewise-linear function. The place where the piecewise functions of the spline connect are called knots. For a given time step, the control function is divided into a fixed amount, i.e. ten, of piecewise functions for the range of possible PV output power levels. For a PV output power level that is constrained in the interval between two knots, the output value of the controller is defined through linear interpolation. The output value of the local controller at each knot is optimized. Therefore, the more knots that are used, the better the performance of the controller, but the higher the computational complexity. In this work, the amount of knots is limited to ten. This leads to good results, as shown in

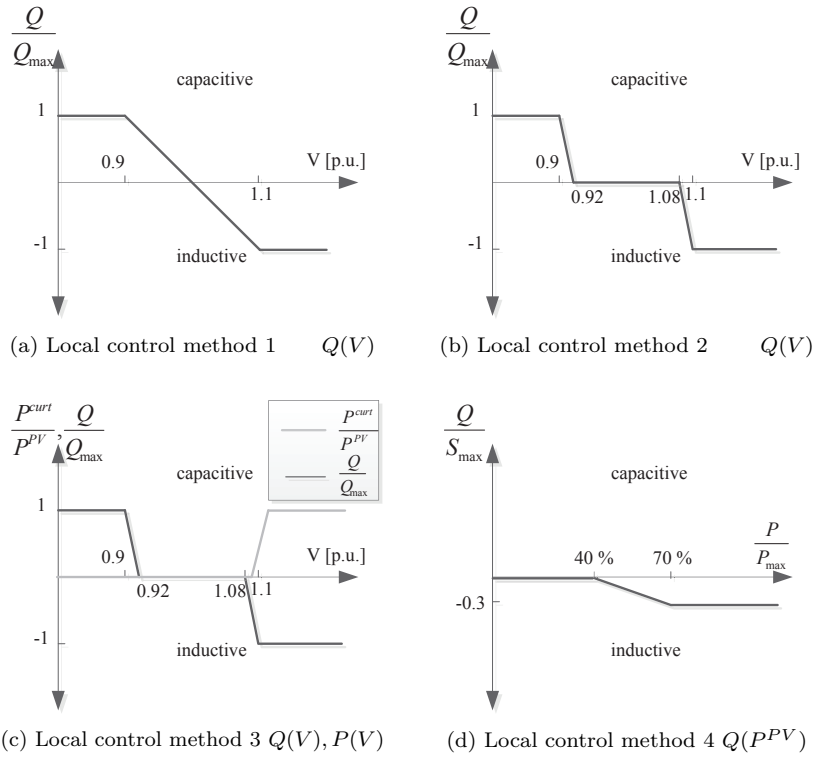

(a) Local control method 1 $Q(V)$ (b) Local control method 2 $Q(V)$

(c) Local control method 3 $Q(V), P(V)$ (d) Local control method 4 $Q(P^{PV})$

Figure 3.2: Four different local control methods.

Section 3.5, and has a limited computational complexity.

Fig. 3.3 shows two local control functions, each consisting of ten piecewise functions. Both curtailed active and reactive power are controlled. The first, local control function is a typical control function of the phase with the highest PV production. Starting from a certain level of power output, reactive power is absorbed to reduce the voltage. For higher power output levels, active power also needs to be curtailed. The second local control function is a typical control function of a phase with less PV production. As was shown in Fig. 3.1, when voltage problems occur i.e. in phase W, due to a higher amount of rated PV power connected to this phase, reactive power injection in phase U can decrease the phase voltage in phase W. Therefore, starting from a certain power output the controller injects reactive power to decrease the voltage in the other phase. From a certain amount of produced power, the voltage will increase in its own phase and the reactive power injection has to be limited. For high amounts

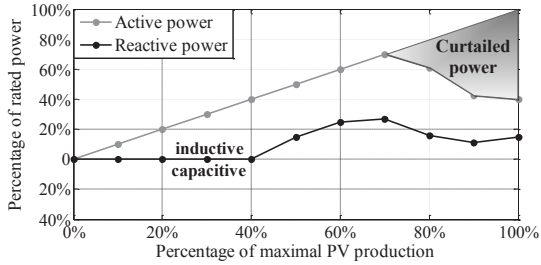

(a) Local control function for a PV unit connected to the phase with the highest PV production.

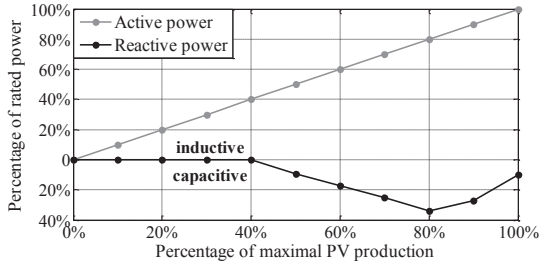

(b) Local control function for a PV unit connected to a phase with less PV production.

Figure 3.3: Example of two optimized local control functions defined by a piecewise linear function with 10 knots.

of produced power, the inverter rating will limit the reactive power injection. Active power need only to be curtailed at very high production levels. The knots of the splines are marked by dots in this figure. By regularly retuning the knots of the splines, i.e. every 15 minutes, the local controller that reacts on the produced power can adapt to increasing and decreasing loads, i.e. during lunchtime.

At night, when the produced PV power is zero, the proposed method reduces to a standard, central, reactive voltage control method, where the reactive power injected, or absorbed, by the PV inverters remains constant until the next central optimization of reactive power takes place. There is a lower correlation between load profiles, resulting in smaller voltage fluctuations in the time between two optimization steps at night, justifying a constant, reactive power control.

3.3 Optimization Problem

The centralized control system should determine setpoints of the reactive power and curtailed power of PVs, based on the expected PV output power during the next time period. In practice, however, the PV output power in the next time period can vary significantly due to the movement of clouds and is uncertain. To cope with this uncertainty, the local controllers are tuned by the central optimization for different possible PV production levels. These different levels are discretised, using e.g. ten points, which form the knots of a first order spline. Constraints are then defined for each possible knot of the spline. Two examples of optimized, local control functions defined by splines were already presented in Fig. 3.3.

The PV inverter complex output power is limited by the nominal inverter apparent power rating $|S_h^{\text{Nom}}|$:

$$\left(P_{p,h}^{\text{PV}} - P_{p,h}^{\text{curt}}\right)^2 + \left(Q_{p,h}^{\text{PV}}\right)^2 \leq \left(|S_h^{\text{Nom}}|\right)^2 \tag{3.1}$$

Where

- $P_{p,h}^{\text{PV}}$ is the produced PV power by the inverter connected to node h, for knot p $[kW]$;
- $P_{p,h}^{\text{curt}}$ is the curtailed PV power by the inverter connected to node h, for knot p $[kW]$;
- $Q_{p,h}^{\text{PV}}$ is the reactive power by the inverter connected to node h, for knot p $[kvar]$;

If a spline of 10 knots is applied, each inverter has 10 complex output power constraints (3.1), as for each possible PV output power level, the inverter rating should be respected. The inverter can not curtail more than the produced PV power, which requires constraint:

$$0 \leq P_{p,h}^{\text{curt}} \leq P_{p,h}^{\text{PV}} \tag{3.2}$$

A constraint on the power factor can be set by a linear constraint:

$$Q_{p,h}^{\text{PV}} \leq \varsigma \left(P_{p,h}^{\text{PV}} - P_{p,h}^{\text{curt}}\right) \tag{3.3}$$

where ς is a constant defining the allowable ratio between reactive and active power.

The first-order splines formed by the knots $P_{p,h}^{\text{curt}}$ and $Q_{p,h}^{\text{PV}}$ define the functions $P^{curt} = f_P\left(P^{PV}\right)$ and $Q^{PV} = f_Q\left(P^{PV}\right)$. All the points of these functions

will satisfy constraints (3.1), (3.2) and (3.3). The convexity of these constraints implies that any point on a straight line between two points in the convex set is part of the set and, therefore, satisfies the inverter limits. This justifies the discretization to a limited amount of points.

For all different PV output levels, the voltage should remain within limits. The influence of PVs on the voltage magnitude can be approximated with a linearized model [41, 49, 86, 94], resulting in an affine constraint. The voltage at node h, for a set of possible output powers $P^{\mathrm{PV}}_{p,\tilde{h}}$, can be defined as:

$$|V_{p,h}| = |V_h^{\mathrm{base}}| + \sum_{\tilde{h}=1}^{n_{\mathrm{nodes}}} \left(\mu^P_{h,\tilde{h}} \left(P^{\mathrm{PV}}_{p,\tilde{h}} - P^{\mathrm{curt}}_{p,\tilde{h}} \right) + \mu^Q_{h,\tilde{h}} Q^{\mathrm{PV}}_{p,\tilde{h}} \right) \tag{3.4}$$

Where

- V_h^{base} is the voltage at node h due to the load of the households during the previous time step $[V]$;
- $V_{p,h}$ is the voltage at node h with the local controllers activated $[V]$;
- $\mu^P_{h,\tilde{h}}$ is the sensitivity of the voltage magnitude in node h by active power injected at node $\tilde{h}$ $[\frac{V}{kW}]$;
- $\mu^Q_{h,\tilde{h}}$ is the sensitivity of the voltage magnitude in node h by reactive power injected at node $\tilde{h}$ $[\frac{V}{kvar}]$;

For each set of possible output powers $P^{\mathrm{PV}}_{p,\tilde{h}}$ a voltage $V_{p,h}$ exists. Due to the small geographical area, the produced PV output power $P^{\mathrm{PV}}_{p,\tilde{h}}$ relative to the nominal power production $|S^{\mathrm{Nom}}|$ could be considered as equal. Having a spline of 10 knots for each PV inverter will then result in 10 possible voltages at each node h.

In practice, the irradiation between different PV panels can slightly differ due to cloud movement. When using splines with 10 knots, the amount of possible combinations, and therefore also possible voltages to include, equals n^{10}_{nodes}. A lot of these combinations are very unlikely or can be neglected, i.e. all combinations with only low PV production levels will not cause any problems. Some relevant combinations of different irradiation levels could also be included by sampling some scenarios. These scenarios represent a realistic cloud pattern with lower irradiation in a certain area of the distribution grid. This will increase the number of constraints. Simulation results, though, show that defining the

splines, based on the assumption of equal relative PV output power level, gives good results, even when the relative output power is not equal.

Typically, the voltages of a limited number of control points at the end of the feeders have to be considered, as these are subject to the largest voltage deviations. This can, again, significantly reduce the number of constraints.

The voltage estimation is done based on information of the previous time step. It is considered that households are equipped with smart meters. This way, the voltage at node h, caused by the load of the households V_h^{base}, can be calculated by performing a load-flow with the load of the households. An alternative way to obtain V_h^{base} is to use a measurement of the voltage in node h and subtract the influence of the PV units on this voltage during the previous time step by making use of the sensitivity factors.

All the possible voltages should be limited between a minimum and maximum voltage:

$$V^{\min} \leq |V_{p,h}| \leq V^{\max} \tag{3.5}$$

where $V^{\min}$ and $V^{\max}$ are the minimum and maximum allowed voltage. As previously stated, the voltages in the beginning of the feeder should not be considered to reduce the amount of constraints. Small violations of constraint (3.5) can exist, due to limited variations of the base load and linearization errors by the linear models. This can be avoided by introducing a small extra conservative margin in the limits of (3.5). The voltage is limited to $\pm$ 10 % of the nominal voltage, but to include a conservative margin, $V^{\min}$ and $V^{\max}$ are chosen to be $\pm$ 9 % of the nominal voltage. All possible voltages should comply with the voltage limits. Due to the convexity of constraints (3.4) and (3.5), every voltage caused by a linear interpolation obtained by the splines will comply with these limits when the relative output power of each PV inverter is equal.

The objective of the controllers is to curtail as little active power as possible. A small penalty term for reactive power is added to the objective function to avoid the use of reactive power when no critical voltage conditions can be reached. The unnecessary use of reactive power could lead to increased losses. The total amount of reactive power is automatically constrained by the limits of the inverters. A small weighting factor w, equal to 0.01, is introduced to ensure that the reduction of curtailment dominates the penalty term for reactive power. Smaller, positive weighting factors can be applied. The final optimization

problem is defined as:

$$\underset{P_{p,h}^{\text{curt}}, Q_{p,h}^{\text{PV}}}{\text{minimize}} \quad \sum_{p=1}^{10} \sum_{h=1}^{n_{\text{nodes}}} \left(w \left(Q_{p,h}^{\text{PV}} \right)^2 + (1-w) P_{p,h}^{\text{curt}} \right) \tag{3.6}$$

$$\text{subject to} \quad (3.1 - 3.5)$$

The solution of this convex optimization problem defines all the knots of the piecewise-linear, local control functions. The active and reactive power are defined in kW and $kvar$.

Different, extra constraints can be added to optimization problem (3.6). Fair, active power curtailment can be imposed by the next constraint:

$$\frac{P_{p,h}^{\text{curt}}}{S_h^{\text{Nom}}} = \frac{P_{p,z}^{\text{curt}}}{S_z^{\text{Nom}}} \tag{3.7}$$

This constraint results in an equal percentage of curtailed power when PV panels produce the same percentage of the nominal power. Note that this constraint imposes fair curtailment within this feeder, but not in the overall system.

Another possibility is to allow only active power curtailment, as in [22]. This can be achieved by adding a constraint that makes $Q_{p,h}^{PV}$ equal to zero. If transformer overloading can take place, a constraint on the maximal apparent power can be introduced. Again, this constraint has to hold for all possible PV output power levels:

$$\left(\sum_{h=1}^{n_{\text{nodes}}} P_{p,h}^{\text{PV}} - P_{p,h}^{\text{curt}} - P_h^L \right)^2 + \left(\sum_{h=1}^{n_{\text{nodes}}} Q_{p,h}^{\text{PV}} - Q_h^L \right)^2 \leq \left(S^{Max} \right)^2 \tag{3.8}$$

where P_h^L and Q_h^L form the load of the household connected to node h and S^{Max} is the maximal apparent power going through the transformer. The sum of the (estimated) active and reactive household loads can be replaced with an estimate of the total active and reactive load.

In this work, the adaptive central controller is compared to the local control methods of Fig. 3.2 and compared to a static central controller. In a static central optimization, the setpoints for the reactive power and curtailed active power are defined and do not depend on local measurements of the produced power.

A prediction of the PV output power during the next 15 minutes is used by the static central optimization to define the setpoints. The static central optimization needs short-term forecasts with a high spatial resolution. The two

most popular very short-term forecast methods are based on stochastic learning techniques or on total sky imagery. The simplest stochastic learning technique is the persistence model which is based on current or recent PV power plant or radiometer output and is extrapolated to account for changing sun angles [95–97]. Total sky imagery consists of the acquisition and analysis of sky images to estimate the cloud cover. This improves the PV power prediction. It, however, requires a Whole Sky Imager device [95]. Also, for PV power predictions with time scales shorter than one hour, forecasts based on a persistence model tend to outperform satellite based forecasting methods and numerical weather prediction models [95–97]. Therefore, for the static central optimization the persistence model will be used as a forecasting method in this work. Typical accuracies for these forecasting methods can be found in [96, 97]. Developing advanced stochastic learning methods for the prediction of PV power is outside the scope of this work. Note that the field of solar and photovoltaic forecasting is rapidly evolving and further improvements in very-short term power forecast methods are expected [95]. Fig. 3.4 shows the 15 minute ahead prediction by a persistence model for a sunny and cloudy day. It is clear that forecast errors increase in the presence of clouds and, therefore, the performance of a static central controller will decrease. The smaller the time period between consecutive optimizations, the faster the central controller can correct for prediction errors due to clouds. The static calculation of both reactive and curtailed active power becomes:

$$
\begin{aligned}
\underset{P_h^{\mathrm{curt}},Q_h^{\mathrm{PV}}}{\text{minimize}} \quad & \sum_{h=1}^{n_{\mathrm{nodes}}} \left(w \left(Q_h^{\mathrm{PV}}\right)^2 + (1-w) P_h^{\mathrm{curt}} \right) && (3.9)\\
\text{subject to} \quad & 0 \leq P_h^{\mathrm{curt}} \leq \mathbf{E}(P_h^{\mathrm{PV}}) \\
& \left(\mathbf{E}(P_h^{\mathrm{PV}}) - P_h^{\mathrm{curt}}\right)^2 + \left(Q_h^{\mathrm{PV}}\right)^2 \leq \left(S_h^{\mathrm{Nom}}\right)^2 \\
& V^{\min} \leq |V_h| \leq V^{\max} \\
& |V_h| = |V_h^{\mathrm{base}}| + ... \\
& \qquad + \sum_{\tilde{h}=1}^{n_{\mathrm{nodes}}} \left(\mu_{h,\tilde{h}}^{P} \left(\mathbf{E}(P_{\tilde{h}}^{\mathrm{PV}}) - P_{\tilde{h}}^{\mathrm{curt}}\right) + \mu_{h,\tilde{h}}^{Q} Q_{\tilde{h}}^{\mathrm{PV}} \right)
\end{aligned}
$$

where $\mathbf{E}(P_h^{\mathrm{PV}})$ is the expected power production of the PV unit connected to node i, during the next time step, as predicted by the persistence model. The obtained setpoints P_h^{curt} and Q_h^{PV} can be locally overruled when inverter constraints are not met because of forecast errors. I.e. when the PV production suddenly drops unexpectedly, the curtailed active power remains limited to this level.

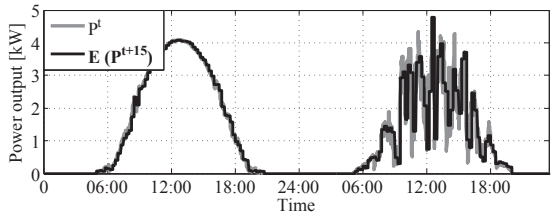

(a)

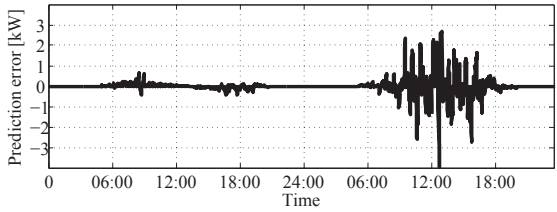

(b)

Figure 3.4: Measured PV profile P^t and 15 minutes ahead PV prediction $\mathbf{E}(P^{t+15})$ for both a sunny and cloudy day (Top) and the prediction error for both days (Bottom).

3.4 Simulated Network

The network used in the simulations is the same, existing, three-phase, four-wire, radial distribution system that was already presented in Fig. 2.1. It has been used to investigate the impact of an increasing amount of PV [14, 94] in public, low voltage distribution networks. It was shown that it can cope with PV units installed at the rooftop of 50 % of all the houses. Overloading of the transformer did not occur.

All households were assumed to have a single-phase connection with a nominal line-to-neutral voltage of 230 V and are equally spread across the three phases. The voltage at the secondary side of the transformer is considered to be 235 V during no load, which can be considered as a typical LV transformer tap to avoid low voltages at the end of the feeder. Statistically representative, residential load profiles are available to perform load-flow simulations. A constant power load model was assumed. Generation of these load profiles is described in [73]. In [73], the privacy problem of data provided by electrical companies is bypassed by transforming a large dataset of residential load profiles into a model that is able to create a set of synthetic, non-aggregated load profiles. This model was

trained based on a large database of measured residential load profiles provided by the DSOs in Flanders. No data of reactive power consumption by loads was available and reactive power by loads is, therefore, neglected in the simulation.

The PV profile was measured at a fixed rooftop PV installation at KU Leuven, with a time step of one minute. All PV panels are assumed to have equal orientation. The PV generation units have a nominal capacity of 5 kVA and are unequally spread across the phases. All households connected to phase U have a PV unit, whereas only 50 % of the other households have a PV unit. The voltage is limited to $\pm$ 10 % of the nominal voltage. The time step used in the simulation is one minute.

3.5 Results

In this section the four, local controllers of Fig. 3.2 are compared both with the adaptive central control method that tunes the local control functions by solving (3.6) and with the static central optimization (3.9) of the PV inverters.

One week in summer is simulated on a one minute basis. To take into account cloud movement, the PV profiles of all households with an index higher than 40 were delayed by one minute to obtain more realistic PV profiles [98]. The local control functions, though, are tuned under the assumption that the PV profiles of all households are equal. Even with this assumption, performance of the adaptive controller is superior, as will be shown in this section. All voltages are obtained by applying the backward-forward sweep power flow method [61]. Convergence problems due to the non-differentiable points of the voltage-dependent, local controllers [25] are mitigated by applying a diminishing step size in the backward-forward sweep power flow method. The adaptive central controller updates the local control parameters every 15 minutes, whereas the static central controller updates the setpoints of the reactive power and curtailed active power every 15 minutes. No constraint to impose fair active power curtailment (3.7) is added in the first simulation.

In Fig. 3.5, an empirical cumulative distribution function (CDF) plots the maximum voltage occurring in the grid. Voltages above 1.1 p.u. need to be avoided. The first local control method shown in Fig. 3.2 reduces the maximum voltage, but fails to avoid voltages above 1.1 p.u. With this local control method, all PV panels will absorb high amounts of reactive power. However, due to the neutral point shifting effect discussed in section 3.2, reactive power absorption in one phase can increase the voltage in another phase. In unbalanced, three-phase, four-wire grids, this will result in higher voltages of the phase with the highest installed PV generation. The fourth local control method also absorbs high

amounts of reactive power in all phases at the same time, and therefore, reduces the voltage insufficiently. The second local controller only absorbs reactive power in phases with high voltages, which clearly improves the voltage reduction. To further reduce high voltages, active power curtailment can be added to the second local control method, which is done in the third local control method. This further improves the performance of the voltage control. The static central controller is unable to adapt to quickly changing conditions, i.e. to a sudden increase of irradiation in the area. The combined central and local control approach is better at adapting to these changing conditions and significantly reduces excessive voltages. To avoid excessive high voltages, the third local control method and the proposed combined central and local control approach should be preferred.

An advantage of centrally-coordinated controllers is that they can ask to inject/absorb reactive power in one phase to avoid excessive voltages in another phase. Therefore, reactive voltage support is more equally spread across the three phases, resulting in decreased losses. The individual reactive power support by each household is presented in Fig. 3.6. In this figure, a modified box plot [94] is applied to display the reactive power support. An additional box, spanning the 5th to 95th percentiles, is added to the standard box plot. Phase U has a higher loading, due to the higher penetration level of PV generation. High voltages mainly occur in this phase. The first local control method results in excessive reactive power support by each household. With the second and third local control method, only nodes with high voltages will absorb reactive power to reduce the voltage. The last local control method results in equal reactive power absorption of all nodes, including the nodes of low loaded phases, which is less efficient. The adaptive central method results in both reactive power injection and absorption of all nodes. Depending on the phase of the connection, PV units absorb or inject reactive power. This is because excessive voltages occur mainly in phase U due to the higher PV penetration. Injecting reactive power in phase V reduces the voltage in phase U due to the neutral point shifting.

The application of the first local control method results in excessive use of reactive power and, therefore, an unnecessary extra loading of grid components. The application of the second and third local control method results in increased loading of the highest-loaded phase U, whereas applying the last local control method results in an equal increased loading of each phase. Avoiding the extra power through the highest-loaded phase is beneficial for the system losses.

A comparison between the losses and the amount of curtailed energy is provided in Table 3.1. A traditional voltage control is added, where a PV installation will disconnect for 10 minutes in case of any voltage limit violation and reconnect when the voltage is within limits again. This type of control results in a high

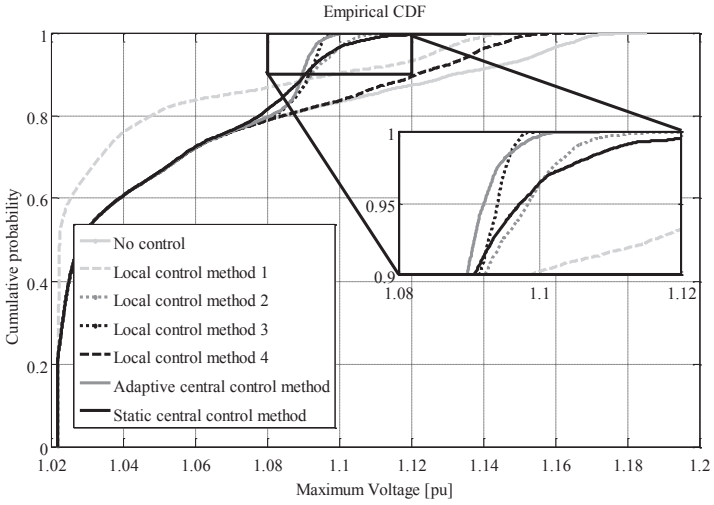

Figure 3.5: Empirical cumulative distribution function (CDF) of the maximum grid voltage for different control methods.

amount of curtailed energy. Due to the disconnection of many units, the peak load seriously drops, which results in a significant decrease of the average amount of losses. Without any type of voltage control, the losses are lower than with reactive voltage control. No reactive power is absorbed or injected. The assumed, constant power model of both the loads and the PV-units will then result in smaller currents in case of higher voltages. The central methods have smaller losses than the local methods, due to the more optimal use of reactive power. If necessary, a limited amount of active power is curtailed by the central methods. The average, daily produced energy in the grid during this week in summer equals 810 kWh, so the amount of curtailed energy is almost negligible. Local control method 3, which had a similar performance in avoiding voltage limit violations as the proposed combined central and local control approach, has increased losses and curtails more energy. In case of a failure in the communication system, local control method 3 could be applied as a less optimal backup for the proposed method.

In the previous simulation, active power curtailment was unfair: customers connected to phase U curtailed more power. By adding constraint (3.7) to the optimization formulation of the local control functions, all PV panels will curtail an equal percentage of the generated power. This will result in an increased total amount of curtailed energy, because PV panels to non-problematic phases will also curtail produced energy. The total active power produced for both

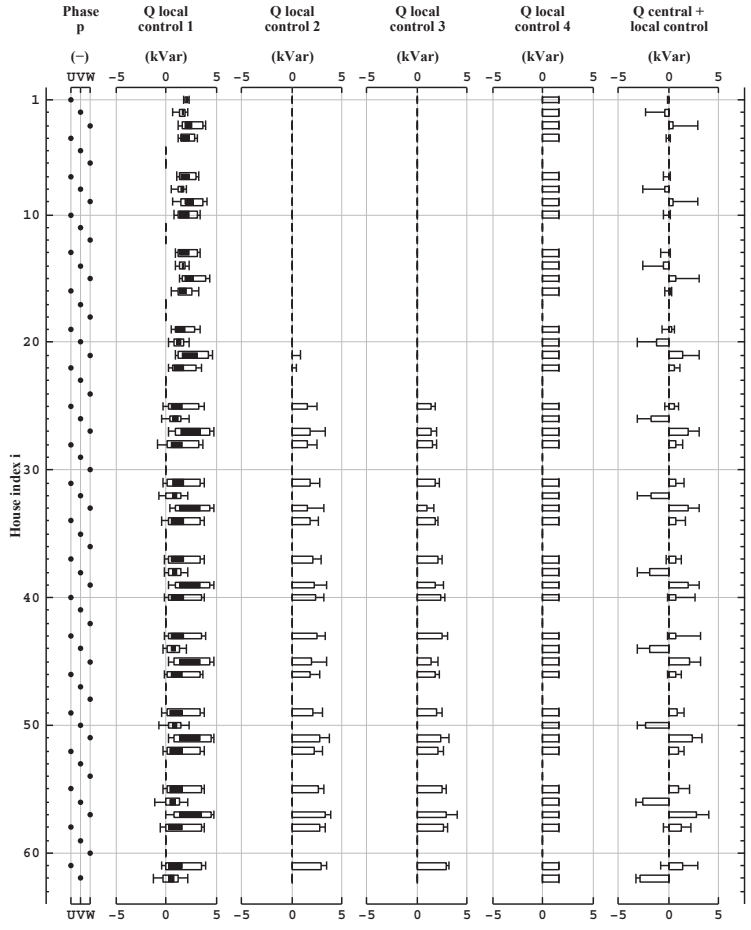

Figure 3.6: Reactive power support of each household for different control methods. A modified box plot is used, where the whiskers extend to the minimum and maximum values.

Table 3.1: Average, daily system losses and the average total amount of curtailed active power in the grid for different control methods.

Control method	**Average daily system losses**	**Average daily curtailed active power**
No control	26.19 kWh	0 kWh
Traditional voltage control	9.81 kWh	257.13 kWh
Local control method 1	82.77 kWh	0 kWh
Local control method 2	33.21 kWh	0 kWh
Local control method 3	31.05 kWh	8.96 kWh
Local control method 4	30.97 kWh	0 kWh
Static central control	28.38 kWh	0.49 kWh
Adaptive central control	28.16 kWh	0.47 kWh

fair and unfair curtailment is plotted in the upper part of Fig. 3.7. In case of fair curtailment, the extra reduction of produced power is limited due to the intelligent application of reactive power. There is a limited amount of increased curtailed energy during peak production only.

The lower part of Fig. 3.7 plots the total produced power for both fair and unfair curtailment when reactive power injection or absorption by the PV generation is not permitted. Without reactive power control, the active power curtailment has to be increased to comply with the voltage limits. Fair active power curtailment will then result in a significant reduction of the produced power. This emphasizes the need for reactive power support by PV panels when the goal is to produce a maximum amount of renewable energy without violating voltage limitations. The individual, average daily active power curtailment for each PV unit is shown in Fig. 3.8. In case of unfair curtailment, only a handful of customers is curtailing power. Especially the customers connected at the end of the feeder to phase U will have the disadvantage of increased curtailment. The extra cost of fair curtailment will be significantly higher without reactive power control. This cost depends on the compensation the DSO will pay to the owners of the PV panels due to the reduction of generated energy and the cost of grid losses. An economic analysis is outside the scope of this text.

3.6 Conclusions

This chapter describes a combination of a central and local control method for voltage control by PV inverters in unbalanced distribution grids. It was shown that in unbalanced, three-phase, four-wire grids the neutral point shifting

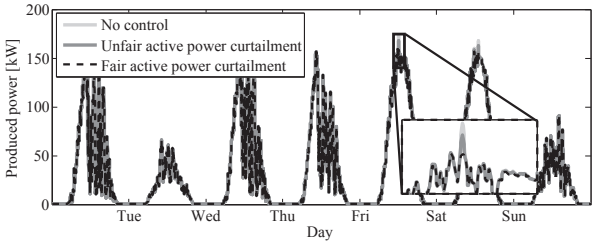

(a) With reactive power control

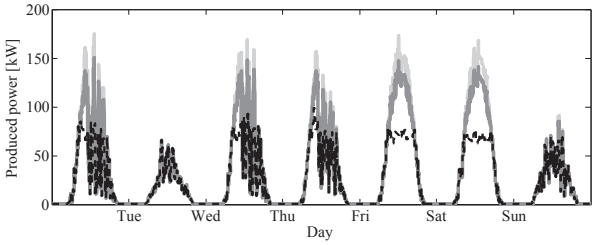

(b) Without reactive power control

Figure 3.7: Total produced power for fair and unfair active power curtailment with and without reactive voltage control.

effect requires special care for active and reactive power control. The reactive and curtailed active power controlled by the PV inverters are a function of the produced PV power and are defined by a first-order spline. The parameters of all the splines are regularly retuned by a central convex optimization program, i.e. every 15 minutes. This way, the local controllers can respond quickly to changing conditions, while a central optimization of the local parameters guarantees a near-optimal use of the reactive power and a minimum amount of curtailed active power.

Simulations show that the proposed control ensures that the voltage complies with the limits, while it results in less losses than the local control methods. It curtails less active power than local control methods that curtail active power and is able to curtail active power in a fair way.

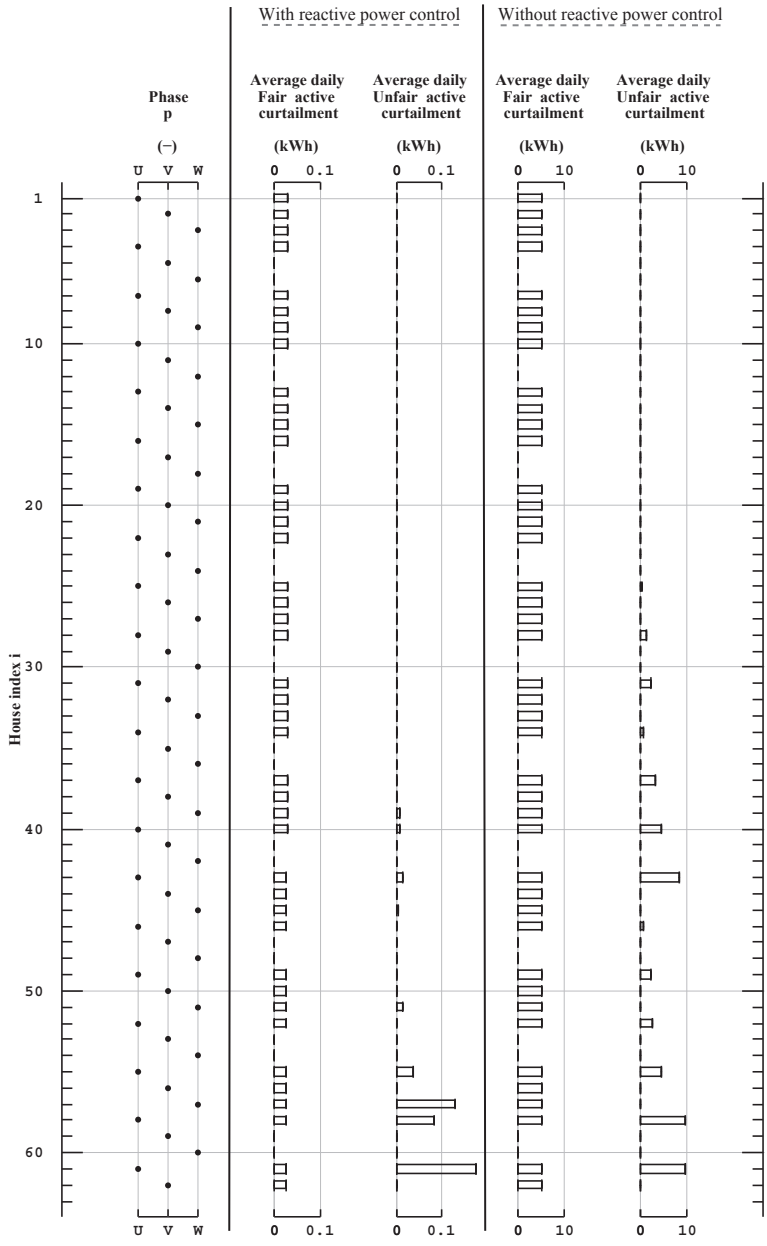

Figure 3.8: Individual, average, daily curtailed active power of each household for fair and unfair active power curtailment, with and without reactive voltage control.

Chapter 4

Load Balancing with EV Chargers and PV Inverters

Load Balancing with EV chargers and PV inverters in Unbalanced Distribution Grids

Sam Weckx, Johan Driesen

Published in IEEE Transactions on Sustainable Energy, vol.6, no.2, pp.635-643, April 2015

4.1 Introduction

A high penetration of distributed photovoltaic generators (PV) and electric vehicles (EVs) may lead to power quality problems in low voltage (LV) distribution networks. European LV distribution networks are often of the three-phase four-wire type. Both PVs and EVs are often not equally spread across the three phases of the distribution network, which will increase the load unbalance [13, 15, 99–101]. An unbalanced operation of the network will result in a serious increase in the system losses, voltage problems and voltage

The first author is the main author of the article. The contributions of the first author include the literature study, the development of the model and the analysis of the simulation results.

unbalance. Furthermore, an unbalanced network can host less PV generation before the critical voltage limit is reached. PVs can extend the transformer life [102], but a high amount of EVs will decrease it.

Different approaches are proposed to balance the load in the three phases. A first solution for the Distribution System Operator (DSO) is manually switching the phase to improve the distribution of the load across the three phases [103]. This can become very costly and the more switching actions, the higher the cost for the DSO. An alternative is dynamically-switching residential load from one phase to another [11, 104]. This requires the use of static transfer switches. In [105], a droop control for negative-sequence currents is proposed. [106] develops a control scheme for a three-phase, four-wire inverter to deliver negative-sequence currents, based on measurements of the negative-sequence voltage. Another approach is applied in [107], where the inverter has a resistive behaviour towards the zero-sequence and negative-sequence component of the node voltage. Most of the work described in the literature is focused on the control schemes of inverters capable of providing negative- and zero-sequence currents [108–110]. This work is focussed on the effect that optimally controlling these balancing inverters has on the network.

Many central and local control strategies have been described in literature, where EVs [111–118] or PVs [22, 50, 119–121] are controlled to improve the power quality in distribution grids. Types of control are reactive power compensation, active power curtailment, disconnecting PV, and coordinated charging of EVs. Reactive power compensation can require additional inverter capacity [122] and might increase grid losses. Active power curtailment of PV panels will result in a lower amount of energy produced and a lower revenue for their owners. EV charging power curtailment can reduce the voltage drop caused by the charging of EVs, but can lead to an unwanted extension of the charging time [123]. Disconnecting PV units, in case of a voltage violation, can lead to a cascade of disconnections [124]. In [43, 125], a battery energy storage system is controlled to limit the voltage deviations caused by PV production. Some of these methods are applied to unbalanced, three-phase, four-wire grids, but none of these control strategies consider the possibility to transfer power from one phase to another by means of an EV charger or PV inverter.

By replacing classical, single-phase, or three-phase PV units by three-phase, balancing PV units that are able to inject more power in one phase than in the other phases, the total power can be more equally spread across the three phases. The majority of houses have a single-phase power supply, but larger houses may have three-phase connections [11, 126]. In the houses with a three-phase connection, a balancing charger or inverter can be installed. Solar cells rarely produce maximal power and, therefore, it is often possible to inject the majority of the generated power into the phase with the highest power consumption,

without overloading of the inverter. Similarly, EVs are only charged for a limited time during the day, so an off-board charger capable of balancing the network can be used extensively for this purpose. In this work, a charger, or inverter, with six inverter legs is used as an alternative to standard three-phase units for the connection of three-phase PV or EV units to the distribution network. This inverter can be interpreted as three single-phase inverters with a common DC-bus. Special care is required for the DC-bus voltage control [106]. Units with a rating of more than 5 kVA may not be connected to one single phase[127]. The use of three, separate single-phase inverters is often already more interesting for PV units than the use of one, three-phase inverter, due to disconnection regulations [127]. If the voltage rises above a certain threshold, typically +10%, the inverter has to disconnect. If three separate single-phase inverters are used, only the inverter connected to the overloaded phase has to disconnect. This results in lower amounts of curtailed energy. The higher possible charging power can make the three-phase charger interesting for an EV owner.

The inverters and chargers will be controlled to balance the load in the three phases. By transferring power from highly loaded to less loaded phases, system conditions will be improved. A simplified representation of the working of a balancing inverter during the day and the night is presented in Fig. 4.1. The width of the arrows represents the amount of active power flowing through the connection. In previous work, we introduced this concept for three-phase PV inverters [128].

PV inverters will mainly improve the grid conditions in the evening. In the evening, when no PV power is generated and high peak loads occur, full inverter capacity can be used to balance the grid. Power extracted from a phase with a low consumption can be injected into a phase with a high consumption. On the other hand, balancing off-board EV chargers will improve the grid conditions, mainly during the day, as the EV will often be absent during this time. Therefore, both types of balancing are complementary.

Our first contribution is the adaptation of a coordinated charging formulation for EVs that includes the possibility to balance the grid with EV chargers. Secondly, balancing PV inverters are added in this formulation. Several load-flow simulations with realistic data show a significant improvement of the network conditions. Finally a local control approach is proposed. This avoids the need to have a real-time communication channel.

This paper is structured as follows: the distribution grid used in the simulation results is described in Section 4.2. In Section 4.3, a coordinated charging problem of EVs with grid balancers is presented. Finally, the local control rule is described in Section 4.4.

4.2 Simulated Network

The network used in the simulations is the same, existing, three-phase, four-wire, radial distribution system that was already presented in Fig. 2.1. 62 statistically representative residential load profiles were available to perform load-flow simulations. A constant power load model was assumed. Generation of these load profiles is described in [73]. In [73], the privacy problem of data provided by electrical companies is bypassed by transforming a large dataset of residential load profiles into a model that is able to create a set of synthetic, non-aggregated load profiles. This model was trained based on a large database of measured residential load profiles provided by the DSOs in Flanders. Reactive power consumption data was not available and, therefore, all loads are assumed to have a $cos(\phi)$ equal to 0.95. Load profiles were assigned randomly to households. Every house is equipped with a PV generator. The average power rating of PV units connected to phase U and V equals 2.2 kW, while PV units connected to phase W have an average rating of 3.3 kW. The PV profile was measured at a fixed rooftop PV installation at KU Leuven. The PV profile was scaled to the inverter size. All PV panels are assumed to have equal orientation. As the geographical area was small, the power output of all PV installations relative to their rated capacity was considered to be equal. Nodes 40 and 62 are equipped with a three-phase, balancing inverter. The rated capacity of the three-phase PV installations is 6 kW. To transfer power from one phase to another, or to inject all of the power into only one phase, the balancing inverter should be able to control the zero-sequence current. Standard inverters with three inverter legs are unable to control the zero-sequence current. To control the zero-sequence current a fourth inverter leg can be added. Alternatively, three separate inverters with a common DC-bus can be used.

Each household with an odd number has an EV. The maximum charging power equals 3.3 kW. Households 51 and 57 have an off-board, three-phase charger with a maximum charging power of 6.6 kW. The EV driving behavior is based

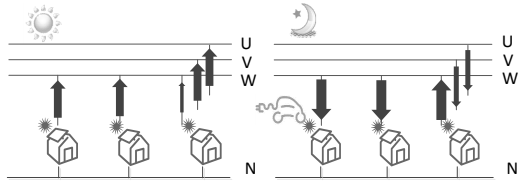

Figure 4.1: Simplified representation of the working of the balancing inverter during the day and the night. At night power is extracted from phase U and V and is injected into the highly loaded phase W.

on a statistical availability model [129]. This model uses statistical data on Flemish transportation behavior to create a realistic driving pattern for each vehicle. The voltage at the primary side of the transformer was assumed to be constant and equal to 1 pu. The nominal line-to-neutral voltage is 230 V. Distribution grid conditions are calculated with a backward-forward sweep algorithm [61] and a time resolution of 15 minutes.

4.3 Coordinated Charging of EVs with Load Balancing by PV Inverters and EV Chargers

A popular, coordinated charging scheme for EVs is the minimization of load variance, also called valley filling [130–133]. The minimization of the load variance leads to low system losses and generally avoids the violation of the lower voltage limitations [130]. It is an easy to solve, convex optimization problem [76].

This work is focussed on three-phase, four-wire networks. These networks require special care when minimizing the load variance. If the variance of the sum of all phases would be minimized, load peaks might still exist on each phase separately. This can result in severe voltage drops in the phase with the highest loading and will increase the system losses. It is, therefore, recommended to minimize the sum of the load variances of each phase, which will result in a more equal loading of the three phases. The following, three-phase formulation is preferred:

$$\begin{aligned}
\min_{P^{\mathrm{EV}}} \quad & \sum_{t=1}^{T} \sum_{i\in\{U,V,W\}} \left(\sum_{h=1}^{N} \left(P_{h,i,t}^{\mathrm{load}} + P_{h,i,t}^{\mathrm{PV}} + P_{h,i,t}^{\mathrm{EV}} \right) \right)^2 \\
\text{subject to} \quad & C_{h,t+1} = C_{h,t} + \psi_h \sum_{i\in\{U,V,W\}} P_{h,i,t}^{\mathrm{EV}} \Delta t \\
& 0 \leq C_{h,t} \leq C_h^{\max} \\
& C_{h,t^{\mathrm{departure}}} = C_h^{\max}
\end{aligned} \tag{4.1}$$

Where

- $P_{h,i,t}^{\mathrm{load}}$ is the consumed power, excluding the EV, by the household connected at node h to phase i at time step t;

- $P^{\text{PV}}_{h,i,t}$ is the generated power of the PV unit connected at node h to phase i at time step t;
- $P^{\text{EV}}_{h,i,t}$ is the charging power of the EV connected at node h to phase i at time step t;
- $C_{h,t}$ is the stored energy in the EV connected at node h at time step t;
- $C^{\max}_{h}$ is the maximal stored energy of the EV connected at node h ;
- ψ_h is the charging efficiency of the EV connected at node h ;

For single-phase EV chargers energy can only be extracted from the phase of connection k:

$$\begin{aligned} &\textbf{if } i = k \\ &0 \leq P^{\text{EV}}_{h,i,t} \leq P^{\text{EV,max}}_{h} \\ &\textbf{else} \\ &P^{\text{EV}}_{h,i,t} = 0 \end{aligned} \tag{4.2}$$

where $P^{\text{EV,max}}_{h}$ is the maximal charging power of the EV connected at node h. In case of a three-phase EV charger capable of balancing the network, the energy can be extracted from each phase. The net energy exchange is constrained to be positive, but the power exchanged with one of the phases can be negative:

$$0 \leq \sum_{i \in \{U,V,W\}} P^{\text{EV}}_{h,i,t} \leq P^{\text{EV,max}}_{h} \tag{4.3}$$

Besides that, the limits of the three single-phase inverters, out of which the balancing off-board charger consists, need to be respected:

$$-\frac{P^{\text{EV,max}}_{h}}{3} \leq P^{\text{EV}}_{h,i,t} \leq \frac{P^{\text{EV,max}}_{h}}{3} \tag{4.4}$$

It is assumed that the three single-phase inverters all have an identical rating of $\frac{1}{3}$ of the total charger rating $P^{\text{EV,max}}_{h}$.

In a classic coordinated charging algorithm, the off-board three-phase charger is unable to balance the network and the charging power in each phase needs to be equal:

$$P^{\text{EV}}_{h,U,t} = P^{\text{EV}}_{h,V,t} = P^{\text{EV}}_{h,W,t} \tag{4.5}$$

Typically, the PV production is an uncontrollable variable. The power injected in the network for a single-phase PV panel is, therefore, fixed. In case of a

three-phase inverter capable of balancing, the power injected in each phase becomes a variable that can be controlled in an optimization problem (4.1). The sum of the power injected in each phase should then equal the total power production and the limitations of the three single-phase inverters, out of which the balancing three-phase inverter is composed, need to be respected:

$$\begin{aligned} \sum_{i \in \{U,V,W\}} P_{h,i,t}^{\mathrm{PV}} &= P_{h,t}^{\mathrm{PV}} \\ -\frac{P_h^{\mathrm{PV,max}}}{3} \leq P_{h,i,t}^{\mathrm{PV}} &\leq \frac{P_h^{\mathrm{PV,max}}}{3} \end{aligned} \tag{4.6}$$

where $P_{h,t}^{\mathrm{PV}}$ is the total, produced power by the PV panel at time step t and $P_h^{\mathrm{PV,max}}$ is the rating of the balancing three-phase inverter connected at node h. Note that at night, when P_h^{PV} equals zero, the full inverter rating can be used to balance the grid.

The strict majority of the time, the off-board EV charger will be able to balance the grid, as the maximum charging capacity will rarely be used to meet the required amount of energy by the time of departure of the EV owner. This depends on the driving pattern of the EV owner.

The full capacity of each of the single-phase inverters of a balancing PV inverter will only be used when the solar irradiation is optimal. This occurs for only a fraction of the year, so, the majority of the time, the PV inverter can balance the grid.

Optimization problem (4.1), with additional constraints (4.2-4.6), is an easy to solve quadratic program [76]. By solving this problem the charging profiles for all EVs are defined, as well as the set points of the balancing chargers and inverters. In this work, CPLEX [134] is applied to solve this problem.

An equal loading of the three phases is beneficial for the voltages in the network. When power is transferred from the highest loaded phase, to the one with the lowest loading, the voltage drop in this phase will reduce. A special effect, called neutral point shifting [12,14], occurs in three-phase, four-wire distribution grids. When power is consumed in one phase, it will result in a voltage drop in this phase, but in a voltage increase in the two other phases. Therefore, the increased power consumption in the phase with the lowest loading will lead to a further improvement of the voltage of the phase with the highest loading. Balanced networks are, therefore, able to host significantly more PV and EVs.

In this work, reactive power compensation is not considered. It can require additional inverter capacity [122] and might increase grid losses. Therefore, the proposed control will try to use the full inverter and charger capacity for

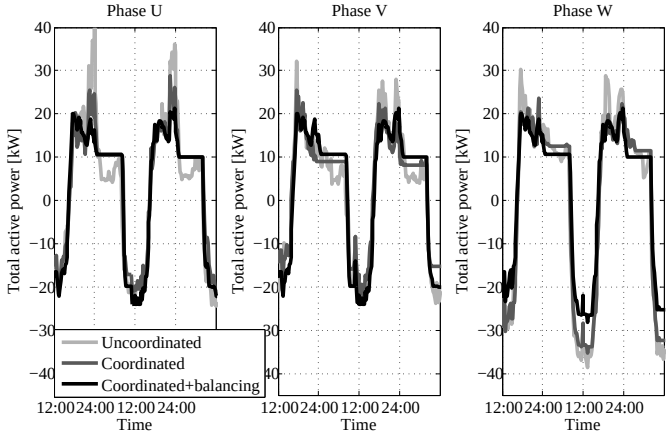

Figure 4.2: Total active power in each phase in case of classic coordinated charging and coordinated charging with balancers

balancing the active power consumption in each of the phases of the three-phase, four-wire distribution network.

The coordinated charging problem is tested on the network discussed in Section 4.2. Fig. 4.2 shows the total, active power in each of the three phases $\left(\sum_{h=1}^{N}\left(P_{h,i,t}^{\text{load}}+P_{h,i,t}^{\text{PV}}+P_{h,i,t}^{\text{EV}}\right)\right)$, for a period of two days, during the summer. A negative value indicates a reverse power flow, which occurs when there is a higher PV production than consumption in this phase. When there is more consumption than production, the total, active power in a phase will be positive. Compared to the case of uncoordinated charging, the load peaks are diminished. However, due to the typical mismatch between PV production and the energy required by the EVs, the classic coordinated charging can only slightly reduce the maximum reverse power flow in phase W in case of a high PV production. When the extra flexibility is added by the two three-phase balancing EV chargers and the two three-phase balancing PV inverters, the reverse power flow in phase W can be diminished by balancing the three phases. This will result in a higher reverse power flow in phase U and V. The more equal division of the load will reduce the system losses and the voltage rise in phase W. This figure also shows that a manual redistribution across the three phases would not be a suitable solution. The highest reverse power flow occurs in phase W, however reconnecting some of these customers to phase U or V would increase the load peaks in the evening in these phases. The consumption in the evening is already higher in phase U and V than in phase W.

In a second simulation, one summer month is evaluated. Fig. 4.3 presents the voltages in each node for the simulated period. In this figure a modified box plot [94] is applied. An additional box, spanning the 5th to 95th percentiles, is added to the standard box plot. As expected, the classic coordinated charging avoids a violation of the lower voltage limit. However, it fails to avoid excessive high voltages that occur during time periods of high PV production, due to the mismatch between PV production and the energy required by the EVs. When the two three-phase EV chargers and the two three-phase PV inverters can balance the network, the coordinated charging can avoid these excessive voltages.

There are many practical concerns when implementing a coordinated charging strategy. For example, in many EV charging algorithms [118, 130, 131, 133, 135], the arrival time and charging demand of each EV was assumed to be known in advance, before the arrival of the EV. Besides that, perfect predictions of the household load and PV production are assumed to be available by most algorithms. However, in reality, estimates of these parameters will have to be used. In [135], a coordinated charging strategy was extended to cope with this problem. Another disadvantage of the coordinated charging algorithm is the need for a real-time communication channel and the high computational power. Privacy barriers and technical constraints can make this gathering of information unrealistic. Privacy sensitive information, such as the departure time, is preferably not communicated to a central instance. Communicating privacy-sensitive information can be avoided by applying distributed algorithms [133, 136]. However, these methods still rely on real-time communication. In this work, it was assumed that the coordinated charging algorithm had perfect predictions in the previous simulations concerning EV behavior, load profiles and PV production. Therefore, the results of the simulations are a benchmark solution that indicates what is maximally possible with the balancing inverters.

4.4 Local Charging of EVs with Load Balancing by PV Inverters and EV Chargers

The need for a communication infrastructure and the high computational burden are serious disadvantages of the coordinated charging strategy. Therefore, a simple and purely-local control approach is implemented, which does not rely on any form of communication or load predictions. The application of the local control of the EVs and PV panels will, however, lead to a sub-optimal solution which will be compared with the benchmark of the coordinated charging algorithm.

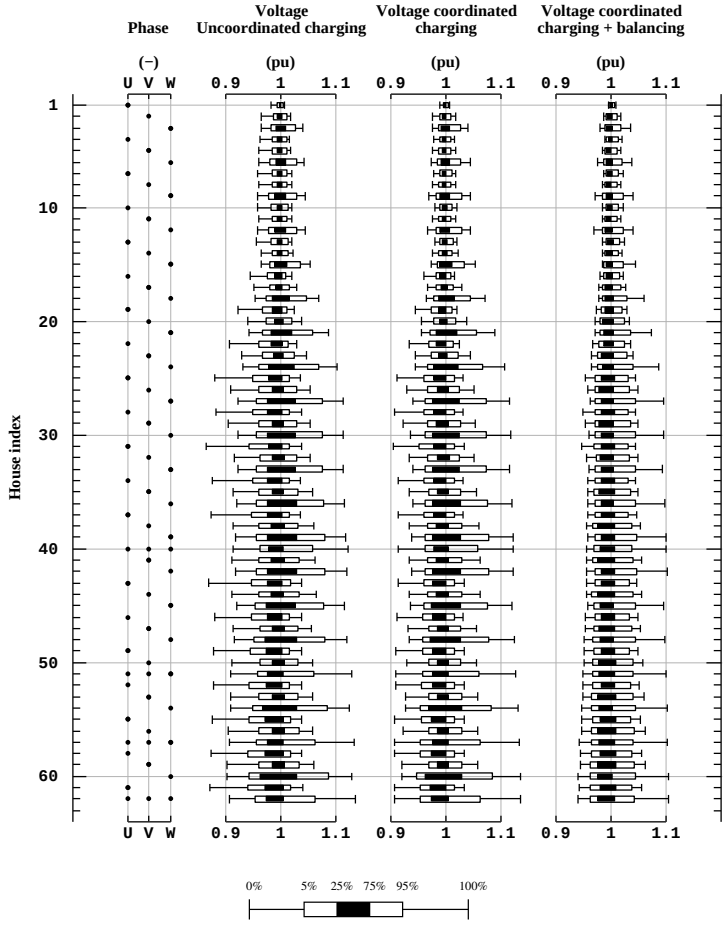

Figure 4.3: Modified boxplot of the node voltages for centralized charging strategies

4.4.1 Local Control of a Balancing EV Charger

For the local control of each off-board, balancing EV charger, only the absolute values of the local voltage measurements are used. No information about the grid is needed. Phases with a lower voltage have a higher active power consumption, due to the voltage drop over the mainly resistive distribution cables. Therefore, it is interesting to absorb more power out of the phases with the highest voltage. This is translated in the following droop relationship:

$$\begin{aligned}(P_U - P_V) &= \eta\,(|V_U| - |V_V|)\\ (P_U - P_W) &= \eta\,(|V_U| - |V_W|)\\ (P_V - P_W) &= \eta\,(|V_V| - |V_W|)\\ (P_U + P_V + P_W) &= P^{\mathrm{EV}}\end{aligned} \tag{4.7}$$

Where

- $|V_U|$ is the absolute value of the voltage of phase U;
- $|V_V|$ is the absolute value of the voltage of phase V;
- $|V_W|$ is the absolute value of the voltage of phase W;
- η is a parameter controlling the inter-phase power delivery $\left[\frac{W}{V}\right]$;

If the magnitude of the voltage in one phase is higher than in another phase, the power difference between the phases is equal to the voltage difference between the phases, multiplied by the constant η. For example, a constant η of $100\frac{W}{V}$ will result in a power difference between the two phases of $100W$ per Volt. This makes inter-phase balancing possible. η can, therefore, be interpreted as a three-phase droop constant. It is a tuning parameter of the local controller. Simulations can be made to evaluate the performance for different values of η [128].

The charging power set point of an EV, P^{EV}, is equal to the minimum power that is needed to fully charge the EV battery during the time before departure. It is defined by dividing the required amount of energy by the available time period. This type of charging will be called EV-based peak-shaving. This simple method of charging improves grid conditions significantly, compared to uncoordinated charging [123].

Eq. (4.7) can be rewritten as:

$$
\begin{aligned}
P_U &= \frac{P^{\mathrm{EV}} + \eta\left(|V_U| - |V_V|\right) + \eta\left(|V_U| - |V_W|\right)}{3} \\
P_V &= P_U - \eta\left(|V_U| - |V_V|\right) \\
P_W &= P_U - \eta\left(|V_U| - |V_W|\right)
\end{aligned}
\tag{4.8}
$$

These formulations do not take into account the constraints of the inverter. Each of the single-phase inverters has a maximum power throughput of $\frac{P_n^{\mathrm{EV,max}}}{3}$, which defines a feasible set for the powers of each inverter. To comply with these constraints, the powers obtained by equation (4.8) are projected on the feasible set:

$$
\min_{P^*} \|P^*_{U,V,W} - P_{U,V,W}\|_2^2 \tag{4.9}
$$

subject to

$$
-\frac{P_h^{\mathrm{EV,max}}}{3} \leq P^*_{U,V,W} \leq \frac{P_h^{\mathrm{EV,max}}}{3}
$$

$$
(P^*_U + P^*_V + P^*_W) = P^{\mathrm{EV}}
$$

Where

- $P_{U,V,W}$ is a vector containing the solution obtained by (4.8)
- $P^*_{U,V,W}$ is the projection on the feasible set. The three obtained values are the setpoints for the power injection/absorption in each phase.

The first constraint guarantees that the nominal power of each of the three single-phase chargers is not exceeded and the second ensures that the total power exchanged with the grid is equal to the power requested by the EV chargers. If the operating point obtained by (4.8) was already part of the feasible set, then (4.9) does not change the operating point.

Fig. 4.4 illustrates the operation of the local controller during a partly-cloudy day in spring. It depicts the power in each of the three phases of the charger, in this case allocated in node 57, as well as the voltage in node 57 for a η equal to $250\frac{W}{V}$.The sum of the powers in each phase is always equal to the EV charging power. As previously discussed, the charging power is defined as the minimum power that is needed to get the EV battery fully charged during the time before departure. When the EV is absent, the sum of the powers equals zero. The

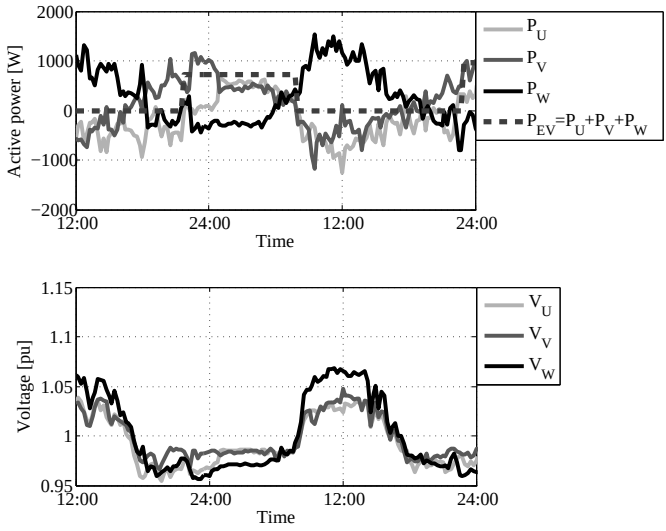

Figure 4.4: Power of the balancing EV charger as a function of the grid voltage in node 57.

charger tries to balance the grid. It is clear from this figure that, during the day, when there is a higher voltage in phase W, due to a higher PV production in this phase, power is consumed in phase W by the charger, while it injects this power back into the other phases. When the EV needs to charge, the majority of the energy is extracted from the phase with the highest voltage.

4.4.2 Local Control of a Balancing PV Inverter

The local control of the balancing PV inverters is similar to the control of the EV chargers (4.7). The sum of the power exchanges in each phase with the network equals the total produced power P^{PV}:

$$\begin{aligned}(P_U - P_V) &= \eta\,(|V_U| - |V_V|)\\ (P_U - P_W) &= \eta\,(|V_U| - |V_W|)\\ (P_V - P_W) &= \eta\,(|V_V| - |V_W|)\\ (P_U + P_V + P_W) &= P^{\mathrm{PV}}\end{aligned} \tag{4.10}$$

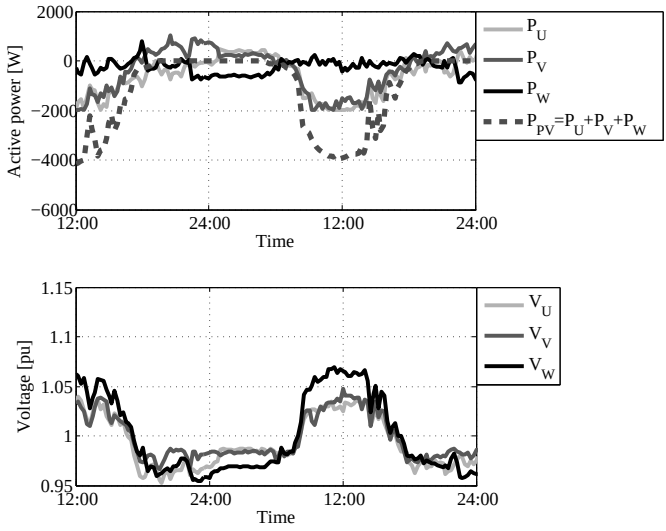

Figure 4.5: Power of the balancing PV inverter as a function of the grid voltage in node 62.

The local control rule of the PV is obtained as in (4.8). If there are regulation limits for the difference in power levels injected between the phases [127], then such requirements can be added to optimization problem (4.9).

Fig. 4.5 illustrates the operation of the local controller for a balancing PV inverter in node 62. As can be seen, the majority of the produced power during the day will be injected in phases U and V. The voltage in these phases indicates a smaller, reverse power-flow in these phases. At night, power is injected into phase W, which has the lowest voltage. The lower voltage in phase W indicates a higher consumption in this phase. Since the power production by the PV panel is zero at night, the power injected into phase W needs to be extracted from the two other phases. These cases are numerical examples of the working of the balancing inverter presented in Fig. 4.1.

The total active power in each of the three phases, for the same two days during summer of Fig. 4.2, are now shown for the EV-based peak shaving, with and without the balancing in Fig. 4.6. A negative value indicates a reverse power flow. The η is chosen to be $250\frac{W}{V}$. When the two three-phase EV chargers and two PV inverters balance the grid, load peaks are diminished. This has positive effects on the grid voltage. Fig. 4.7 presents the voltages in each node, for the same simulated period as Fig. 4.3. Due to the balancing, the voltages

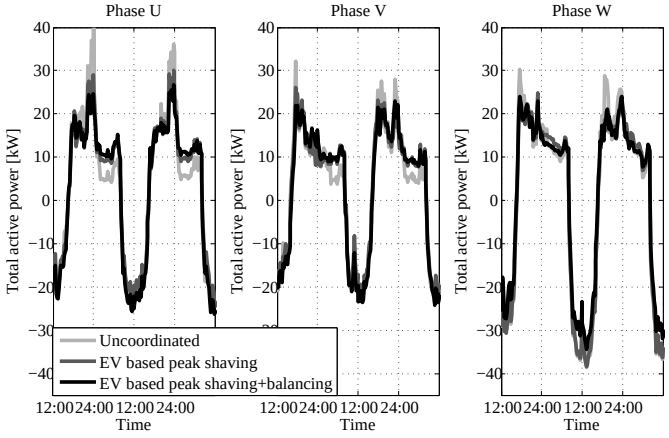

Figure 4.6: Total active power in each phase in case of EV based peak shaving and EV based peak shaving with balancers.

become closer to the nominal voltage. Moreover, when comparing Fig. 4.3 and Fig. 4.7, it is clear that a simple local control approach with two balancing chargers and two balancing inverters outperforms a classic, central coordinated charging strategy without the possibility to balance the grid.

Node 62 is an end node and is, therefore, more vulnerable to voltage problems and severe voltage unbalance. Fig. 4.8 compares the Voltage Unbalance Factor (VUF) occurring in this node for the different control strategies. According to the European standard, the VUF is defined as the magnitude of the ratio of the negative-sequence voltage to the positive-sequence voltage [137]. The Cumulative Distribution Function (CDF) of the VUF is presented for a simulated period of one summer month. The improvements with balancing are clear. Also, when there is no PV production or EV available, the balancers further improve the grid conditions, which explains the significant improvement. An increasing amount of EVs and PVs typically worsens the voltage unbalance [13], but, by promoting the installation of balancing chargers and inverters, the voltage unbalance will be improved, compared to the situation without EVs or PVs.

A final constraint that can limit a further integration of EVs and PV panels in the distribution grid are the transformer and line loading limits. The CDF of the maximum apparent power through the three phases of the transformer is plotted in Fig. 4.9. It is clear that, when the grid is equipped with balancers, the peak loading reduces. The installation of these balancers is, therefore, beneficial for the lifetime of the transformer.

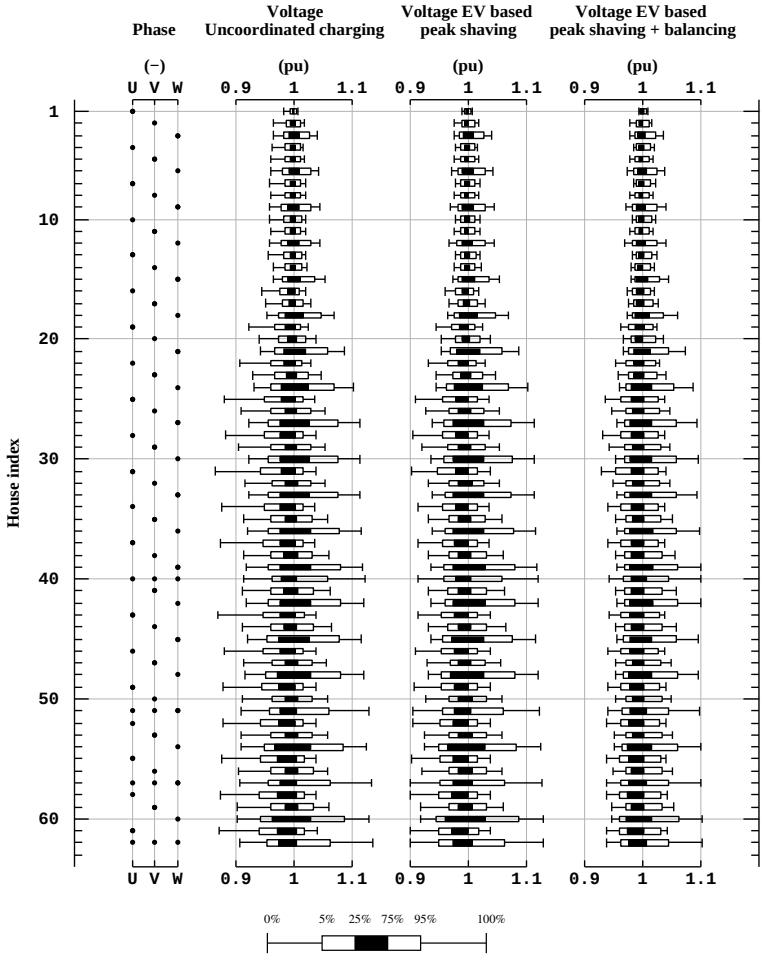

Figure 4.7: Modified boxplot of the node voltages for local charging strategies.

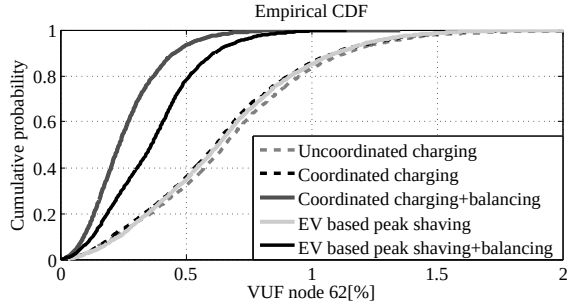

Figure 4.8: Cumulative distribution function of the voltage unbalance factor in node 62.

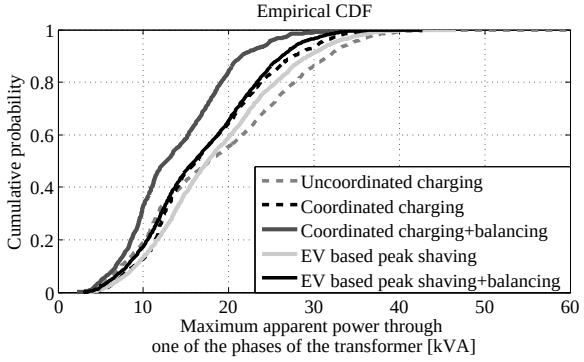

Figure 4.9: Cumulative distribution function of the maximum apparent power through one of the phases of the transformer.

The balanced grid operation is also beneficial for the grid losses, as these increase with the square of the line currents. Table 4.1 compares the possible reduction of grid losses, compared to uncoordinated charging. Again, the simple, local EV-based peak shaving with balancing chargers and inverters outperforms the classic coordinated charging problem without balancing.

The benefit of the proposed balancing strategy is, therefore, that it has a positive effect on both component loading, voltage unbalance, grid voltages and grid losses. Other control strategies often fail to improve all of these indicators. I.e. reactive power control by PV inverters can significantly improve the grid voltages, but might increase the component loading and the grid losses [50, 82].

The location of the inverters balancing the grid influences the effectiveness of

Table 4.1: Reduction of grid losses compared to uncoordinated charging. The average daily system losses in case of uncoordinated charging were equal to 32.91 kWh.

Charging strategy	Reduction [%]
Classic coordinated charging	16
Coordinated charging + balancing	28
EV based peak shaving	7
EV based peak shaving + balancing	19

the proposed method. Grid unbalance is always more severe at the end of the feeder [13]. Therefore, the further the balancing inverter is located from the substation, the higher the expected improvement. Further research involves the optimal placement of balancing inverters and the development of a prototype. Besides that a compensation method will have to be developed to reimburse the customers that install a balancing inverter or charger for the increased cost of the installation.

4.5 Conclusion

The grid impact of the increasing amount of EV charging and PV production can be substantially reduced if they would be able to balance the grid. Both off-board, three-phase EV chargers and three-phase PV units can be adapted to balance a three-phase, four-wire distribution grid. Grid conditions will be improved by absorbing power from a phase with a lower loading and injecting this power into the phase with the highest loading. A centralized coordinated EV charging problem is adapted in this work to evaluate the effects of the extra flexibility added by these balancers. Several load-flow simulations with realistic data are performed and show a significant improvement of component loading, voltage unbalance, grid voltages and grid losses when some three-phase chargers and PV-units are adapted to balance the grid. Thanks to these units, more PVs and EVs could be connected to the distribution network, before critical limits are reached.

Even with a simple, local control rule, two off-board EV chargers and two PV inverters that are able to balance the grid, will improve the grid conditions more than a computationally and communicationally intensive, classic coordinated EV charging strategy. An affordable implementation of these types of balancers can, therefore, become a cost-effective option for DSOs to cope with the increasing amount of EVs and PV panels.

Chapter 5

Locational Pricing in Distribution Grids

Locational pricing to mitigate voltage problems caused by high PV penetration

Sam Weckx, Reinhilde D'hulst, Johan Driesen

Published in Energies 2015, Vol. 8, 4607-4628

5.1 Introduction

The electricity grid is going through a transition period. A high penetration of PV panels and the ongoing electrification of the transport system requires new strategies for the operation and management of the electricity grid. Typically, the high power injection of PV panels does not coincide with periods of high demand. The resulting, high, reverse power-flow can cause a significant rise in the grid voltage. The maximum amount of PV generation that can be connected to a Low Voltage (LV) network is typically limited by this voltage rise [22, 121]. In current regulations, a PV panel has to disconnect from the

The first author is the main author of the article. The contributions of the first author include the literature study, the development of the model and the analysis of the simulation results.

distribution grid as soon as the maximum voltage is reached. However, this can lead to unnecessary curtailed green energy to keep the voltage within limits. Traditionally, Distribution System Operators (DSOs) are responsible for keeping the grid voltage within limits, and, today, more advanced methods may be needed to control the grid voltage.

Different control strategies have been proposed to control the grid voltage and avoid damage to the grid. A first method consists of PV panels that curtail part of the active power to reduce the voltage [22, 121]. Another option is to use the remaining inverter capacity of a PV panel to do reactive voltage control [25, 138]. Furthermore, flexible loads, like electric vehicles, can increase or decrease their consumption to regulate the grid voltage [112]. All of these methods are effective in managing the grid voltage, but do not give a real-time incentive to the customers to control the voltage. Also, these strategies should be combined to achieve optimal grid voltage control and the most cost effective option should be chosen to comply with the voltage limits.

Real-time pricing is a well-known demand response technique. When real-time pricing is applied, electricity consumers are charged with prices that can vary over short time intervals. This can thus be used to encourage the desired energy consumption behavior among users and to keep the total consumption level below the power generation capacity [139]. It is an incentive that is offered by the grid operator[140, 141]. In this work, a real-time pricing strategy is used to control the grid voltage. The distribution system operator can adapt the real-time energy price to keep the voltage within limits. This price will give an incentive to inject or consume reactive power to control the voltage, or, if necessary, to curtail active power, or adapt the consumption of the flexible load. The most cost-effective solution will be obtained. The prices are defined by a distributed gradient algorithm, based on a two-way communication system. The pricing is applied to unbalanced distribution networks, which requires special care, due to the neutral point shifting. In previous work, this pricing strategy was tested for active power only [54]. In this work, incentives will be given for reactive voltage control as well.

Finally, arbitrage will be analysed. Arbitrage is possible when the same asset, in this case energy, does not trade at the same price at different locations. PV generation is not necessarily spread equally across the three phases. This can lead to higher voltages in the phase with the highest power production [142] and, therefore, a lower price for energy that is injected into this phase. When there is a price difference for the energy in the three different phases, at the same location, power can be transferred from the phase with the lowest price to the phase with the highest price. This can be done with adapted PV inverters. PV inverters rarely operate at their maximal power production. If a three-phase PV inverter consists of three single-phase inverters with a common DC-bus, it

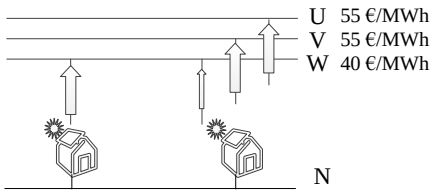

Figure 5.1: Representation of the arbitrage by a balancing PV inverter. When the price is higher in phase U and V than in phase W, more power will be injected into these phases. The width of the arrows represents the amount of active power flowing through the connection.

is possible for the majority of the produced power to be injected into the phase with the highest power consumption, or to transfer power from highly loaded to less loaded phases, without overloading the PV inverter. This principle is illustrated in Fig. 5.1.

This chapter is structured as follows: in Section 5.2, the distribution grid used in the simulation results is described and special attention is given to effects in unbalanced grids, because these will have implications on the locational grid prices. Section 5.3 describes the system model that defines the optimal response of the flexible loads and PV units and Section 5.4 elaborates on the distributed pricing strategy that results in the same response as the optimization problem, which was defined in Section 5.3. Finally, Section 5.5 presents some results and shows how PV panels, flexible loads and three-phase PV inverters that perform arbitrage react to the locational prices.

5.2 Simulated Network

The network used in the simulations is the same existing three-phase, four-wire, radial distribution system that was already presented in Fig. 2.1. All households were assumed to have a single-phase connection, except households 41 and 62, which have a three-phase connection to the network. The households with a single-phase connection are spread equally across the three phases in the order U,V,W,U,V,W, etc... The voltage at the secondary side of the transformer is considered to be 230 V during no load. All households have a PV installation. The PV inverter rating of the households connected to phase U and V equals

2.2 kW, while the households connected to phase W have a rating of 3.3 kW. These assumptions will create unbalance in the network. The households with a three-phase connection have a three-phase PV installation with a rating of 6 kW.

A remarkable and important effect in three-phase, four-wire grids is the neutral point shifting [12]. When a single-phase load consumes active or reactive power, a current will flow through the neutral conductor. This results in a voltage drop over the impedance of the neutral conductor and the neutral voltage experienced by all customers will shift. As a consequence of the neutral shift, reactive power absorption in phase U significantly increases the phase voltage of phase W and decreases the phase voltage of phase V. To decrease the voltage in one phase, it can be more beneficial to inject reactive power into another phase than to absorb reactive power into this specific phase itself [50]. This is important for the locational pricing approach that will be developed. When voltage problems occur in one phase, the DSO should give an incentive to inject reactive power into another phase. Another consequence of the neutral shift is that consuming power in one phase, will decrease the voltage in this phase, whereas the voltage in the other two phases will slightly increase.

Voltage limits are the major concern when integrating distributed generation in distribution networks. Like in DC power-flow models [142], AC models can be approximated with a linear model to describe the influence of PV panels and flexible loads on the voltage magnitude [41, 49, 94]. The voltage at a node m can be approximated by:

$$|V_h| \approx |V_h^{\text{base}}| + \sum_{\tilde{h}=1}^{N} \left(\mu^P_{h,\tilde{h},i} P_{\tilde{h},i} + \mu^Q_{h,\tilde{h},i} Q_{\tilde{h},i} \right) \tag{5.1}$$

where

- $\mu^P_{h,\tilde{h},i}$ is the sensitivity of the voltage magnitude in node h by active power injected at node $\tilde{h}$ into phase i;
- $P_{\tilde{h},i}$ is the active power injected or consumed at node $\tilde{h}$ into/from phase i by a PV panel or a flexible load;
- $\mu^Q_{h,\tilde{h},i}$ is the sensitivity of the voltage magnitude in node h by reactive power injected at node $\tilde{h}$ into phase i;
- $Q_{\tilde{h},i}$ is the reactive power injected at node $\tilde{h}$ into phase i by a PV panel;
- V_h^{base} is the voltage at node h due to the uncontrollable load of the households;

- V_h is the expected voltage at node h;
- N is the number of nodes;

The voltages are limited between a minimum and a maximum voltage:

$$V^{\min} \leq |V_h| \leq V^{\max} \tag{5.2}$$

where $V^{\min}$ and $V^{\max}$ are the minimum and maximum allowed voltages. In this work, $V^{\min}$ and $V^{\max}$ are chosen to be $\pm$ 10% of the nominal voltage of 230 V. The voltages of control points at the end of the feeders have to be monitored and controlled, as these are subject to the largest voltage deviations. These voltages are measured and communicated to the DSO. In this work, nodes 44 and 62 are these controlled nodes.

Using the linear voltage model described in (5.1) has various advantages. First of all, the DSO does not need to know the actual uncontrollable load of the households to approximate the voltage caused by the uncontrollable load alone. Since this could contain privacy sensitive information, the customers preferably do not share this information with a central instance [140]. If the DSO knows the consumption of the PV panels and of the flexible loads during the voltage measurement, he can calculate the effect these had on the voltage measurement with the voltage sensitivity factors. With this information, he can then obtain the voltage caused by only the uncontrollable base load V_h^{base}, without having information on the uncontrollable household consumption.

A second advantage is that the voltage constraints (5.1) and (5.2) remain an easy to handle, convex set. Another advantage is that these sensitivity factors can be approximated based on historic smart meter data, without having information about the exact grid topology [143].

In real-life conditions, the uncontrollable load can vary. The obtained V_h^{base} is, therefore, an estimate of the voltage, caused by only the uncontrollable base load, at the next time step. Furthermore, in the linear model, linearization errors should also be taken into account. It is, therefore, advised to include a small, extra conservative margin in the limits of (5.2). $V^{\min}$ and $V^{\max}$ can be chosen to be $\pm$ 9% of the nominal voltage, whereas the actual limits equal $\pm$ 10% of the nominal voltage. As could be seen in chapter 2 the linearization error remains in the order of 0.5%. The effect of sudden load variations can be easily analysed with the voltage sensitivity factors $\mu^P_{h,\tilde{h}}$. The voltage sensitivity factors $\mu^P_{h,\tilde{h}}$ express the change in voltage of node h in case of a load variation in node $\tilde{h}$. If information on typical load variations is available, the typical sudden voltage variations can be calculated and the conservative margin can be adapted. The typical load variations depend on the time step of the algorithm.

If the time step is larger, larger load variations can be expected. Note also that voltage limits are based on 10 minute mean RMS values. Therefore, if a voltage limit would be violated during one or two minutes, the conservative margin can be adapted to guarantee that the 10 minute mean RMS value remains below the limit. The preferred time step for an update of the network price will be one or two minutes. The price has to be regularly updated, because the PV power output will be variable. Note again that voltage limits are based on 10 minute mean RMS values, so this will provide sufficient time to correct for short periods of a voltage out of limits. Alternatively, the price update can be event-based. As long as the voltage remains close but below the voltage limits, there is no need for an update.

5.3 System Model

The purpose of the DSO is to keep the voltage within limits in an optimal way, without hindering the normal market operation. To do this, it will have to steer the consumption of flexible loads and single- and three-phase PV panels.

The flexible consumption is modelled by utility functions. The utility function reflects the customer satisfaction for the consumption of their flexible loads. The higher their satisfaction, the higher the price they are willing to pay for the requested energy. In this work, quadratic utility functions are considered, which are one of the most widely used utility functions [139, 144]:

$$U\left(P_{\tilde{h},i}^{\text{flex}}\right) = \omega_{\tilde{h}} P_{\tilde{h},i}^{\text{flex}} - \frac{\beta_{\tilde{h}}}{2}\left(P_{\tilde{h},i}^{\text{flex}}\right)^2 \quad \text{for} \quad 0 \leq P_{\tilde{h},i}^{\text{flex}} \leq P_{\tilde{h}}^{max} \tag{5.3}$$

Where

- $P_{\tilde{h},i}^{\text{flex}}$ is the flexible power consumption of the load connected to node $\tilde{h}$ at phase i;
- $\beta_{\tilde{h}}$ and $\omega_{\tilde{h}}$ are confidential parameters characterizing customer types;
- $P_{\tilde{h}}^{max}$ is the maximal consumption of the flexible load connected to node $\tilde{h}$;

For an announced price $\Lambda_{\tilde{h}}$, each customer determines the optimal $P_{\tilde{h},i}^{\text{flex}}$ from:

$$\min_{P_{\tilde{h},i}^{\text{flex}}} \quad -U\left(P_{\tilde{h},i}^{\text{flex}}\right) + \Lambda_{\tilde{h}} P_{\tilde{h},i}^{\text{flex}} \tag{5.4}$$

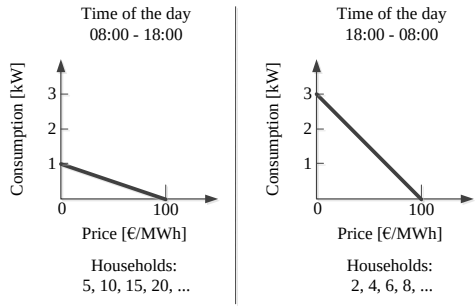

Figure 5.2: Response of the flexible loads on the electricity price for different moments of the day.

It can be proven that a quadratic utility function leads to a consumption $P_{\tilde{h},i}^{\text{flex}}$ that is linearly dependent on the electricity price [145]. Typically, the available flexibility depends on the time of the day. During the day, consumers are often absent and the available flexibility is small. In the evening, the amount of flexibility is higher. Therefore, the confidential parameters $\omega_{\tilde{h}}$ and $\beta_{\tilde{h}}$ are chosen such that a price of 0 €/MWh results in a consumption of 1 kW and a price of 100 €/MWh results in a consumption of 0 kW between 08:00 and 18:00 for all houses with a house number which is a multiple of five. The other houses are assumed to have no available flexibility at that moment. In the evening, the parameters are chosen as such that a price of 0 €/MWh results in a consumption of 3 kW and a price of 100 €/MWh results in a consumption of 0 kW for all houses with a number which is a multiple of 2. Fig. 5.2 gives a summary of the responsiveness of the loads at different moments. The price $\Lambda_{\tilde{h}}$ is the electricity price charged by the provider. This price consists of the generation cost, the taxes and the fixed network tariffs. Further on in this work, a variable network price will be added to control the grid voltage. The price $\Lambda_{\tilde{h}}$ can differ between providers. For the ease of simplicity, all of the households received the same price $\Lambda_{\tilde{h}}$ in this work. However, results can be generalized to a situation where all customers have a different electricity price $\Lambda_{\tilde{h}}$.

Single-phase PV units will always inject the produced power into their phase of connection. Part of the produced power can be curtailed to support the network, but the PV unit will never consume power. The remaining capacity of the PV inverter can be used to inject or absorb reactive power.

Three-phase PV installations inject power into each of the three phases. The three-phase PV inverter usually injects the same amount of active and reactive

power into each phase. However, when the three-phase inverter consists of three single-phase units with a common DC-bus, the unit can inject a different amount of active or reactive power into each phase. This type of inverter is referred to as a balancing inverter.

The DSO will try to optimally-steer the flexible loads and PV units to avoid voltage limit violations in the grid. If all of the information of the flexible loads and the PV panels could be centralized at one location, the DSO would solve the following problem:

$$\min_{P^{\text{flex}}_{\tilde{h},i}, P^{\text{PV,curt}}, Q^{\text{PV}}} \underbrace{\sum_{\tilde{h}\in\{\theta_{\textbf{flex}}\}} -U\left(P^{\text{flex}}_{\tilde{h},i}\right) + \Lambda_{\tilde{h}} P^{\text{flex}}_{\tilde{h},i}}_{\textbf{Flexible loads}} + \tag{5.5}$$

$$\underbrace{\sum_{\tilde{h}\in\{\theta_1\}} -\Lambda_{\tilde{h}}\left(P^{\text{PV}}_{\tilde{h},i} - P^{\text{PV,curt}}_{\tilde{h},i}\right) + \alpha\left(Q^{\text{PV}}_{\tilde{h},i}\right)^2}_{\textbf{Single-phase PV}} + \tag{5.6}$$

$$\underbrace{\sum_{\tilde{h}\in\{\theta_3\}} \sum_{i\in\{U,V,W\}} \left(-\Lambda_{\tilde{h}}\left(P^{\text{PV}}_{\tilde{h},i} - P^{\text{PV,curt}}_{\tilde{h},i}\right) + \alpha\left(Q^{\text{PV}}_{\tilde{h},i}\right)^2\right)}_{\textbf{Three-phase PV}} \tag{5.7}$$

subject to

$$P^{\text{PV}}_{\tilde{h},i} - P^{\text{PV,curt}}_{\tilde{h},i} \geq 0 \quad \tilde{h} \in \theta_1 \tag{5.8}$$

$$\sum_{i\in\{U,V,W\}} \left(P^{\text{PV}}_{\tilde{h},i} - P^{\text{PV,curt}}_{\tilde{h},i}\right) \geq 0 \quad \tilde{h} \in \theta_3 \tag{5.9}$$

$$\left(Q^{\text{PV}}_{\tilde{h},i}\right)^2 + \left(P^{\text{PV}}_{\tilde{h},i} - P^{\text{PV,curt}}_{\tilde{h},i}\right)^2 \leq S^2_{\tilde{h},i} \quad \tilde{h} \in \theta_1 \tag{5.10}$$

$$\left(Q^{\text{PV}}_{\tilde{h},i}\right)^2 + \left(P^{\text{PV}}_{\tilde{h},i} - P^{\text{PV,curt}}_{\tilde{h},i}\right)^2 \leq S^2_{\tilde{h},i} \quad \tilde{h} \in \theta_3 \tag{5.11}$$

$$V^{\min} \leq |V_h| \leq V^{\max} \quad h \in N_{contr} \tag{5.12}$$

$$|V_h| = |V_h^{\text{base}}| + \sum_{\tilde{h}=1}^{N} \left(\mu^P_{h,\tilde{h},i}\left(-P^{\text{PV}}_{\tilde{h},i} + P^{\text{PV,curt}}_{\tilde{h},i} + P^{\text{flex}}_{\tilde{h},i}\right)\right) + \sum_{\tilde{h}=1}^{N} \mu^Q_{h,\tilde{h},i} Q^{\text{PV}}_{\tilde{h},i} \tag{5.13}$$

Where

- $\theta_{\textbf{flex}}$ is the set of all customers with a flexible load unit;
- $\theta_{\textbf{1}}$ is the set of all customers with a single-phase PV unit;
- $\theta_{\textbf{3}}$ is the set of all customers with a three-phase PV unit;
- $P^{\text{PV}}_{\tilde{h},i} - P^{\text{PV,curt}}_{\tilde{h},i}$ is the net injected power into phase i of the PV panel connected at node $\tilde{h}$. For a single-phase PV unit $P^{\text{PV}}_{\tilde{h},i}$ is the total produced

power, for a three-phase unit $P^{\text{PV}}_{\tilde{h},i}$ is one third of the total produced power. Part of the produced power can be curtailed $P^{\text{PV,curt}}_{\tilde{h},i}$;

- $Q^{\text{PV}}_{\tilde{h},i}$ is the reactive power injected/absorbed by the PV panel connected at node $\tilde{h}$ into phase i;
- $S_{\tilde{h},i}$ is the inverter rating of the PV unit connected at node $\tilde{h}$ to phase i. For a three-phase unit $S_{\tilde{h},i}$ is one third of the total three-phase inverter rating;
- α is a parameter to penalize reactive power injection or absorption by a PV panel;

The objective function consists of three terms. The first term (5.5) maximizes the utility of the flexible loads. The second term (5.6) reflects the income of the single-phase PV units. The units get a price of $\Lambda_{\tilde{h}}$ for the injected power and have a decreased income when they have to curtail power. They can also provide reactive power, but this at a small cost characterised by the parameter α. This cost should account for increased losses due to reactive voltage control. α is chosen to be 1 €/$Mvar^2h$. The last term (5.7) of the objective function gives the income of the three-phase PV units. It consists of the income for injecting active power and a penalty for reactive voltage control.

A small penalty term is added to the objective function that penalizes the balancing inverter for injecting a different amount of active power into the three phases. This term ensures that when there are no voltage problems the same amount of power is injected in each phase. This term is small compared to the other terms and, for the ease of simplicity, this term is not presented in the objective function.

Constraint (5.8) ensures that a single-phase PV unit does not curtail more energy than the produced amount. Constraint (5.9) ensures the same for a three-phase PV unit. The amount of reactive power absorbed, or injected, by a single-phase PV unit is limited by constraint (5.10), while constraint (5.11) limits the reactive power by a three-phase unit. When the three-phase inverter does not consist of three single-phase units, the active and reactive power injection in each phase have to be equal. This can be implemented by adding the following constraints:

$$\begin{aligned} P^{\text{PV}}_{\tilde{h},U} &= P^{\text{PV}}_{\tilde{h},V} = P^{\text{PV}}_{\tilde{h},W} \\ Q^{\text{PV}}_{\tilde{h},U} &= Q^{\text{PV}}_{\tilde{h},V} = Q^{\text{PV}}_{\tilde{h},W} \end{aligned} \tag{5.14}$$

Constraint (5.12) guarantees that the voltage will stay within limits for all the control nodes N_{contr}.

The solution of this problem will optimally control the flexible loads and PV units. If no voltage problems occur, the PV panels will not curtail any energy, or provide reactive power. Also, the flexible loads will behave in their normal way as described by (5.4). If voltage problems occur, this will change.

Centralizing all information at one location to solve the DSO optimization problem might be complicated. Besides that, privacy sensitive information, like the utility function, is preferably not shared with a central instance. Therefore, there is a need to create a distributed pricing algorithm that, by means of network prices, results in the same, optimal solution, but that does not require all the information to be gathered at one place. This distributed algorithm will rely on duality theory. The DSO optimization problem can be reformulated as a decomposable dual problem and can be solved using a dual ascent method, with the same solution. Strong duality holds, because the primal problem is convex and a strictly feasible point will exist. Dual ascent methods rely on an iterative update of the Lagrange multiplier to obtain the same solution. These methods are also called Lagrange Dual Decomposition methods and are commonly applied in power systems [54, 139, 146]. Other distributed algorithms have been proposed to control the reactive power contribution of PV inverters [147], but these do not make use of a real-time pricing scheme.

The voltage in the network is controlled by constraint (5.12). The Lagrange multipliers Λ^{DSO} of constraint (5.12) have an economical interpretation. They equal the shadow price for creating voltage problems in the control node. This is a price per Volt. To find the price per unit of active or reactive power, one has to multiply this price per Volt by the influence of active or reactive power on the voltage magnitude:

$$\overbrace{\Lambda_h^{DSO}}^{\text{Price per Volt}} \xRightarrow[\text{active power}]{\text{Influence on the voltage of}} \overbrace{\Lambda_h^{DSO}\mu^P_{h,\tilde{h},i}}^{\text{Price per kWh}} \tag{5.15}$$

$$\xRightarrow[\text{reactive power}]{\text{Influence on the voltage of}} \underbrace{\Lambda_h^{DSO}\mu^Q_{h,\tilde{h},i}}_{\text{Price per kVarh}} \tag{5.16}$$

The parameters $\mu^P_{h,\tilde{h},i}$ and $\mu^Q_{h,\tilde{h},i}$ express the influence that a node $\tilde{h}$ has on the voltage of the control node h. They differ between different locations and, therefore, they can differ between different customers. Charging these shadow prices $\Lambda_h^{DSO}\mu^P_{h,\tilde{h},i}$ and $\Lambda_h^{DSO}\mu^Q_{h,\tilde{h},i}$ will result in optimal system behaviour. In the next section will be discussed how these shadow prices can be found without centralizing all information. The dual ascent method applied for this will consist of an iterative update of the Lagrange multipliers, which, in this case, coincide with the network prices.

5.4 Distributed Pricing Algorithm

An iterative, distributed algorithm will solve the dual of the DSO optimization problem by iteratively updating the Lagrangre multipliers of the voltage constraints. The Lagrange multipliers are the shadow prices for creating voltage problems in the control nodes. These should be charged to the customers to obtain the optimal solution. This price is found by an iterative scheme. Every iteration, the flexible loads and PV units receive a network price from the DSO. They respond back to the DSO how they would react to this network price. Based on this information, the DSO can update the network price and send this updated price back to all the PV units and flexible loads. This process continues until the price has converged.

A flexible load will define its planned consumption based on the following problem:

$$\min_{P^{\text{flex}}_{\tilde{h},i}} \quad -U\left(P^{\text{flex}}_{\tilde{h},i}\right) + \Lambda_{\tilde{h}} P^{\text{flex}}_{\tilde{h},i} + \tag{5.17}$$

$$+ \sum_{h=1}^{N_{contr}} \Lambda^{DSO}_{h} \mu^{P}_{h,\tilde{h},i} P^{\text{flex}}_{\tilde{h},i} \tag{5.18}$$

Compared to (5.4), an extra network price $\Lambda^{DSO}_{h}\mu^{P}_{h,\tilde{h},i}$ is added. The price for making use of the network depends on the location and phase of the customer. In case voltage problems occur in a control node, a price Λ^{DSO}_{h} is set for using voltage "resources" in this control node, and the customer is charged, depending on their influence $\mu^{P}_{h,\tilde{h},i}$ on this control node. Due to the neutral point shift, the sign of $\mu^{P}_{h,\tilde{h},i}$ can be both positive and negative, dependent on the phase of connection. Therefore, consumption can both be rewarded and penalized by the DSO. N_{contr} is the number of control nodes. In this work, there are two control nodes: node 44 and 62. The voltages of all the three phases of these nodes are controlled.

PV installations will also respond to electricity prices. They can curtail active power, or provide reactive voltage control to support the network. A single-phase PV unit will define its active and reactive power set point, based on the

following problem:

$$\min_{P^{\mathrm{PV,curt}},Q^{\mathrm{PV}}} \quad -\Lambda_{\tilde{h}}\left(P^{\mathrm{PV}}_{\tilde{h},i}-P^{\mathrm{PV,curt}}_{\tilde{h},i}\right)+\alpha\left(Q^{\mathrm{PV}}_{\tilde{h},i}\right)^2+$$

$$-\sum_{h=1}^{N_{contr}}\Lambda^{DSO}_{h}\mu^{P}_{h,\tilde{h},i}\left(P^{\mathrm{PV}}_{\tilde{h},i}-P^{\mathrm{PV,curt}}_{\tilde{h},i}\right)+ \tag{5.19}$$

$$+\sum_{h=1}^{N_{contr}}\Lambda^{DSO}_{h}\mu^{Q}_{h,\tilde{h},i}Q^{\mathrm{PV}}_{\tilde{h},i}$$

$$\text{subject to} \quad \left(Q^{\mathrm{PV}}_{\tilde{h},i}\right)^2+\left(P^{\mathrm{PV}}_{\tilde{h},i}-P^{\mathrm{PV,curt}}_{\tilde{h},i}\right)^2\leq S^2_{\tilde{h}} \tag{5.20}$$

$$P^{\mathrm{PV}}_{\tilde{h},i}-P^{\mathrm{PV,curt}}_{\tilde{h},i}\geq 0 \tag{5.21}$$

An extra, locational-dependent network price is added compared to the normal objective function defined by (5.6). The same price Λ^{DSO}_{h} is set for using voltage "resources" in this control node, and the customer is charged depending on their influence $\mu^{P}_{h,\tilde{h},i}$ and $\mu^{Q}_{h,\tilde{h},i}$ on this control node. Note that $\mu^{P}_{h,\tilde{h},i}$ is not equal to $\mu^{Q}_{h,\tilde{h},i}$, because active power has a different influence on the voltage of the control node than reactive power. Therefore, the prices for active power are not identical to the prices for reactive power. When analysing this objective function, it is clear that the total price for active power is the sum of the electricity price of the provider and a variable price which depends on the shadow price of the grid voltage $\Lambda_{\tilde{h}}+\sum_{h=1}^{N_{contr}}\left(\Lambda^{DSO}_{h}\mu^{P}_{h,\tilde{h},i}\right)$. As long as this total price for the energy provided is positive, no active power will be curtailed. When there is no reward for providing or absorbing reactive power, the PV units will not provide reactive voltage control.

A three-phase PV unit will define its active and reactive power set point in each phase based, on the following problem:

$$\min_{P^{\text{PV,curt}},Q^{\text{PV}}} \quad \sum_{\substack{\text{i} \in \\ \{U,V,W\}}} -\Lambda_{\tilde{h}} \left(\left(P^{\text{PV}}_{\tilde{h},i} - P^{\text{PV,curt}}_{\tilde{h},i} \right) + \alpha \left(Q^{\text{PV}}_{\tilde{h},i} \right)^2 \right) +$$

$$- \sum_{h=1}^{N_{contr}} \sum_{\substack{\text{i} \in \\ \{U,V,W\}}} \Lambda^{DSO}_{h} \mu^{P}_{h,\tilde{h},i} \left(P^{\text{PV}}_{\tilde{h},i} - P^{\text{PV,curt}}_{\tilde{h},i} \right)$$

$$+ \sum_{h=1}^{N_{contr}} \sum_{\substack{\text{i} \in \\ \{U,V,W\}}} \Lambda^{DSO}_{h} \mu^{Q}_{h,\tilde{h},i} Q^{\text{PV}}_{\tilde{h},i}$$

$$\text{subject to} \quad \left(Q^{\text{PV}}_{\tilde{h},i} \right)^2 - \left(P^{\text{PV}}_{\tilde{h},i} - P^{\text{PV,curt}}_{\tilde{h},i} \right)^2 \leq S^2_{\tilde{h},i} \; i \in U,V,W$$

$$\sum_{i \in \{U,V,W\}} \left(P^{\text{PV}}_{\tilde{h},i} - P^{\text{PV,curt}}_{\tilde{h},i} \right) \geq 0$$

Compared to the single-phase PV panels, three-phase PV panels will receive a network price for each phase. Dependent on the phase of connection of node h, $\mu^{P}_{h,\tilde{h},i}$ and $\mu^{Q}_{h,\tilde{h},i}$ can be both positive and negative, depending on their phase i. This gives an incentive to transfer power from one phase to another.

Once the flexible loads and PV panels have calculated their planned consumption for the given price, they will send this information to the DSO. They do not yet adopt this consumption, as they have to wait for the DSO to inform them that the price has converged. With the planned consumption of each unit, the DSO can calculate the expected voltage magnitude of the control nodes if these plans would be realised:

$$|\widehat{V_h}| \approx |V^{\text{base}}_{h}| + \sum_{\tilde{h}=1}^{N} \left(\mu^{P}_{h,\tilde{h},i} \left(-P^{\text{PV}}_{\tilde{h},i} + P^{\text{PV,curt}}_{\tilde{h},i} + P^{\text{flex}}_{\tilde{h},i} \right) \right) + \sum_{\tilde{h}=1}^{N} \mu^{Q}_{h,\tilde{h},i} Q^{\text{PV}}_{\tilde{h},i} \tag{5.22}$$

The expected voltage should respect the voltage limits. If this voltage is outside the limits, the network price should be increased. If the voltage is clearly inside the limits, the network price might have been too high and can be reduced. As discussed earlier, the network price corresponds to the Lagrange multipliers of constraint (5.12). Only one of the constraints can be active: either the upper voltage limit is reached, or the lower voltage limit is reached. In case the voltage

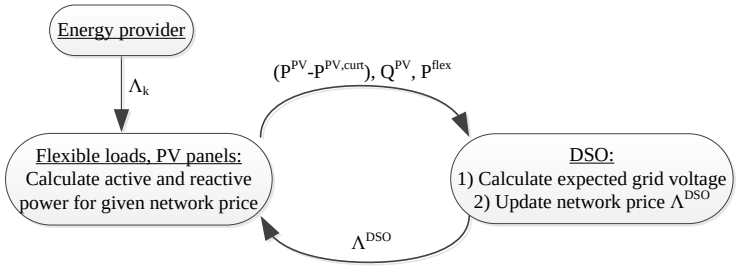

Figure 5.3: Flowchart of the distributed locational pricing scheme.

becomes too high, the update rule of the Lagrange multiplier becomes:

$$\widehat{\Lambda}_h^{DSO} = \Lambda_h^{DSO} + \delta \left(\widehat{V_h} - V^{\max} \right) \tag{5.23}$$

$$\Lambda_h^{DSO} = max \left(\widehat{\Lambda}_h^{DSO}, 0 \right) \tag{5.24}$$

If the voltage has dropped below the limits, the update rule becomes:

$$\widehat{\Lambda}_h^{DSO} = \Lambda_h^{DSO} + \delta \left(V^{\min} - \widehat{V_h} \right) \tag{5.25}$$

$$\Lambda_h^{DSO} = -max \left(\widehat{\Lambda}_h^{DSO}, 0 \right) \tag{5.26}$$

This update rule is a gradient ascent method to find the optimal Lagrange multipliers [148]. Λ_h^{DSO} will only differ from zero when network limits are reached in node h. One iteration consists of a price update from the DSO, followed by a response from all the customers. Fig. 5.3 presents this loop. Only once the price has converged, end-users will be informed that the price has converged and then they will adapt their consumption. In the preliminary iterations, the planned consumption is communicated for the given price, but this consumption is not actually adopted. In this work, a constant stepsize δ is used to update the Lagrange multipliers. Convergence with a constant stepsize is within a near-optimal ball, but it is typically faster than convergence with a diminishing stepsize [148, 149]. To further improve convergence, a quadratic term is added to the single-phase PV optimization problem that penalizes the deviation from the calculated curtailed PV power in the previous iteration. This limits the oscillatory behavior from one iteration to the next [150].

5.5 Results

5.5.1 Simulation of One Time Step of 10 Minutes

The pricing algorithm is tested on the network of Fig. 2.1. The price for electricity $\Lambda_{\tilde{h}}$, excluding the network price, is defined as 50 €/MWh. Consumers can have different providers that charge different electricity prices, but, in this work, all of the consumers are assumed to have an equal, fixed electricity price. In a first simulation, the algorithm is evaluated for one single time step of 10 minutes. This is a time step with a (high) PV production of 90 % of the inverter rating. The load is chosen randomly between 0.5 and 0.7 kW for nodes connected to phase U and between 0 and 0.3 kW for nodes connected to phase V and W. Fig. 5.4 presents the voltage in the network for these conditions when no pricing algorithm is applied. The high PV production leads to an unacceptably high voltage in the nodes at the end of the feeder connected to phase W. Adding a network price will avoid this high voltage, by giving incentives to curtail energy, to provide reactive power, or to transfer power from one phase to another.

Only Active Power Curtailment

When the only form of voltage control is the active power curtailment by PVs and the response of flexible loads, network prices will have to be high. PV units only curtail active power when the network price exceeds the price they would normally receive for the produced energy. The resulting voltage in the network is shown in Fig 5.5. The final network price $\sum_{h=1}^{N_{contr}} \Lambda_h^{DSO} \mu_{h,\tilde{h},i}^{P}$ that mitigates the voltage problems is presented in Fig. 5.6. As can be seen, the network price can drop below -50 €/MWh for nodes connected to phase W at the end of the feeder, making the total price for electricity negative in these nodes. This means that consumers get rewarded for electricity consumption. The price for power consumption only drops for nodes connected to phase W. This is the phase with the highest PV production. Due to the neutral point shifting effect, power consumption in phases U and V can increase the voltage in phase W. Therefore the price for nodes connected to these phases increases. The nodes with the highest influence on the voltage of phase W of the control nodes receive the highest network price. These nodes will curtail active power. The response of the flexible loads and the PV units is also given in Fig. 5.6. Flexible loads connected to phase W will increase their consumption, whereas the other flexible loads will decrease their consumption. Also, note that the

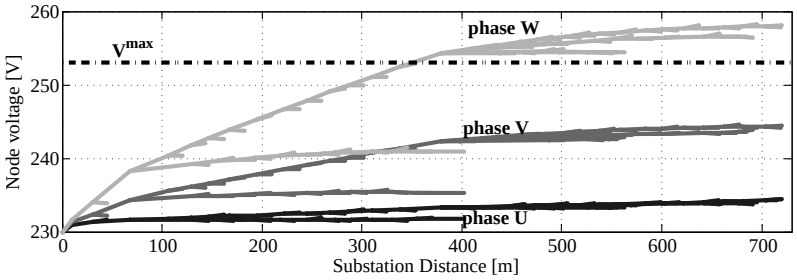

Figure 5.4: Grid voltages when no pricing scheme is used to control the voltage.

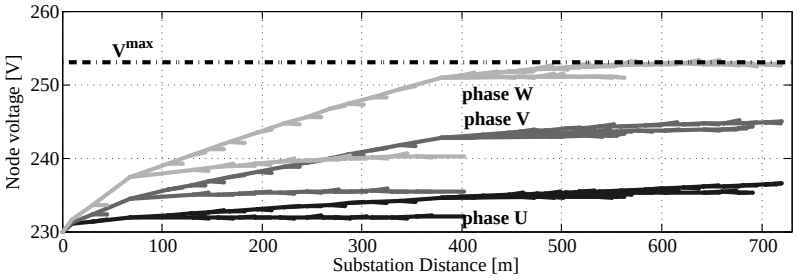

Figure 5.5: Grid voltages when a pricing scheme that gives incentives to adapt flexible consumption and to curtail PV power is used to control the voltage.

nodes with a three-phase PV unit do not curtail power. Arbitrage is not allowed and it is assumed that an equal amount of active power is injected into each phase. The penalty that needs to be paid to inject power into phase W does not outweigh the money received for injecting power into phases U and V.

Active Power Curtailment and Reactive Voltage Control

When reactive power can also be used to control the voltage, the extra network price will remain small. The costs associated with providing reactive power is small for PV units, because of the small α in (5.6) and (5.7). Therefore, small price incentives will suffice to keep the voltage within limits. The resulting voltage in the network is shown in Fig 5.7. The final price obtained by the pricing algorithm that mitigates the voltage problems is presented in Fig. 5.8. The response of the flexible loads and the PV units is also given in this figure. As can be seen, no expensive, active power curtailment takes place. The flexible loads have a limited adaptation of their consumption due to the relatively small

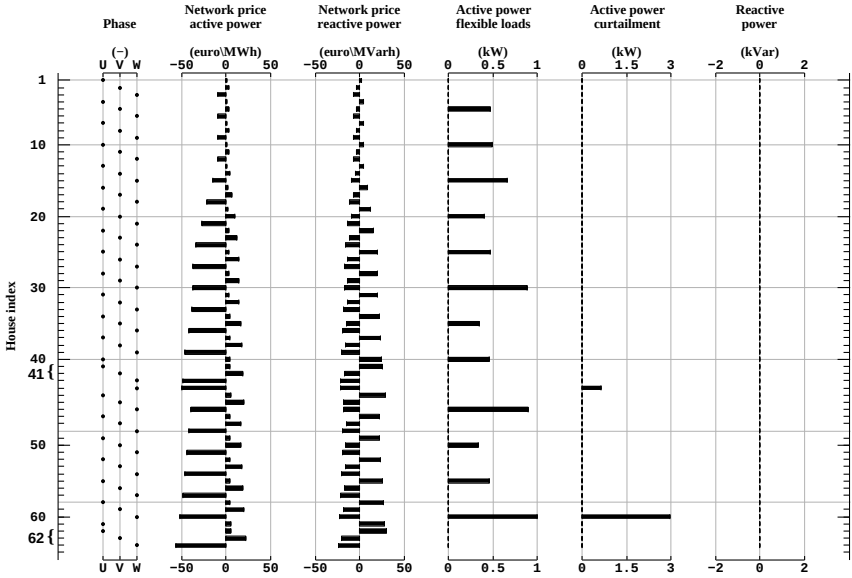

Figure 5.6: Network prices, flexible consumption, curtailed PV power and reactive power provided by PV panels for each node of the grid when a pricing scheme that gives incentives to adapt flexible consumption and to curtail PV power is used to control the voltage.

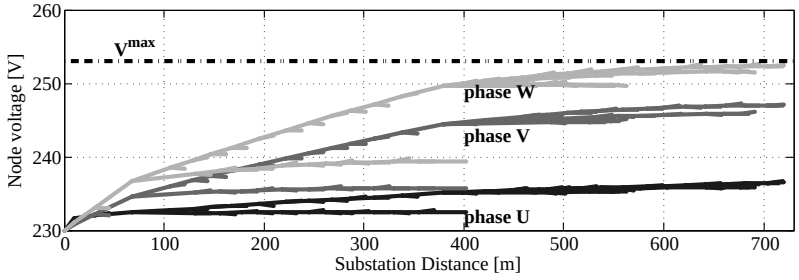

Figure 5.7: Grid voltages when a pricing scheme that gives incentives to adapt flexible consumption or to provide reactive voltage control and to curtail PV power is used to control the voltage.

price changes. The cheaper reactive power control is used to control the voltage. Three-phase PV units need to inject, or absorb, the same amount of reactive power into each phase

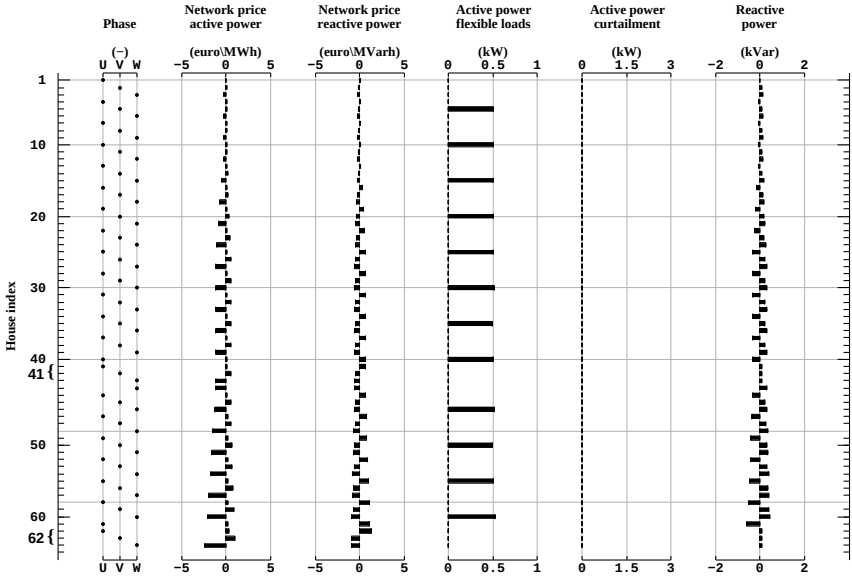

Figure 5.8: Network prices, flexible consumption, curtailed PV power and reactive power provided by PV panels for each node of the grid. The pricing scheme gives incentives to adapt flexible consumption, to provide reactive voltage control and to curtail PV power is used to control the voltage.

The network prices presented in Fig. 5.6 and 5.8 were obtained with the iterative scheme that was presented in Section 5.4. The convergence of the network price is fast. Fig. 5.9 shows the evolution of the network price of the three phases of node 62 for the simulation with reactive voltage control. After 35 iterations, the final price is obtained.

5.5.2 Simulation of One Week

In a second simulation, a sunny week is analysed. 62 statistically representative, residential load profiles were available to perform load-flow simulations. Generation of these load profiles is described in [73]. In [73], the privacy problem of data provided by electrical companies is bypassed by transforming a large dataset of residential load profiles into a model that is able to create a set of synthetic, non-aggregated load profiles. This model was trained based on a large database of measured residential load profiles provided by the DSOs in Flanders. The PV profile was measured at a fixed rooftop PV installation at

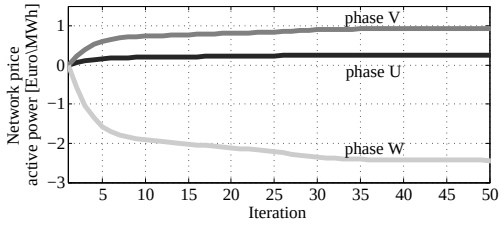

Figure 5.9: Convergence of the network price at node 62.

KU Leuven and scaled to the inverter size. The price charged by the electricity provider $\Lambda_{\tilde{h}}$ was assumed to be 50 €/MWh and constant. Fig. 5.10 presents the minimum and maximum phase voltage in the control nodes and the extra network price charged by the DSO to mitigate voltage problems. Besides the response of the flexible loads, only active power curtailment is allowed. Thanks to the pricing mechanism, the voltage remains in between limits. The majority of the time, the network price $\sum_{h=1}^{N_{contr}} \Lambda_h^{DSO} \mu_{h,\tilde{h},i}^{P}$ is zero. During the day, when there is a high PV production, the price for energy consumed in phase W will drop to increase the flexible consumption and, if necessary, curtail active power. Sometimes, a network price has to be charged to avoid an excessive drop of the grid voltage in the evening. Especially the end nodes have a very volatile price and the difference in price between the phases can become large.

When PV panels can provide reactive power, the price volatility will drop significantly. Fig. 5.11 presents the minimum and maximum phase voltage in the control nodes and the extra network price charged by the DSO to mitigate voltage problems in this case. Again the pricing mechanism can keep the voltage in between the limits, but the network prices are reduced with a factor 10 at least. Note that the price scale is different in Fig. 5.11.

Finally, we analyse the effect of arbitrage. If the three-phase PV inverters are allowed to do arbitrage, the variable network price will drop even further. This is typical for arbitrage, as it has the effect of causing prices in different locations to converge. Fig. 5.12 presents the minimum and maximum phase voltage in the control nodes and the extra network price charged by the DSO to mitigate voltage problems. The network price is reduced, compared to Fig. 5.10 and Fig. 5.11. Fig. 5.13 shows the power exchanged with each phase by the two three-phase PV inverters. During the day, a maximum amount of active power is injected into phases U and V. The remaining power is injected into the overloaded phase W. This, because during the day, the network price in phase W becomes negative, as can be seen in Fig. 5.12. Therefore, the reimbursement

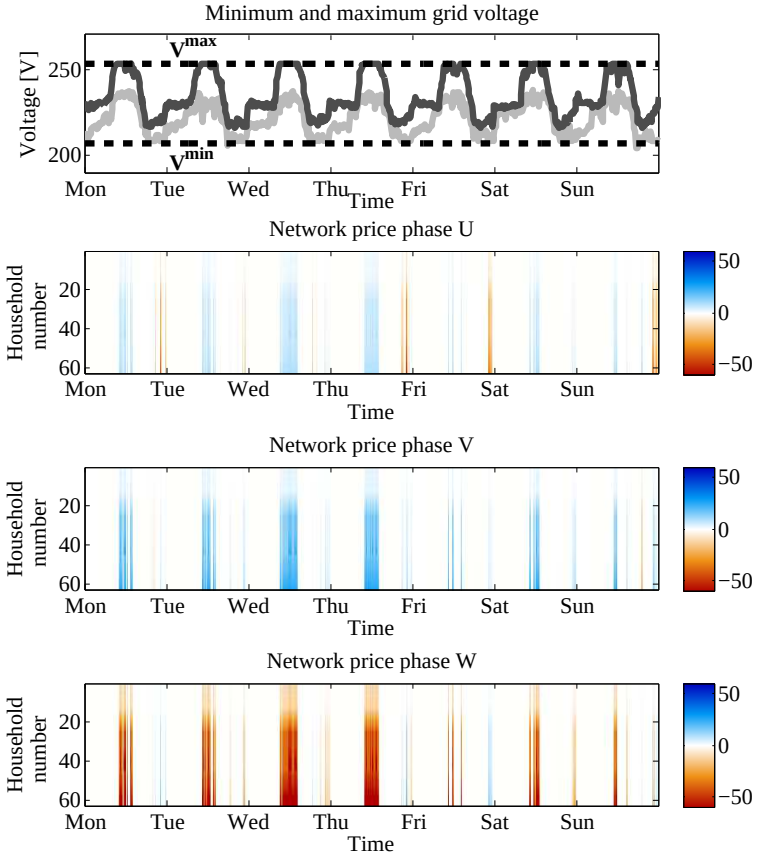

Figure 5.10: The maximum and minimum phase voltage that occurs in the control nodes and the network price at each node for active power during a sunny week in case of active power curtailment only.

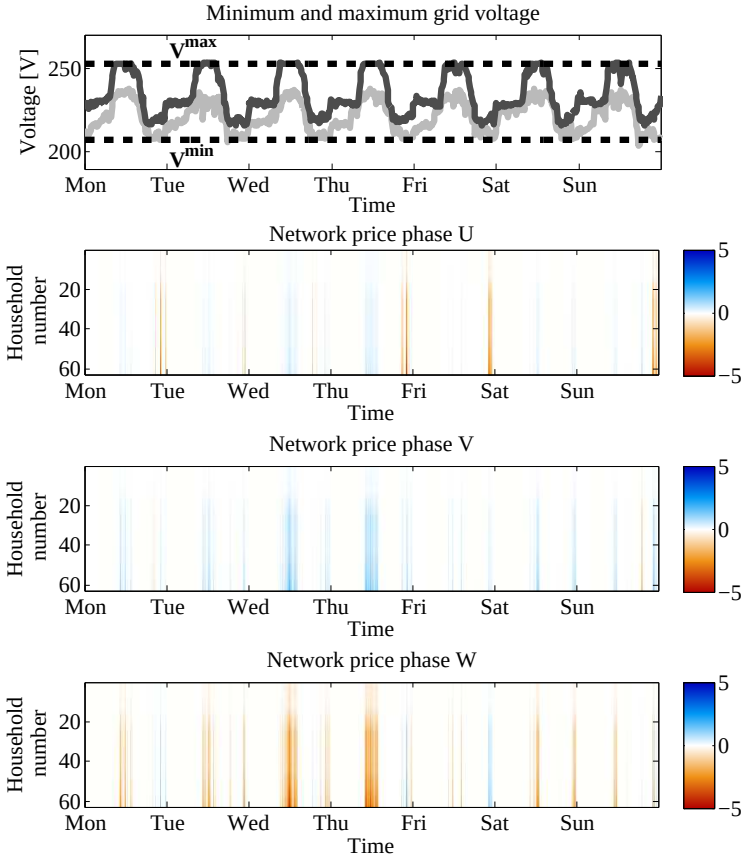

Figure 5.11: The maximum and minimum phase voltage that occurs in the control nodes and the network price at each node for active power during a sunny week in case of both active power curtailment and reactive voltage control.

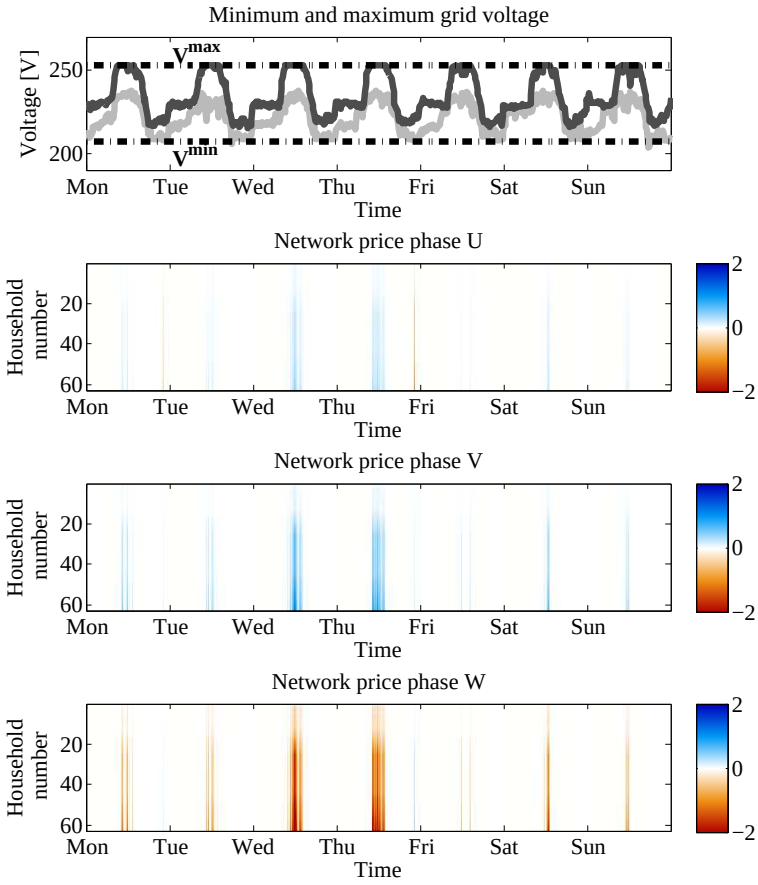

Figure 5.12: The maximum and minimum phase voltage that occurs in the control nodes and the network price at each node for active power curtailment during a sunny week in case of active power curtailment, reactive voltage control and arbitrage.

for injecting power into phase W is smaller. At night, power is extracted from the phases with a low load and injected into phases with a high load.

5.5.3 General Remarks

In this work, it was assumed that the flexible loads and PV units react to the network prices to cover their own cost for the provided network service. They

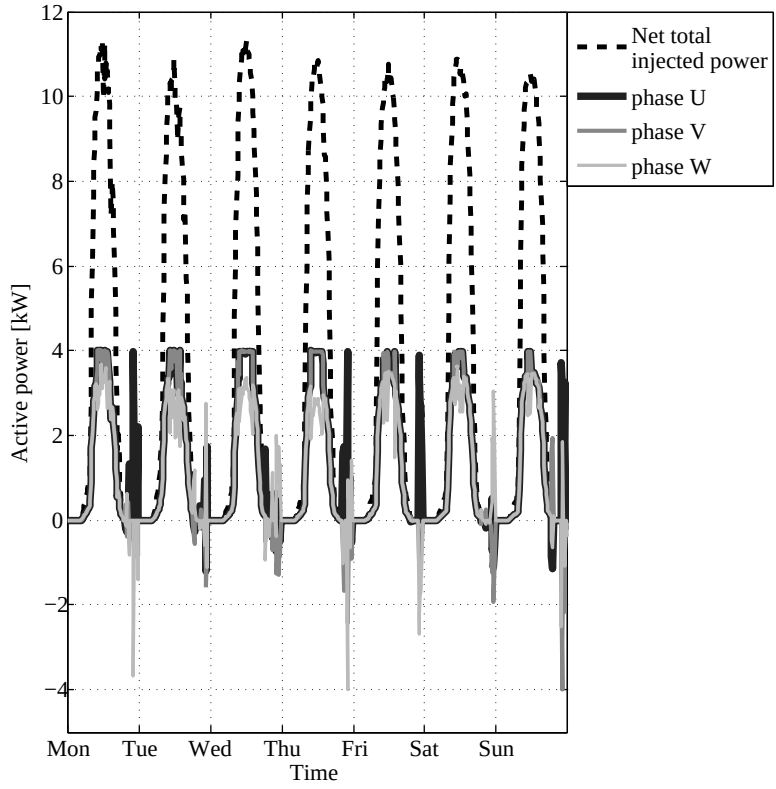

Figure 5.13: The total net injected power by the two balancing inverters and the total injection into each of the phases during the simulated week.

could also respond strategically to the network prices to increase their profit. When only a small amount of loads and PV units react to the network prices, they can increase the network prices by agreeing to adapt their consumption only for a minimum network price. In further research, the effect of this strategic behavior could be explored.

The network price can also be a control signal that is used to control the grid voltage in a distributed way. It is not necessarily charged to the customers. For example, customers participating in the voltage control can be reimbursed for the offered amount of control, for the occasions that the control is activated or by a yearly fixed fee if they participate. One of the main critics in these types of algorithms is the assumption that consumers are very sophisticated, to the level of being daily energy traders that are aware of their costs. This

is absolutely not necessary in the proposed framework. A PV panel can be equipped with a control box, with standard settings for the costs.

5.6 Conclusion

In this chapter, a locational pricing algorithm that takes into account the voltage limitations of unbalanced three-phase, four-wire, radial networks is proposed. When the limits of the maximum or minimum voltage are reached, the system operator defines an extra grid price to give an incentive for reactive voltage control, or to curtail active power. The total price of electricity consists of a price from the provider and a grid price for using the network. The grid prices are defined by a distributed optimization problem. Due to the unbalanced nature of the network, prices can differ between the different phases at one connection point. This gives an incentive to balance the network by transferring power from a phase with a low price to a phase with a high price.

Simulations show that the voltage can be controlled with the pricing scheme. When voltage problems occur, reactive voltage control will mainly be applied. The costs associated with reactive voltage control are smaller than those associated with active power curtailment. The price for making use of the network remains small, as small rewards give sufficient incentive for reactive voltage control. If arbitrage by three-phase PV units is added, the price differences between the phases diminish. When reactive voltage control is not applied, the network price needs to rise significantly to justify the curtailment of active power.

Chapter 6

Multi-Agent Charging of Electric Vehicles Respecting Distribution Network Constraints

Multiagent Charging of Electric Vehicles Respecting Distribution Transformer Loading and Voltage Limits

Sam Weckx, Reinhilde D'hulst, Bert Claessens, Johan Driesen

Published in IEEE Transactions on Smart Grids , vol.5, no.6, pp.2857-2867, Nov. 2014

The first author is the main author of the article. The contributions of the first author include the literature study, the development of the model and the analysis of the simulation results. The practical validation was done in cooperation with Filip Leemans, Marcel Stevens and Johan De Winter.

6.1 Introduction

The number of electric vehicles (EVs) is expected to rise significantly in the future. A high penetration of EVs forms both a threat and an opportunity for the operation of the electricity network. EVs have high energy requirements and, therefore, are a considerable extra load for the distribution network. This can result in severe voltage drops, or overloading of the distribution transformer. On the other hand, EVs are parked longer than required to charge completely, resulting in a significant amount of flexible consumption if the charging power of EVs can be controlled. Therefore, EVs are interesting for the application of Demand Side Management (DSM), where the charging of EVs is shifted to reduce generation costs.

In case of a high excess of wind energy, or the availability of cheap electricity, all available EVs will preferably charge at maximum power. This might overload the low voltage network distribution transformer, or make it difficult to comply with national standards for keeping the voltage within acceptable limits. The preferable implementation of DSM is able to combine both objectives by reducing generation costs, without jeopardizing the grid. In case the charging commands by an EV aggregator result in local grid problems, the system operators should have the option to intervene in demand response signals to ensure security of supply and quality of service.

As DSM will eventually involve millions of customers, centralized control will not be manageable because limits of computational complexity and communication overhead will be reached [151]. Different authors, therefore, propose multi-agent systems to obtain a scalable system. Algorithms based on dual decomposition and the alternating direction of multipliers (ADMM) are characterised by the iterative exchange of signals to obtain the optimal charging pattern for all EVs. These typically do not take network constraints into account [131, 133, 152]. In [153], ADMM is applied for the control of loads to minimize the losses in unbalanced distribution grids, while taking into account network constraints. The total EV owners convenience is maximized for a single period without violating branch constraints by means of ADMM in [154]. The required, iterative form of communication in these control algorithms might hinder a practical implementation and, therefore, is avoided in this work.

Many other multi-agent systems were proposed to coordinate the charging of EVs in a scalable way. In [155], a multi-agent system is applied to maximize the load factor by the iterative exchange of price signals. Reducing peak demand is also obtained with decentralized control in [156]. A multi-agent based Virtual Power Plant consisting of domestic devices was created in [157] to compensate imbalance caused by wind energy. The extra voltage drop caused by the charging

of EVs, which is one of the main concerns of the Distribution System Operator (DSO), is, however, not taken into account in these control systems. [158] takes into account voltage constraints, but requires an exhaustive search to find the combination of schedules that minimizes the cost of charging the EVs.

In this chapter, an existing, scalable market control system for DSM [159–163] of EVs is analysed and extended. Many extensions to this control heuristic have already been developed [151, 164, 165], and practical test sites exists where the market-based control is tested [165]. Our first contribution to this control framework is a mathematical proof that shows that this control heuristic is, in fact, a method to solve a distributed utility maximization problem. The underlying problem is identical to the one of [152, 166], but the solution method does not result in an iterative form of communication. Secondly local distribution network constraints in unbalanced three-phase, four-wire, radial grids are added to this framework. Only those agents that are responsible for LV networks with network problems need to be updated. Both transformer overloading and voltage problems can be avoided. Finally, reactive power is added as a control variable. It is shown that special care is required for reactive voltage control in three-phase, four-wire, unbalanced, radial distribution networks.

This chapter is structured as follows: In Section 6.2, the market-based multi-agent control framework is introduced. This framework is proven to be a distributed implementation of a utility maximization problem in section 6.3. In the second part of this section, the distributed utility maximization problem is extended with some network constraints and reactive voltage control in unbalanced networks is discussed. In Section 6.4, the framework is compared to other algorithms to solve the utility maximization problem in a distributed way. The test system is described in Section 6.5. Finally, Section 6.6 discusses the obtained results.

6.2 Market Based Multi-Agent Control

The proposed multi-agent control is based on [159–163]. This control heuristic is based on a tree structure of three types of agents: device agents, substation agents and an auctioneer agent. All controllable consumer devices are equipped with a device agent. In a first step, each device agent defines a bid function where the customer assigns the price, which is limited by the interval $[0, 1]$, to have a certain power consumption level.

In a second step, the device agents discretize the bid function and send it to a substation agent. This substation agent sums-up the bid functions of all the underlying devices in a low voltage network. The substation agents, in

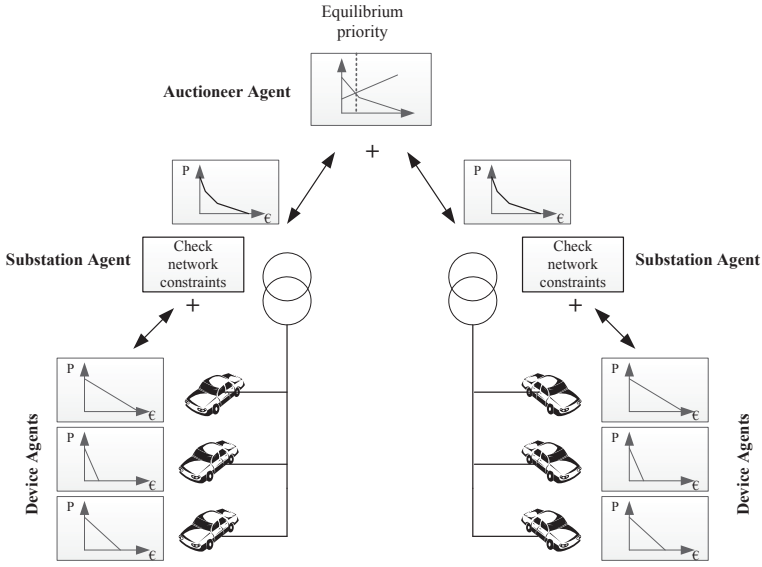

Figure 6.1: Market-based control of an electric network

turn, send the bid function to a unique auctioneer agent. This significantly reduces the amount of communication required and makes the system scalable. Finally, the auctioneer agent will define the equilibrium price as the intersection of the aggregated bid functions and the supply bid function. The supply bid function represents the prices that the producer, or balancing party, will accept for different generation levels. When the equilibrium price is defined, this value is sent back to all the device agents that will select their corresponding power level. Fig. 6.1 presents this information hierarchy.

In this work, extra intelligence is added to the substation agent. The substation agent will only add up powers for a certain possible equilibrium price if these will not result in violation of the transformer or voltage limits. Moreover, it will apply the offered flexibility to avoid voltage problems. In this work, the focus is on EVs, however, the framework can be extended to other types of devices.

In [151, 164, 167, 168], an extension is made to the auctioneer agent to include planning in the framework. Based on this planning, the auctioneer is able to define the supply bid function for the real-time control. In this work, the method of [151, 164] is applied, with the purpose of minimizing the total charging cost given a known day-ahead price. The charging should not lead to problems in the low voltage network. Other objective functions can be applied. More details about the applied approach can be found in [151, 164].

6.3 An Optimization Perspective on Market Based Control

In this section, it will be proven that the heuristic described in Section 6.2 can be interpreted as a utility maximization problem. This utility maximization problem can be extended with distribution network constraints and be solved in a distributed way.

6.3.1 Utility Function of an EV

Depending on their state, energy may be worth a different value for each device. This is generally expressed by a utility function, a concept applied in microeconomics. In this work, it is assumed that utility functions are decomposable in time. Popular decomposable utility functions $U(P_h)$ are the linear and quadratic utility function [166], where P_h is the power consumption level for a specific time and $U(P_h)$ is the utility function of the EV h. An EV h that consumes P_h kW electricity at a rate of λ per kWh is charged λP_h per hour. Hence, the welfare of each user is defined as [139]:

$$W\left(P_h\right) = U\left(P_h\right) - \lambda P_h \tag{6.1}$$

where $W\left(P_h\right)$ is the users welfare function. Given a certain price λ, the power $P_h^*(\lambda)$ that maximizes the welfare of EV h is therefore defined as:

$$P_h^*(\lambda) = \underset{P_h}{\text{argmax.}}\ U\left(P_h\right) - \lambda P_h \tag{6.2}$$

The function defined by $P_h^*(\lambda)$ is the optimal bid a device would make to an auction-based market. When this bid is used, each price will result in maximum welfare of the device. When the utility function is linear or quadratic, and the feasible sets are intervals, an explicit solution exists for $P_h^*(\lambda)$ [169]. The graphs shown at each EV in Fig. 6.1 are optimal bids that correspond to a quadratic utility function. A simple way of calculating a bid function for an EV is by using a corner price p_r [80,170], which is applied in this work. More on defining bid functions for EVs can be found in [80, 151]. In the heuristic described in Section 6.2, the price λ is not necessarily an actual price, but can be interpreted as a control signal.

The utility functions are not limited to linear or quadratic functions, but are assumed to be decomposable in time, non-decreasing and concave [139]. While the class of utility functions that fulfill these conditions is very large, it is convenient to have a quadratic utility function and the corresponding linear bid function [139, 144].

6.3.2 Utility Maximization Problem

In a utility maximization problem, the sum of all utilities of the customers, minus the cost $C(H)$ to deliver the total power H, is maximized [139]. This results in the following minimization problem:

$$\min_{P,H} \quad -\sum_{h=1}^{N} U\left(P_h\right) + C\left(H\right) \tag{6.3}$$

$$\text{subject to} \quad \sum_{h=1}^{N} P_h = H \tag{6.4}$$

The constraint of this optimization problem ensures that the sum of the individual consumption of all EVs equals the total consumption of all EVs. The cost function $C(H)$ is assumed to be convex.

The total power $H^*(\lambda)$ that maximizes the welfare of the supplier is defined as:

$$H^*(\lambda) = \underset{H}{\text{argmax.}} \; -C\left(H\right) + \lambda H \tag{6.5}$$

$H^*(\lambda)$ equals the supply bid function as presented in Section 6.2.

The dual of problem (6.3) is defined as:

$$\max_{\lambda}.\min_{P,H}. -\sum_{h=1}^{N} U\left(P_h\right) + C\left(H\right) + \lambda\left(\sum_{h=1}^{N} P_h - H\right) \tag{6.6}$$

where λ is the Lagrange multiplier of the constraint (6.4). It will be shown in this section that the Lagrange multiplier equals the price charged to the customers in (6.1), (6.2). Therefore, the same symbol is applied.

The Lagrangian dual function is decomposable in P and H and can be solved in a distributed way. The auction-based heuristic is a distributed algorithm that solves the dual problem. If strong duality holds, then the solution of the dual problem (6.6) equals the solution of the primal problem (6.3). It is supposed that there is a feasible solution and, therefore, Slater's condition holds [76]. This ensures a zero duality gap, and that optimal Lagrange multipliers exist.

The dual function can first be decomposed into subproblems that can be solved by each LV substation. It is assumed that there are K substations. A substation agent is responsible for a subset of all the EVs, described by the set n_k. Each

EV is part of one subset and the union of all subsets covers all EVs N. The subproblem of a LV substation k in control of the subset of EVs n_k is:

$$\min_{P} \quad -\sum_{h \in n_k} U\left(P_h\right) + \lambda \sum_{h \in n_k} P_h \tag{6.7}$$

In the auction-based heuristic a bid $P_h^*(\lambda)$ of a device h corresponds to the solution of a subproblem of the dual function, as can be recognised in (6.2). The task of the substation agent is to add all the bids up to obtain $\sum_{h \in n_k} P_h^*(\lambda)$, which is the solution of subproblem (6.7) for each possible λ. Afterwards, each substation agent sends the total consumption of their cluster, for each possible equilibrium price, to the auctioneer agent. The auctioneer adds-up all these aggregated bids to obtain $\sum_{h=1}^{N} P_h^*(\lambda)$ and compares it to the power that the energy provider will produce given a certain price $H^*(\lambda)$ [139].

The market is cleared when the aggregated bids $\sum_{h=1}^{N} P_h^*(\lambda)$ equal $H^*(\lambda)$. It can be shown that $\sum_{h=1}^{N} P_h^*(\lambda) - H^*(\lambda)$ equals the subgradient of the dual problem [139, 148]. Therefore, making the aggregated bids $\sum_{h=1}^{N} P_h^*$ equal to H^* comes down to solving the dual problem (6.6). The Lagrange multiplier λ of the dual problem is the equilibrium price, which is sent to the substation and EV agents.

6.3.3 Utility Maximization Problem with Transformer and Voltage Constraints

The purpose of this work is to include transformer and voltage limitations in the scalable heuristic. These network constraints can be included in the utility maximization formulation. Different constraints need to be added to the subproblem (6.7) of each LV substation. First of all, transformer overloading in a LV substation k has to be avoided. Therefore, a constraint on the maximal apparent power is introduced:

$$\left(P_k^L + \sum_{h \in n_k} P_h\right)^2 + \left(Q_k^L + \sum_{h \in n_k} Q_h\right)^2 \leq \left(S_k^{\max}\right)^2 \tag{6.8}$$

where P_k^L and Q_k^L are the uncontrollable active and reactive load flowing in the transformer of substation k during the previous time step. P_k^L and Q_k^L can be obtained from a measurement of the total load flowing in the transformer, of which the load of the n_k EVs is subtracted. The substation agents know the charging powers of all EVs during the previous time step. During the next time step, the sum of the uncontrollable load and the assigned charging power of the EVs may not trespass the maximal allowed apparent power $S_k^{\max}$.

As the uncontrollable load might change slightly during the next time step and system losses will increase for high loads, it is recommended to include a small, conservative margin on the maximal allowed apparent power $S_k^{\max}$. In a three-phase system, constraint (6.8) has to be formed for each separate phase.

A second issue that has to be taken into account is the significant voltage drop caused by the charging of EVs in LV networks. The influence of EVs on the voltage magnitude can be approximated with a linear model [41, 49, 86, 94], resulting in an affine constraint. The voltage at a node h connected to a substation k can be approximated as:

$$|V_h| \approx |V_h^{\text{base}}| + \sum_{\tilde{h} \in n_k} \left(\mu_{h,\tilde{h}}^P P_{\tilde{h}} + \mu_{h,\tilde{h}}^Q Q_{\tilde{h}} \right) \tag{6.9}$$

where

- $\mu_{h,\tilde{h}}^P$ is the sensitivity of the voltage magnitude in node h by active power injected at node $\tilde{h}$;
- $\mu_{h,\tilde{h}}^Q$ is the sensitivity of the voltage magnitude in node h by reactive power injected at node $\tilde{h}$;
- V_h^{base} is the voltage at node h due to the base load of the households;
- V_h is the expected voltage at node h with EVs charging;

All the voltages should be limited between a minimum and maximum voltage:

$$V^{\min} \leq |V_h| \leq V^{\max} \tag{6.10}$$

where $V^{\min}$ and $V^{\max}$ are the minimum and maximum allowed voltage. Typically, the voltages of a limited amount of control points at the end of the feeders have to be considered, as these are subject to the largest voltage deviations. It is assumed that these voltages are measured and communicated to the substation agent. The substation agent knows at what rate the EVs were charging during the previous control time step. With the voltage sensitivity

factors, the substation agent can calculate the effect these EVs had on the voltage during that measurement, to obtain the voltage caused only by the base load V_h^{base}. This voltage by the base load V_h^{base} can then be used to plan the consumption of the EVs during the next time step of the control framework.

In real-life conditions, the base load will vary during the next time step of the control framework. Therefore, the obtained V_h^{base} is only an estimate of the voltage that will occur during the next time step by the base load only. This could result in small violations of constraint (6.10). Besides that, there will be linearisation errors by the linear model. Therefore, a small extra conservative margin is introduced in the limits of (6.10). In this work, $V^{\min}$ and $V^{\max}$ will be chosen to be $\pm$ 9% of the nominal voltage, whereas the actual limits equal $\pm$ 10% of the nominal voltage. A justification for this 1% margin can be found in chapter 5.

An important advantage of the application of the linear voltage model is that the substation agent does not need to know the actual, inelastic base load of the households to approximate the voltage caused by the base load only. The inelastic load profiles might contain privacy sensitive information. Another reason for the application of the linear model is that the constraints remain a convex set. This will reduce the computation time. The sensitivity factors can be based on off-line calculations that are seldom updated depending on the network operation, e.g., heavy or light loading conditions [46]. Another advantage is that these sensitivity factors can be approximated based on historic smart meter data, without having information about the exact grid topology [75].

For a single-phase line, with mainly resistive line impedance, reactive power has a limited effect on the voltage [25, 93]. However, special care is required in three-phase, four-wire distribution grids. The connection of single-phase loads and EVs to three-phase, four-wire LV networks will not only alter the voltage profile in the connected phase, but also the two other phase voltages due to a neutral point shift [12]. I.e. in grids with mainly resistive line impedance, reactive power absorption in phase U will reduce the phase voltage of phase U, while it significantly increases the phase voltage of phase W and decreases the phase voltage of phase V. The neutral-point shift origins from the return current through the neutral conductor. This effect is exploited by the substation agent, as will be shown in section 6.6.

The remaining capacity of the EV charger can be applied to reactive voltage support in the network by the substation agent. When reactive voltage control is applied, customer utility can be increased for low equilibrium prices, as the reactive power injection partly compensates the voltage drop caused by the

increased load. The EV charger complex output power is limited by:

$$(P_h)^2 + (Q_h)^2 \leq \left(S_h^{\text{Nom}}\right)^2 \tag{6.11}$$

Where

- Q_h is the reactive power by the EV charger connected to node h;
- S_h^{Nom} is the nominal apparent power of the EV charger connected to node h;

To add this constraint to the subproblem of the substation agent, it is assumed that, besides the bid function, the EV also sends $|S_h^{\text{Nom}}|$ to the substation agent. If this is not communicated, the substation agent can replace $|S_h^{\text{Nom}}|$ with $P_h^{\max}$, which the substation agent can extract from the received bid function. A constraint on the power factor can be set by a linear constraint:

$$Q_h \leq \varsigma P_h \tag{6.12}$$

where ς is a constant defining the allowable ratio between reactive and active power. In this work, the constraint on the power factor is omitted and it is assumed that the full nominal apparent power can be used for reactive power control, if necessary. When reactive power is used, it is advised to add a small, quadratic penalty term for reactive power to the objective function of the utility maximization problem, to avoid the use of reactive power when no voltage problems occur.

The utility maximization problem with transformer and voltage constraints becomes:

$$\begin{aligned} \underset{P,Q,H}{\text{min.}} \quad & -\sum_{h=1}^{N} U\left(P_h\right) + C\left(H\right) \\ \text{subject to} \quad & \sum_{h=1}^{N} P_h = H \\ & (6.8 - 6.10)\ \forall\ k = 1...K \\ & (6.11 - 6.12)\ \forall\ h = 1...N \end{aligned} \tag{6.13}$$

Constraints (6.8-6.10) have to hold for each of the K LV substations, making scalability even more important. Constraints (6.11-6.12) are only added when the substation agent also applies reactive power for grid voltage control. These constraints are specific for each EV, and, therefore, need to be handled in a

scalable way. For the ease of simplicity the small, quadratic penalty term for reactive power is not presented in the objective function of (6.13).

By relaxing the first constraint of (6.13), the following dual formulation is obtained:

$$\begin{aligned} \max_{\lambda} \quad & \min_{P,Q,H} \; -\sum_{h=1}^{N} U\left(P_h\right) + C\left(H\right) + \lambda\left(\sum_{h=1}^{N} P_h - H\right) \\ & \text{subject to} \quad (6.8-6.10) \\ & \qquad\qquad\quad (6.11-6.12) \end{aligned} \tag{6.14}$$

The Lagrangian dual function is decomposable in P and H and can be solved in a distributed way. There will be a substation agent at each LV substation of the grid. Each of the substation agents will solve a subproblem of (6.14). The subproblem of a substation agent located at a LV substation k equals:

$$\begin{aligned} \min_{P,Q} \quad & -\sum_{h\in n_k} U\left(P_h\right) + \lambda \sum_{h\in n_k} P_h \\ \text{subject to} \quad & (6.8-6.10) \\ & (6.11-6.12) \end{aligned} \tag{6.15}$$

Compared to the subproblem of (6.7), transformer and voltage constraints have been added. The substation agent receives the utility function of all EVs of its cluster and solves optimization problem (6.15) for each possible equilibrium price λ. In a practical implementation, possible equilibrium prices are limited between 0 and 1. This interval is divided into 100 possible equilibrium prices ($\triangle\lambda = 0.01$). Optimization problem (6.15) will be solved for each of these 100 possible prices at the substation level. Gurobi is applied to solve this optimization problem [171]. The solution $\sum_{h\in n_k} P_h^*(\lambda)$ of subproblem (6.15) is sent to the auctioneer agent who can clear the market after adding up all of the solutions of the K substation agents. It can again be shown that $\sum_{h=1}^{N} P_h^*(\lambda) - H^*(\lambda)$ equals the subgradient of the dual problem [148] and that making the aggregated bids $\sum_{h=1}^{N} P_h^*$ equal to H^* comes down to solving the dual problem (6.14). Note that this solution complies with all network limitations in the LV substations for each equilibrium price. The outcome of the market clearing by the auctioneer agent results in an equilibrium price λ^*, which is sent to the substation agents.

The substation agents can then send the active and reactive power setpoint to each EV.

One could argue that solving optimization problem (6.15) for each possible equilibrium price is very time consuming. However, optimization problem (6.15) is convex and can, therefore, be solved very efficiently for each possible equilibrium price. The different optimization problems can easily be parallellized. To further reduce the amount of computations, it can first be checked for which prices the network constraints (6.8-6.10) will be violated. Only for those prices, optimization problem (6.15) will have to be solved, whereas, for the prices without network problems it suffices to just add the different bids as done to solve the problem without network constraints (6.7). The prices that cause network constraint problems can be found in one load-flow. After this, optimization problem (6.15) is solved for all of the problematic prices. Further reductions in computation time can be obtained by approximating constraint (6.11) by a polygon [94].

The total procedure is presented in Fig. 6.2. After the devices have sent their utility function, the substation agents can start maximizing total consumer welfare for all possible equilibrium prices. They start with an initial, small price and keep on incrementing the possible equilibrium price until the maximum price is reached. Results for both active and reactive power are stored by the substation agents. When the power consumption levels are defined for all the possible equilibrium prices, the aggregated bid function is sent to the auctioneer agent. This agent can then define the final equilibrium price λ^*. Once this final price is received by the substations, the substation agents can look-up the power setpoints and send them to all EVs. For the ease of presentation, the substation agent calculations are presented as a loop, however, the substation agent can also compute the aggregated bids in parallel.

One of the advantages of the suggested approach is that neither the device agents, nor the auctioneer agents, have to change, compared to the existing market-based control of Section 6.2. All intelligence is added to the substation agents, who are the only agents that have to be aware of the grid conditions. It is possible to equip only those LV networks that are sensitive to network problems with the substation agent that takes into account the network limitations, or to gradually introduce the new substation agent in the market-based control of Section 6.2.

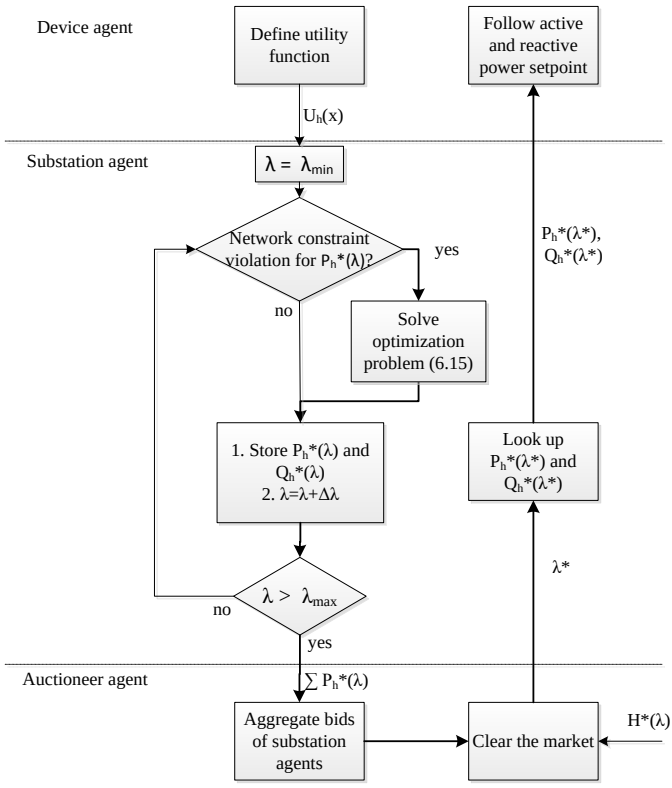

Figure 6.2: Flowchart of the distributed utility maximization that incorporates network constraints.

6.4 Comparison with other Distributed Utility Maximization Algorithms

Distributed utility maximization algorithms in smart grid literature are mainly based on dual ascent methods [133, 136, 139, 149, 152, 169] to solve the dual problem (6.14). In a dual ascent method, an iterative exchange of messages is applied to find the optimal solution of the dual problem. Each iteration, the central agent broadcasts a price. The device agents send back their planned consumption for this price. After this iteration, the price is updated by the central agent and a new iteration starts. These iterations continue until convergence of the price takes place.

Both dual ascent methods, as well as the proposed heuristic, can be used to solve the exact same problem, but they differ in their communication and computational requirements. The proposed method has some advantages and some disadvantages compared to these dual ascent methods.

6.4.1 Comparison of Communication Requirements

The proposed heuristic has mainly communicational benefits, compared to the dual ascent methods. First of all, it is not based on an iterative communication procedure in contrast to dual ascent methods. The device agents only communicate their utility function to the substation agents once. The utility functions can be compressed for an efficient communication, i.e. quadratic utility functions can be represented by three constants. The substation agents aggregate the bids and deliver these to the auctioneer agent. When the auctioneer agent has received all of the aggregated bids, it can immediately define the Lagrange multiplier of the dual problem (6.6), resulting in convergence in a single iteration. Only one price is sent back by the central agent. In a dual ascent implementation, the central agent needs to communicate a possible equilibrium price to all of the device agents every iteration. Therefore the amount of communication from the central agent to the device agents is significantly higher. Each iteration, the device agents need to respond to the higher agents when dual ascent methods are applied. So, the amount of communication from the device agents to the substation agent can be expected to be higher. Besides that, iterative algorithms will have a higher overhead, i.e. a connection needs to be established at each iteration to send a packet. Moreover, in a realistic communication environment, the underlying infrastructure places constraints on the communication, such as delays, or maximum throughput [164]. Similarly as in chapter 5, the equilibrium price can be updated in the range of one or two minutes. This provides sufficient reaction time to keep the 10 minute mean RMS values within limits.

Alternatively, the communication system can be made event-based. In case of an unforeseen constraint violation, the substation agent performs an optimization step and the set-points can be adapted. Event-based communication systems can more easily cope with a realistic communication environment [164]. Just as in the dual ascent methods, the utility function of each consumer remains unknown to the central agent, due to the aggregation of the individual utility functions at the substation level, ensuring privacy.

6.4.2 Comparison of Computational Requirements

In this paragraph we will compare the computational load of the proposed heuristic and the dual ascent methods and we will suggest methods to reduce the computational load of the proposed heuristic. Besides that, the restrictions of the utility functions by both methods are discussed.

A clear disadvantage of the proposed method is that the substation agent also solves (6.15) for values of λ that are far from optimal, whereas dual ascent methods converge towards the optimal λ. If the optimal λ always evolves smoothly in time, these less-efficient computations can be avoided by only solving the required problem (6.15) in the neighbourhood of the previous optimal λ. If this neighbourhood covers only 10 % of the total range of possible equilibrium prices, then only these 10 % of equilibrium prices need to be evaluated by the substation agent and, therefore, the computational load can be reduced with approximately a factor of 10.

Another disadvantage, compared to the dual ascent methods, is the requirement that utility functions have to be decomposable in time. The utility functions should reflect who has the highest need for the available energy, at the actual time step, independent of future information. To counteract this disadvantage, a planning approach is developed in [151, 164, 167, 168] to optimize the supply bid function at each time step.

An advantage of the proposed heuristic is that it can work with utility functions that are just convex and not necessarily strict convex. It can even handle binary behaving devices [168]. The local subproblem of the substation agent (6.15) then becomes an integer problem, which can be efficiently solved locally at the substation agent. Dual ascent methods can not guarantee convergence for this type of problem [172]. Dual ascent methods also require special care for a good step-size selection. Another benefit of the proposed heuristic is that the local intelligence at the device level is minimal. There is no need to solve an optimization problem at the device level, in contrast to many dual ascent methods. This can reduce hardware and software requirements at the device level.

6.5 Simulated Network

The network used in the simulations is the same, existing, three-phase, four-wire, radial distribution system that was already presented in Fig. 2.1.

All households have a single-phase connection, with a nominal line-to-neutral voltage of 230 V, and are equally-spread across the three phases. Statistically representative residential load profiles are available to perform load-flow simulations. A constant power load model was assumed. Generation of these load profiles is described in [73]. In [73], the privacy problem of data provided by electrical companies is bypassed by transforming a large dataset of residential load profiles into a model that is able to create a set of synthetic, non-aggregated load profiles. This model was trained based on a large database of measured residential load profiles provided by the DSOs in Flanders. No data was available on reactive power consumption by the loads, which is, therefore, neglected in the simulation.

The time step used in the simulation is one minute. EVs are connected by single-phase connections to the network, with a maximum capacity of 3.3 kW. Each household is assumed to possess an EV. The EV charging energy and the arrival and departure time are modelled based on Flemish data on travel behavior, as described in [129]. It is assumed that they will only charge at home.

The 10 minutes mean r.m.s. voltage is limited to $\pm$ 10% of the nominal voltage. According to Belgian regulation, the DSO has to comply with the power quality standard EN-50160. The voltage control by the substation agent is executed every 15 minutes in this work. Therefore, it is possible that, due to a sudden increase of the base load, the voltage drops further below the acceptable limits as set by the standard, and the substation agent cannot respond fast enough to keep the 10 minutes mean r.m.s. voltages within the required range of $\pm$ 10% of the nominal voltage. This is a rare event and the 10 minutes mean r.m.s. voltage remains within the range of $\pm$ 10% of the nominal voltage, during more than 95% of the time, as will be shown in Section 6.6.

6.6 Results

In a first simulation, the focus is on a single time step at 8 pm. The aggregated bid function of only one substation agent will be investigated, to give a clear presentation of the results. The different grid conditions that will occur as a function of each possible equilibrium price are shown in Fig. 6.3. In Fig. 6.3a,

the aggregated bid function of the substation agent $\sum_{h \in n_k} P_h^*(\lambda)$ is plotted as a function of the equilibrium price. For equilibrium prices close to zero, an extra consumption of more than 160 kW can be activated. However, the distribution grid cannot host this extra consumption. From a certain equilibrium price, voltage drops caused by the charging of EVs become severe, as presented in Fig. 6.3b. It is shown that, starting from a price of $\lambda = 0.25$, the voltage in phase V according to the linear model of (6.9), is expected to reach the minimum allowed voltage of 0.91 p.u. To be able to still increase the consumption in phase V, reactive power will be injected in phase V and U, and absorbed in phase W, as shown in Fig. 6.3c. Due to the neutral point shift, reactive power absorption in phase W can boost the voltage in phase V. For lower equilibrium prices, the consumption in phase W increases, and the absorption of reactive power in this phase needs to be reduced. Starting from a price of $\lambda = 0.05$, the aggregated bid function will be lower than for the case without network control, because the available reactive power is insufficient to compensate for the voltage drop caused by the charging of the EVs. In Fig. 6.3d, the loading of each phase of the transformer is depicted. The transformer capacity is high enough, so no transformer overloading takes place. The loading with and without the active and reactive power control is similar.

In a second test case, the same time step is investigated, but the maximum capacity of the transformer is cut in half to 125 kVA. Obviously, an extra consumption of 160 kW would damage the transformer. From a certain equilibrium price, the sum of the inelastic load and the extra consumption by EVs reaches the maximum capacity of the transformer. No more extra consumption can be activated for lower equilibrium prices. For this case there is almost no benefit of reactive power control, as it only causes an extra loading of the distribution transformer. This is shown in Fig. 6.4. For equilibrium prices lower than approximately 0.25, each of the phases would be loaded with more than the allowed 125/3 kVA. The available reactive power to solve voltage issues is, therefore, strictly limited. The total power consumption of the cluster of loads is now limited to approximately 100 kW.

In the next simulation, a time period of three days is investigated. A vehicle fleet needs to be charged as cheap as possible, given the day-ahead price. A day-ahead price of the Belgian spot market is used. During the night, electricity prices are lower, which is, therefore, the preferred time period for charging all the EVs. At the time period of the lowest price, all available cars preferably charge at maximum power. Even with a low base load, this will result in a severe voltage drop. The supply bid function in each time step is defined by the method developed in [151, 164]. Fig. 6.5 plots the power consumed during three days and the minimum 10 minute mean r.m.s voltage in the grid.

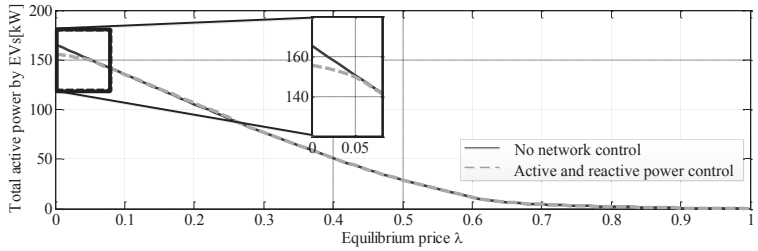

(a) The total consumption by the cluster as a function of the equilibrium price.

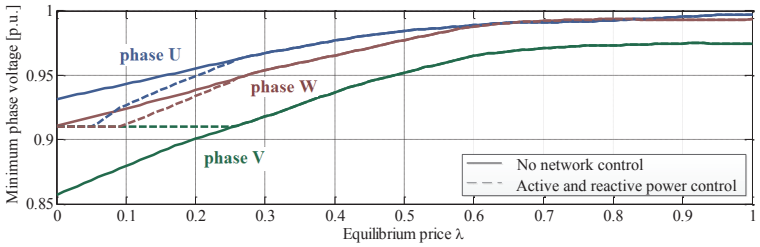

(b) The expected minimum phase voltages according to the linear model as a function of the equilibrium price.

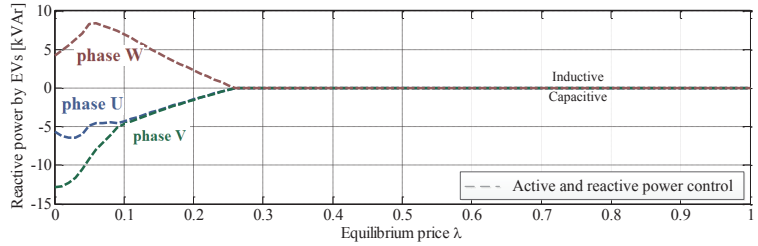

(c) The required reactive power by the EVs as a function of the equilibrium price.

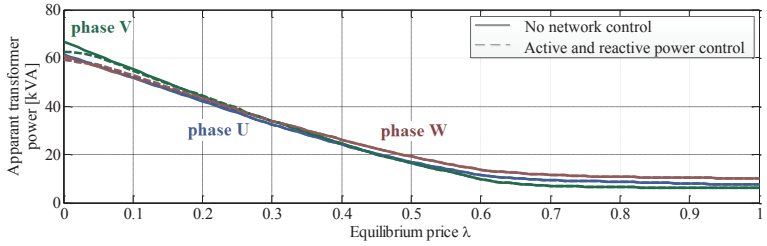

(d) The expected transformer loading as a function of the equilibrium price.

Figure 6.3: Expected grid conditions as a function of the equilibrium price for a transformer with a capacity of 250 kVA.

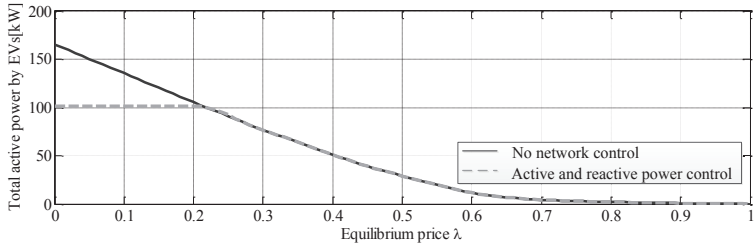

(a) The total consumption by the cluster as a function of the equilibrium price.

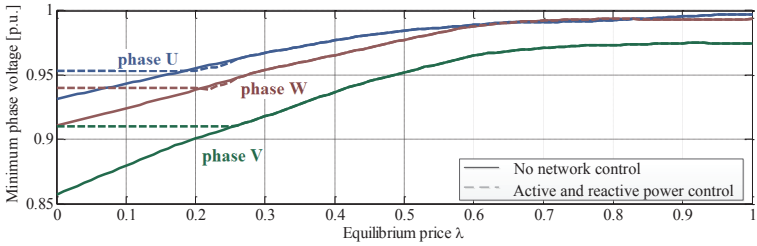

(b) The expected minimum phase voltages according to the linear model as a function of the equilibrium price.

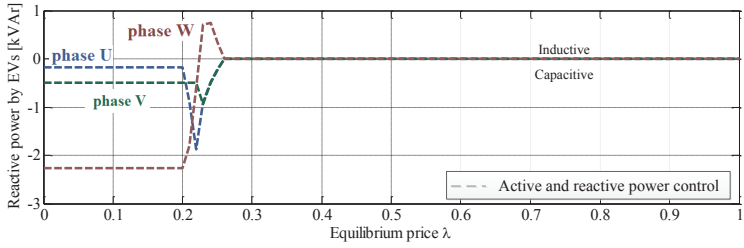

(c) The required reactive power by the EVs as a function of the equilibrium price.

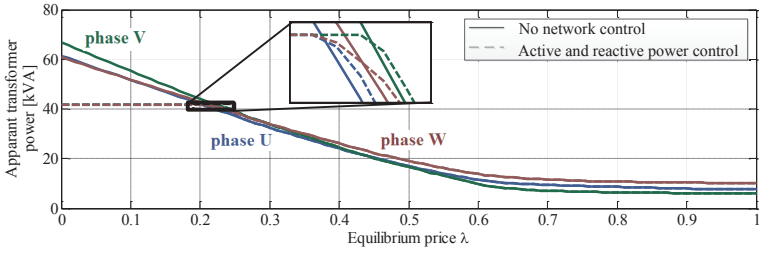

(d) The expected transformer loading as a function of the equilibrium price.

Figure 6.4: Expected grid conditions as a function of the equilibrium price for a transformer with a capacity of 125 kVA.

All voltages are obtained by applying the backward-forward sweep power flow method [61]. To clearly present the algorithm, the data of only one substation is plotted. The high peak due to the simultaneous charging of EVs results in severe voltage drops. When the substation agent does take the network constraints into account, the power consumed during the lowest price period slightly drops, but the voltage remains within acceptable limits. If the substation agent can use the remaining capacity of the EV chargers for reactive power support, more EVs can charge simultaneously before voltage limits are reached. The reduced, maximal charging power during the lowest price period results in a small price increase to charge the EV fleet. In comparison to the situation where network limitations are not taken into account, the total charging cost increases with 0.4% when active and reactive power are applied to comply with the network limits and 0.8% when only active power is used.

The same simulation can be performed for transformers with a transformer capacity of only 125 kVA. The peaks due to simultaneous charging of the EVs are now limited, to ensure that the transformer does not get overloaded, as shown in Fig. 6.6. The transformer loading is plotted, instead of the minimum grid voltage, because it is the transformer capacity that limits the total consumption by the EVs in the substation. Due to the strict limitations of the transformer, reactive power control is rarely used by the substation agent. The maximum transformer loading in each phase is now 125/3 kVA. Load variations between two market clearings can result in a short violation of the transformer limits. Due to the lower consumption possible during the lowest price period, the total charging cost increases by 6% for both control approaches.

In Fig. 6.7, one week is simulated and the corresponding, cumulative distribution function of the minimum voltage occurring in the grid is plotted. The voltage clearly complies with the power quality standard EN-50160.

In a final simulation, the computational scalability is investigated. Fig. 6.8 presents the computation time as a function of the number of substations. Each of these substations has the topology of Fig. 2.1, with cable lengths that vary 1%. In the multi-agent algorithm, each substation agent needs to calculate the aggregated bid function before the auctioneer agent can clear the market. The slowest of all agents defines the computation time seen in Fig. 6.8. The addition of a slower agent, therefore, explains the increase in steps of the computation time. It can be seen that substation agent 10 required more time to calculate the aggregated bid function than the first 9 substation agents. All substations that were added to the overall system after substation agent 10 were faster agents. Therefore, substation agent 10 defines the total execution time. The execution time of a centralized algorithm keeps on increasing for the number of substations. The simulations were performed on a workstation using a Intel Xeon (2.4 GHz, 12 MB cache, 4 cores) and 32 GB of RAM. A detailed discussion

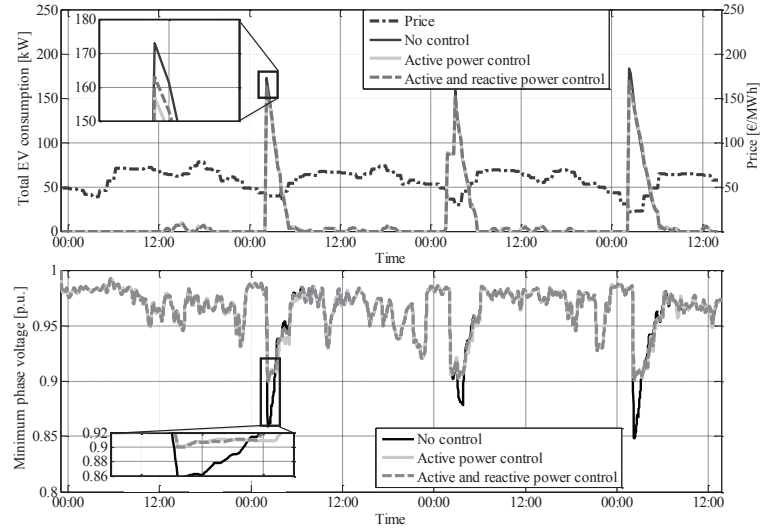

Figure 6.5: Power consumption of the fleet of EVs (Top) and the minimum voltage in the grid (Down).

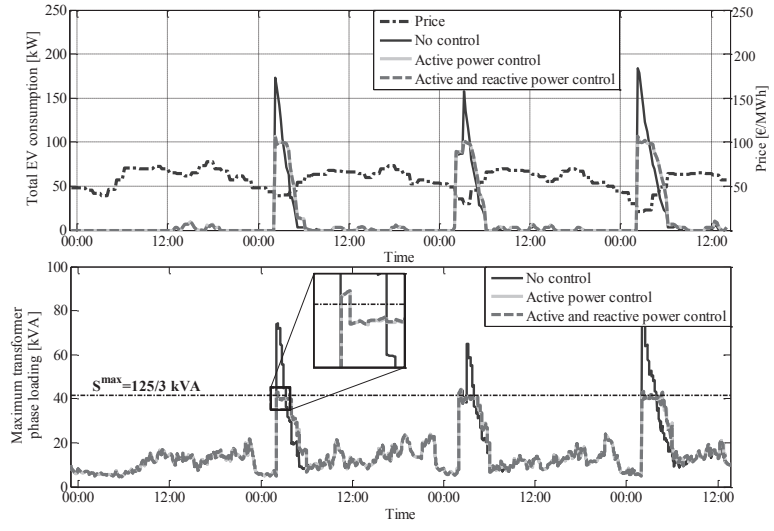

Figure 6.6: Power consumption of the fleet of EVs (Top) and the maximum transformer loading for a transformer with a reduced transformer capacity of 125 kVA (Down).

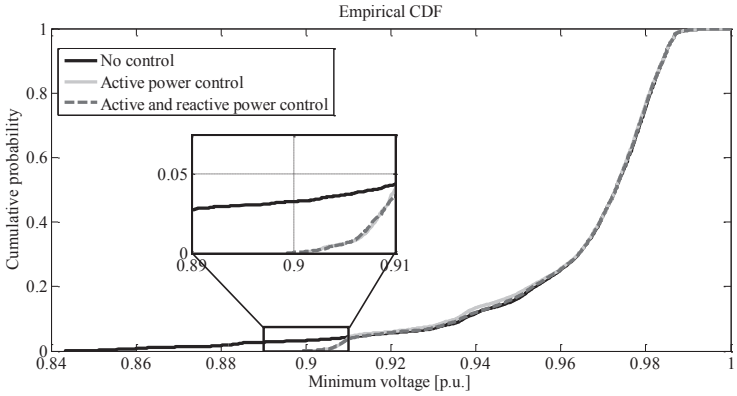

Figure 6.7: Cumulative distribution function of the minimum voltage.

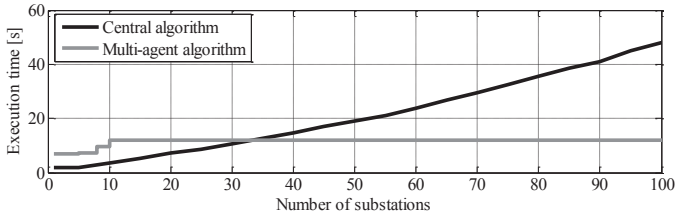

Figure 6.8: Execution time for an increasing amount of substations.

of the scalability of the original framework described in Section 6.2 can be found in [151].

6.7 Conclusion

In this work, a multi-agent market-based control is proposed that takes into account transformer and voltage limitations. The control framework solves a utility maximization problem with LV network constraints. With the mutual exchange of only one message between the different agents, the utility maximization problem is solved. It is, however, required that the applied utility functions are decomposable in time.

Simulations show that, with the proposed structure, the fleet of EVs can be charged at minimum cost, without harming the network and while customer welfare remains maximal at all times. The remaining capacity of the EVs is used

to provide reactive voltage support. Due to the application of reactive voltage control, more EVs can simultaneously charge before the voltage reaches critical limits. Therefore, more EVs can charge at the same time during periods of low energy costs. Special attention has been given to the neutral point shift effect when applying reactive voltage control in unbalanced, three-phase, four-wire LV grids. Reactive voltage control has no benefits if the transformer capacity limits the amount of EVs that can charge simultaneously.

The focus of further and ongoing work is on an event-based implementation, as in [164], rather than having fixed moments for the communication between the agents. Interaction between the agents could be made event-driven, such as the arrival of a new EV, or the violation of a voltage limit due to a sudden increase in household loads. This way, the substation agent could react faster to conditions that might harm the LV grid. This can have implications on the preferred communication and metering infrastructure. Besides that, it will be investigated how to incorporate utility functions that are not decomposable in time. Finally, other business cases could be evaluated, like absorbing an unexpected excesses of wind power with the EV fleet.

6.8 Annex

The proposed algorithm was tested in the VITO HomeLab. The grid used was already presented in Fig. 2.8. Four EVs were emulated by means of electric heaters. Therefore, no reactive power could be included in the tests. Two of the EVs could modulate their active power consumption by means of a phase angle controller. The phase angle controller adapts the output voltage based on an input voltage between zero and five volts. This input voltage is created by filtering a PWM signal of an Arduino. The two other EVs have a fixed charging power and are controlled by a solid-state relay. The optimization problem (6.15) is, therefore, in this case, an integer problem. The practical implementation setup is presented in Fig. 6.9.

One EV was connected to node 1 (EV1), one to node 2 (EV2), one to node 3 (EV3) and one to node 4 (EV4). Node 1 and 2 are connected to phase U, while node 3 and 4 are connected to phase V. EV1 and EV3 can modulate their consumption and have a maximal consumption of 2550 W, while EVs 2 and 4 can only be turned on or off and have a maximal charging power of 1500 W. Square bid functions were used. The different corner priorities can be found in Table 6.1. For the ease of representation, the bid functions were kept constant during the tests. The lower voltage limit was chosen to be 94 % of the nominal voltage. It is assumed that electricity is very cheap at the simulated time period,

Table 6.1: The used corner priorities of the four EVs.

	EV 1	EV 2	EV 3	EV 4
Priority	0.25	0.6	0.5	0.75

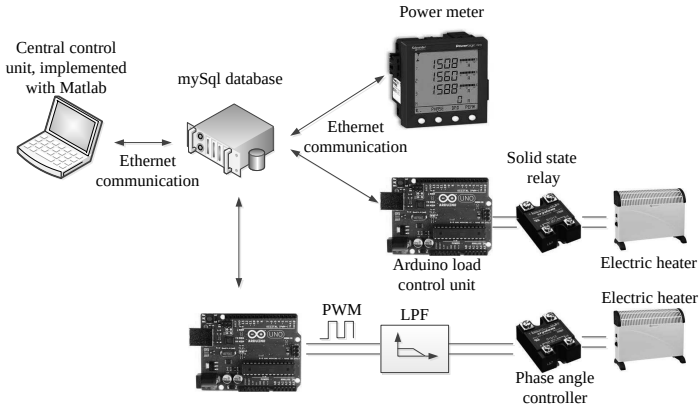

Figure 6.9: Practical implementation of the voltage control strategy.

and, therefore, all EVs would preferably charge at maximal power. However, the substation agent needs to take into account the minimum grid voltage.

The total, active power in each phase is depicted in Fig. 6.10, while the voltage is shown in Fig. 6.11. It can be seen that EVs 2 and 4 are charging most of the time. Only when the uncontrollable load is very high they stop charging. The EVs that can modulate their consumption (EVs 1 and 3) adapt their consumption to avoid voltage problems. The last two EVs also have a lower priority of charging and are filling the valleys. The voltage remains close around the minimum voltage. EVs 1 and 3, therefore, consume as much as they can, while respecting the voltage limits.

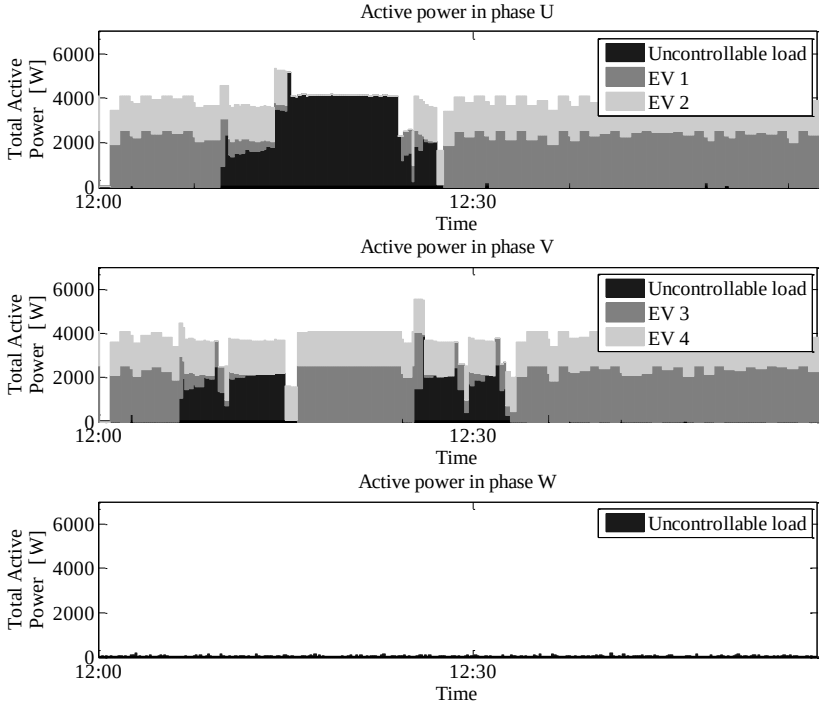

Figure 6.10: The total active power consumption in phase U, V and W when two EVs are connected to phase U and two EVs are connected to phase V.

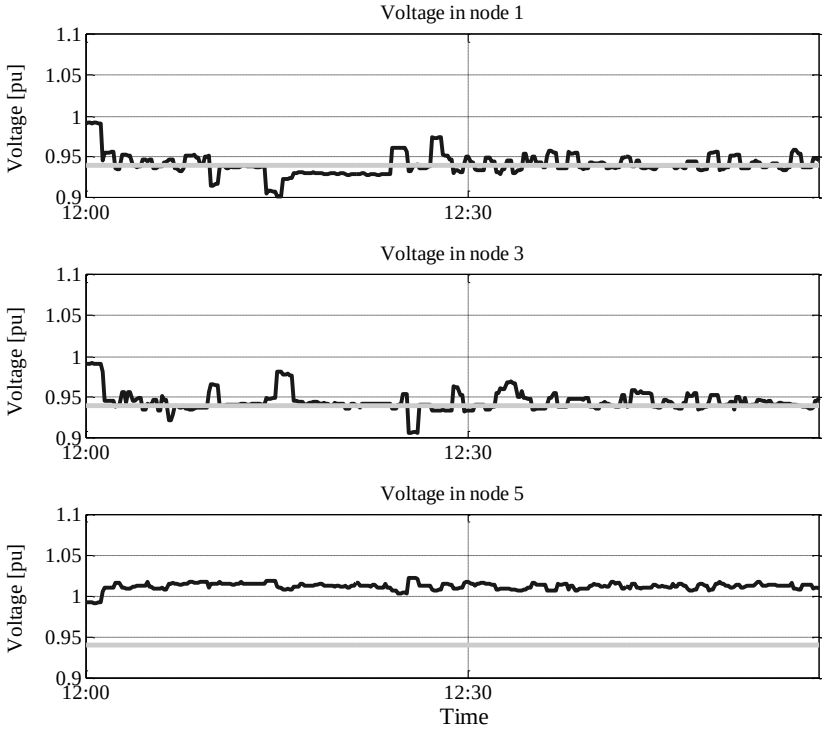

Figure 6.11: The voltages of nodes connected to phase U (node 1), V (node 3) and W (node 5) when two EVs are connected to phase U and two EVs are connected to phase V.

Chapter 7

Frequency Support by a Multi-Agent Demand Control System

Primary and secondary frequency support by a multi-agent demand control system

Sam Weckx, Reinhilde D'hulst, Johan Driesen

Published in IEEE Transactions on Power Systems, vol.30, no.3, pp.1394-1404, May 2015

7.1 Introduction

A high penetration of renewable energy sources challenges the future grid operation. In a power system, the imbalance between generation and demand should be minimized as much as possible to ensure frequency stability and avoid blackouts. Renewable energy sources, like solar and wind power, are

The first author is the main author of the article. The contributions of the first author include the literature study, the development of the model and the analysis of the simulation results

characterised by fluctuating power generation, while the amount of dispatchable power generation reduces. This makes it harder to match the production of energy to the demand. By controlling demand, the more expensive alternative of flexible, additional, back-up generation can be avoided. The residential demand side can make a significant and reliable contribution to primary frequency response [36]. Different types of demand can be applied for frequency support, including fridges, freezers, HVAC and water heaters [36, 173, 174]. In, [175] thermostatically-controlled loads respond to the frequency by making their setpoints dynamic. The introduction of electric vehicles (EVs) in the electric network is another form of controllable load that can react to the frequency [4,176]. It is shown in [177] that EVs can significantly reduce frequency deviations in isolated power systems.

Three levels of control are generally used to maintain the balance between supply and demand. Primary frequency control is a local, automatic control that adjusts the active power generation and consumption to quickly restore the balance between load and generation [31]. Secondary frequency control is a centralized, automatic control that adjusts the active power production, or consumption, to restore the frequency and the interchanges with other systems to their target values following an imbalance [31]. Tertiary frequency control consists of redispatching the generating units [31]. The response time of each type of control is different. The primary frequency control reacts very quickly, within the first few seconds after a disturbance. The secondary reserves can be activated in 30 s to 15 min. Tertiary reserves are manually activated after the secondary reserves.

In the literature, there are still multiple issues concerning the application of dynamic loads as frequency reserves. First of all, the contribution of dynamic demand to primary and secondary reserves could be combined with a classical demand response system, where the consumption of these loads is shifted in time. To be able to provide reserves, the load aggregator, that provides reserves by dynamic residential demand, needs to manage his cluster of loads so that the consumption can always be increased or decreased. The amount of reserves needs to be known by the aggregator and, for primary frequency reserves, the response of the cluster to frequency changes needs to be controlled.

In the literature, the power-frequency relationship of a device that participates in frequency control is not assumed to depend on the utility function of that device. A utility function describes the degree of well-being the product provides for consumers. Therefore, at an instance of frequency support by dynamic demand, social welfare is not maximized. An EV with a near departure time and a high requirement for sufficient energy will have a higher utility for power than an EV with an expected departure the next day. Therefore, when reducing demand to support the frequency, welfare maximization would result in decreasing the full

charging power of the second EV while keeping the charging power of the EV with near departure time constant, rather than reducing both charging powers by an equal percentage. A similar analogy can be made for electric water heaters, fridges and freezers. The value of power for a fridge is indirectly incorporated by making the frequency-power relationship of the fridge dependent on temperature in [173]. In [178], the cost for providing a certain amount of symmetric primary reserves is minimized, where comfort constraints of the devices are taken into account to order the activation of binary behaving devices. However a more general tool to define the value of power for a certain device is their utility function. Given the utility of a device, social welfare can be maximized. In previous work [79], this concept was applied to primary frequency reserves.

In this chapter, a multi-agent control framework is presented that can shift demand through time and can activate primary and secondary reserves provided by a cluster of loads. While the focus at this work is on the activation of frequency reserves, the reservation is outside the scope. During activation of the reserves provided by dynamic demand, social welfare remains maximal. The chapter is structured as follows: in Section 7.2, utility functions that describe the value of energy for different types of devices are presented. Section 7.3 introduces the market-based, multi-agent control used and shows how the multi-agent control framework activates contracted fast spinning reserves provided by the cluster of loads. In Section 7.4, a rolling horizon control is presented that determines the consumption plan of the cluster and that ensures the availability of the contracted reserves. Finally, Section 7.5 discusses different simulation results of the proposed algorithm.

7.2 Utility Function of a Device

Energy can have a different value for each device, depending on its state. This is generally expressed by a utility function, a concept applied in microeconomics. It should be strictly distinguished from the electric utility, which has another meaning. The utility function applied in microeconomics describes the degree of well-being the product provides for consumers. It, therefore, defines the different responses of different devices to various prices [139]. In this work, we assume utility functions that are decomposable in time and can be created for all types of devices. Popular utility functions include the linear and the quadratic utility function [139] denoted as $U(P_h)$, where P_h is the power consumption level of the device h. A device h that consumes P_h kW electricity at a rate of λ per kWh is charged λP_h per hour. Hence, the welfare for each user is defined as [139, 166]:

$$W\left(P_h\right) = U\left(P_h\right) - \lambda P_h \tag{7.1}$$

Where $W(P_h)$ is the users welfare function. Given a certain price λ, the power $P_h^*(\lambda)$ that maximizes the welfare of device h is therefore defined as:

$$P_h^*(\lambda) = \underset{P_h}{\text{argmin.}} - U(P_h) + \lambda P_h \tag{7.2}$$

The function defined by $P_h^*(\lambda)$ is the optimal bid a device would make to an auction-based market. When this bid is used, each price will result in maximum social welfare for the device. When the utility function is linear or quadratic, and the feasible sets are intervals, an explicit solution exists for $P_h^*(\lambda)$ [79, 169]. Devices that can only be turned on or off require a two-state utility function:

$$U = \begin{cases} \beta_h & \text{if device is turned on} \\ 0 & \text{if device is turned off} \end{cases} \tag{7.3}$$

Where the parameter β_h characterizes the satisfaction when the device is turned on. The corresponding bid function is:

$$P_h^*(\lambda) = \begin{cases} P_h^{On/Off} & \text{if } \lambda \leq \dfrac{\beta_h}{P_h^{On/Off}} \\ 0 & \text{if } \lambda > \dfrac{\beta_h}{P_h^{On/Off}} \end{cases} \tag{7.4}$$

Where $P^{On/Off}$ is the power consumption when the device is turned on.

A simple way of calculating a bid function for an EV is by using a corner price p_r [80, 170], as depicted in the left of Fig. 7.1. The corner price p_r is the maximal price the EV is willing to pay for electric energy at that time instance and is represented by the following formula:

$$p_r = \frac{\triangle E^{EV}}{P^{max} \triangle t_{dep}^{EV}} \tag{7.5}$$

Where $\triangle E^{EV}$ is the required energy by the time of departure, P^{max} is the maximal charge power and $\triangle t_{dep}^{EV}$ is the time till departure. EVs with high requirements for energy and little time left before departure will have higher bid functions. More on defining bid functions for EVs can be found in [80, 151].

Electric hot water heaters are other devices that offer a great amount of flexibility. Their charging can be shifted with little impact on the comfort of the user. It is assumed that the electric water heaters can not modulate their power consumption and have a fixed power consumption $P_h^{On/Off}$ when they are turned on. The State Of Charge (SOC) is the main indicator of a domestic hot water buffer for any demand response control system [179]. The closer the SOC drops to its minimum, the more urgent its scheduling. Therefore, the bid is

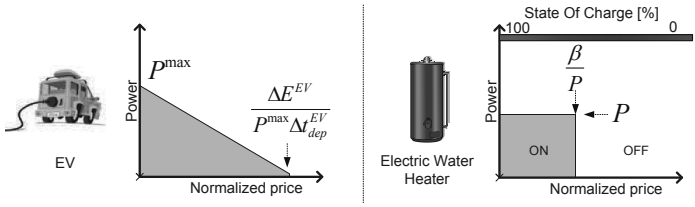

Figure 7.1: Possible ways of defining a bid function $P_h^*(\lambda)$ for EVs and electric water heaters. The bid of an EV depends on the required energy by the time of departure and the time till departure. The bid of an electric water heater depends on the state of charge of the heater.

made inversely proportional to the SOC of the heater. This is done by making β_h of (7.3) and (7.4) inversely proportional to the SOC. In case of a low SOC, the bid will be high and vice versa, as depicted in the right of Fig. 7.1.

A similar reasoning holds for other devices [79]. Note that the optimal bidding is not limited to these types of bids, but can incorporate other factors as well, like consumer preferences or consumer wealth. The utility functions are not limited to the described functions, but are assumed to be decomposable in time and to be non-decreasing. The class of utility functions that fulfil these conditions is very large [139, 144]. When devices compose their own utility function, the assumption that consumers are very sophisticated, to the level of being daily energy traders that are aware of their utility functions, can be avoided. In this work, EVs and electric water heaters are used, as they can instantly adapt their power consumption.

7.3 Auction-Based Control

A scalable, auction-based control framework is applied to control the cluster of loads. It is extended to activate the contracted spinning reserves. The multi-agent control algorithm consists of two parts: one part to control the cluster of loads in real-time to obtain the planned consumption and another part for the planning of the consumption of the cluster of loads over a time horizon. The former is covered in this section, while the latter is discussed in section 7.4.

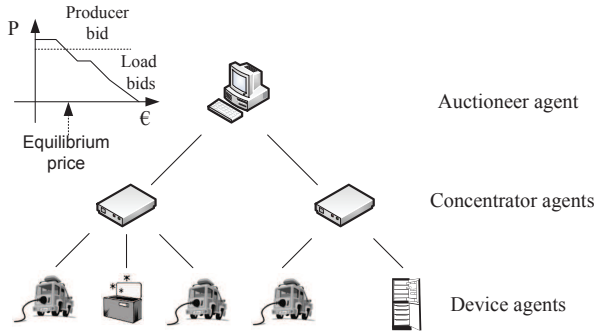

Figure 7.2: Auction-based power market.

7.3.1 Real-Time Control of the Loads

In the real-time operation of the multi-agent algorithm, all the device agents send their bid $P_h^*(\lambda)$ to a concentrator agent. This concentrator agent sums-up the bid functions of their zone $[161, 180]$. The concentrator agents, in turn, send the bid function to a unique auctioneer agent. Finally, the auctioneer agent will define the equilibrium price as the intersection of the aggregated bid functions and the supply bid function. The supply bid function is defined by the consumption level $P_t^{\mathbf{Load}}$ that was planned by the auctioneer agent. How to define this consumption level $P_t^{\mathbf{Load}}$ will be discussed in section 7.4. The auctioneer agent manages and plans the real-time consumption of the cluster of loads of the load aggregator. After the equilibrium price is defined, it is sent back to all of the device agents and these will then select their corresponding power level. This market clearing takes place every 15 minutes, or can be made event-driven. Fig. 7.2 presents this auction-based market approach.

When consumption can be increased, or decreased, given the defined equilibrium price, the cluster of loads is able to provide upward and downward reserves. This is shown in Fig. 7.3. This multi-agent control framework can be extended to cooperate in frequency reserve markets. For the cluster of loads to be activated as reserves, extensions have to be made to the part of the multi-agent system responsible for the real-time operation.

The provided frequency reserves are divided into primary, or Frequency Containment Reserves (FCR), and secondary, or Frequency Restoration Reserves (FRR). The purpose of this work is to imitate these reserves, provided by conventional generators, with a cluster of loads. Primary frequency reserves by conventional generators respond instantaneously to frequency changes. To mimic this behaviour, the instantaneous primary frequency control by dynamic

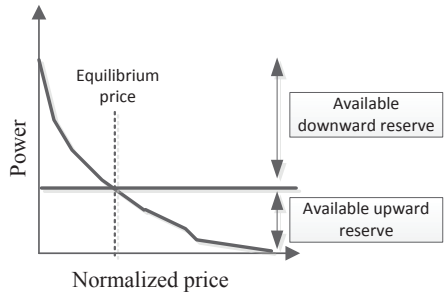

Figure 7.3: Available reserves of the cluster of loads after defining the equilibrium price.

demand cannot be based on any form of communication. Therefore, a local controller taking care of the primary frequency control is added to each device agent. In case of a frequency drop, the power consumption that creates the least welfare should be shut down. In case of a frequency rise, the power consumption that results in the highest extra welfare should be activated. The response of the local controller can be changed and optimized by the auctioneer agent. Secondary reserves should be available between 30 s and 15 min after a request of the transmission system operator and, therefore, a reliable communication system can be applied to activate the required reserves by the dynamic demand. For ease of explanation, the secondary frequency control will be discussed before the primary frequency control by dynamic demand.

7.3.2 Secondary Frequency Control

Due to the slower time scale of secondary control, the auction-based infrastructure, as described in section 7.3.1, can be applied to activate secondary reserves. The total consumption of the cluster of loads $\sum_{h=1}^{N} P_h$ needs to be equal to the sum of the planned load $P_t^{\mathbf{Load}}$ of the cluster at time step t and the activated upward or downward reserves $R_{\mathbf{load}}^{2,+/-}$. To obtain this consumption the auctioneer agent makes the supply bid function equal to $P_t^{\mathbf{Load}} + R_{\mathbf{load}}^{2,+/-}$. The resulting equilibrium price gives rise to the required consumption level of the cluster of loads when sent to all devices.

The secondary frequency control with the multi-agent auction-based control is a distributed utility maximization problem. The utility maximization problem equals:

$$\begin{aligned} \max_{P_h} \quad & \sum_{h=1}^{N} U\left(P_h\right) \\ \text{subject to} \quad & \sum_{h=1}^{N} P_h = P_t^{\mathbf{Load}} + R_{\mathbf{load}}^{2,+/-} \end{aligned} \tag{7.6}$$

The dual of this problem is defined as:

$$\max_{\lambda} \min_{P_h} - \sum_{h=1}^{N} U\left(P_h\right) + \lambda_m \left(\sum_{h=1}^{N} P_h - P_t^{\mathbf{Load}} - R_{\mathbf{load}}^{2,+/-} \right) \tag{7.7}$$

If strong duality holds, then the solution of the dual problem (7.7) equals the solution of the primal problem (7.6). For integer problems, strong duality in general does not hold. In [181] is stated that problems of this type have a diminishing duality gap if the number of subproblems increases. Therefore, solving the dual problem with a high amount of aggregated devices will result in only a small, or even no, error.

The Lagrangian dual function is decomposable in different subproblems. The welfare maximization that each device performs in (7.2) is a subproblem of the dual problem. It can be shown that $\sum_{h=1}^{N} P_h^*(\lambda_m) - P_t^{\mathbf{Load}} - R_{\mathbf{load}}^{2,+/-}$ is a subgradient of the dual problem and, therefore, finding the intersection of the aggregated bid functions $\sum_{h=1}^{N} P_h^*(\lambda_m)$ and the supply bid function $P_t^{\mathbf{Load}} + R_{\mathbf{load}}^{2,+/-}$ comes down to solving the dual problem of the utility maximization problem. The equilibrium price is equal to the lagrange multiplier λ_m of the dual problem.

Intuitively, when all customers receive the same price and this price results in the desired consumption level of $P_t^{\mathbf{Load}} + R_{\mathbf{load}}^{2,+/-}$, the total utility is maximized, as only devices with a sufficient need for energy are turned on.

7.3.3 Primary Frequency Control

Primary frequency reserves are used to stabilise the frequency after a disturbance in the time frame of seconds. Conventional generators react immediately to this disturbance. To mimic the behaviour of these conventional generators, the response of the loads can, therefore, not depend on a communication signal that is sent after the occurrence of such a disturbance. Instead, it is based on a local controller that is added to the device agent.

When the frequency is higher than the nominal value, an incentive for consumption should be given. When it is lower, consumption should be decreased. This can be achieved by adding an extra frequency-dependent price component to the normal price. The market clearing price that customers receive is the price at the nominal frequency, i.e. 50 Hz, which results in a consumption level of $P_t^{\mathbf{Load}} + R_{\mathbf{load}}^{2,+/-}$. A frequency deviation results in a price deviation from that market clearing price. The auctioneer, therefore, does not send only one equilibrium price to all loads, but a price dependent on frequency. The frequency-dependent price is defined by the preferred shape of the frequency response of the cluster of loads. Fig. 7.4 shows the aggregated bid function and the resulting power-frequency droop relationship. The dotted line is the price at 50 Hz. In a deadband around 50 Hz, the price remains unchanged. When the frequency deviates outside the deadband, devices adapt their behaviour as defined by their bid functions. The local control parameters of a device then depend on the bid functions of the device, as described in Section 7.3. The bid function defines the power-price relationship and, therefore, also defines the power-frequency relationship. An example of two EVs is given in Fig. 7.5. The EV with a near departure time and little energy stored in the battery is charging and only stops charging when the frequency significantly drops. The EV with a larger amount of time left before departure only starts charging when the frequency reaches a certain value above 50 Hz.

The aggregated response of all loads mimics the behaviour of a conventional generator. When more devices are involved in the auction-based control the aggregated bid function becomes smoother and, therefore, the smoother behaviour of the conventional generators can be imitated. The primary frequency control can be made both symmetric and asymmetric.

Devices can autonomously adapt their power consumption, based on the frequency-price dependency. This results in consumption levels that are dependent on frequency, while the system welfare remains maximal. As frequency can be measured locally in a cheap way [173], devices can adapt their own price automatically. The devices do not require any information about the system, in contrast to the method described in [182]. The only difference with the classic auction-based control is that, instead of one single equilibrium price, a frequency-price relationship is communicated to all loads. The frequency-price relationship is always equal for all controllable loads. At time steps that loads are not used for primary reserves, the price will be independent of the frequency.

Frequency can be considered to be equal across the system and, therefore, the price increase will be equal for all customers, which will result in maximal system utility. Only small errors on the frequency measurements give rise to minor price differences that could deteriorate the maximal system utility. The effect of

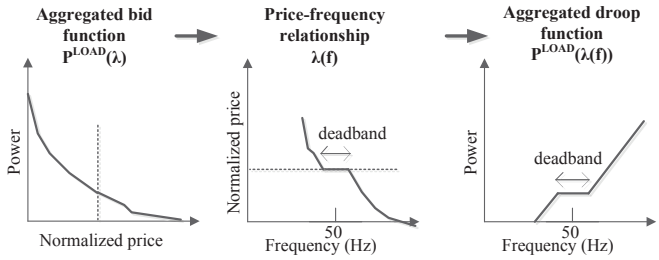

Figure 7.4: To obtain a specific power-frequency, or droop, relationship of the cluster of loads, the price is determined as a function of the frequency. The dotted line is the market price at 50 Hz.

frequency measurement errors on the aggregated droop function is plotted in Fig. 7.6. 5000 EVs and 5000 electric water heaters make a bid. At the top of this figure, the aggregated bid function is shown. The price-frequency relationship that results in the aggregated droop function is also shown. A controller tolerance band of $\pm f_{tol} = 20mHz$ is added to the aggregated droop function [178]. Frequency measurement errors result in a deviation of the reference droop function and can result in difficulties to comply with an acceptable tolerance band. Uncorrelated, Gaussian noise is added to the frequency measurements of the participating devices. Gaussian noise with a σ equal to 0.01 Hz results in a minimal deviation from the reference droop curve and compliance with the tolerance band. A σ equal to 0.1 Hz results in a severe deviation of the reference curve, which does not comply with the accepted tolerance band, as shown in the bottom part of Fig. 7.6. It is, therefore, recommended to reduce the frequency measurement errors to below the tolerance band.

The primary frequency support activation has a distributed optimization interpretation. The purpose of the primary load frequency support by dynamic demand is to eliminate the load-generation mismatch in the whole system, while maximizing system utility. Intuitively, if customers receive the same price and this price converges, the system utility will remain maximal. A mathematical proof can be found in Appendix A.

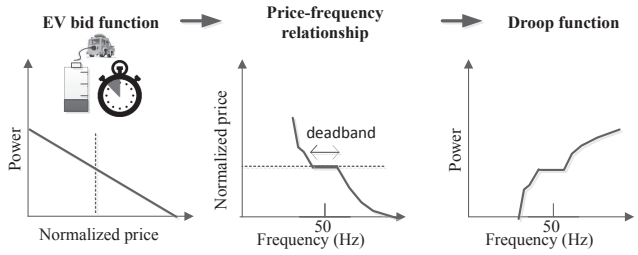

(a) The derived frequency droop function for an EV with a high and urgent need for energy.

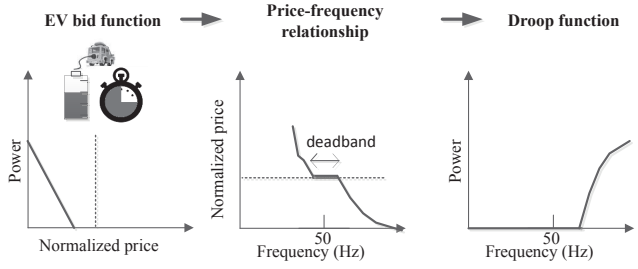

(b) The derived frequency droop function for an EV with a low need for energy.

Figure 7.5: The individual droop relationships for each device depends on their bid function. The price-frequency relationship is always equal for all loads of the cluster. The dotted line is the market price at 50 Hz.

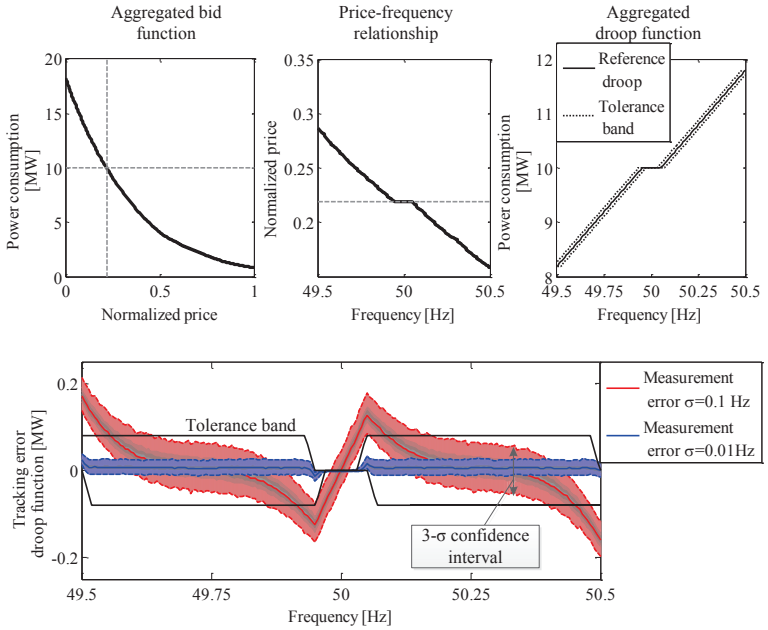

Figure 7.6: Influence of frequency measurement errors on the aggregated droop function.

7.3.4 Practical Considerations

The exchange of information between the different parties is presented in Fig. 7.7. The secondary control actions $R^{2,+/-}_{\mathbf{load}}$ are usually determined at a central dispatch centre, based on the Area Control Error (ACE) [183]. The control signals of the dispatch center are transmitted to the generating units and to the auctioneer agent. The auctioneer agent can adapt the price-frequency relation to comply with the requested action. The maximum amount of time that can elapse between the request from the TSO and the beginning of the response by the loads depends on the country and can range from a few seconds to 5 minutes [31]. Note that this system is perfectly suited for an event-driven implementation [164], where the price-frequency relationship gets updated after each request from the system operator.

The device agent locally measures the frequency, at a sample rate of the order of 1 kHz, and responds to the frequency according to the last received price-frequency relationship. Therefore, the devices can comply with the timing

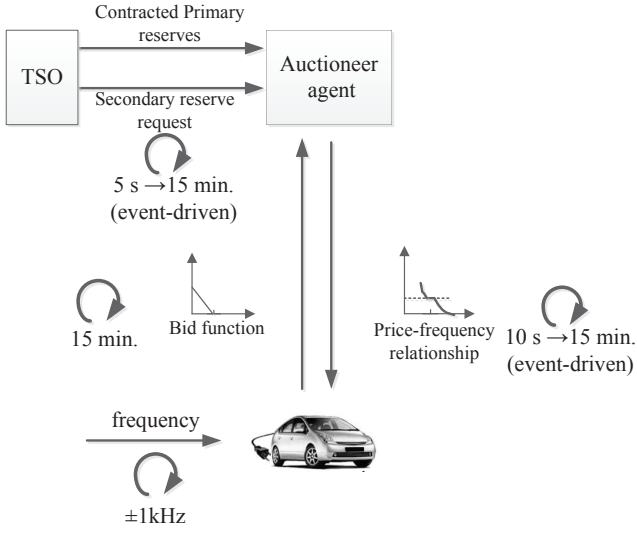

Figure 7.7: The interaction between the different agents. The concentrator agent is not presented.

requirements of the primary frequency reserves. The device agent updates his bid function every 15 minutes, to reflect its actual value for the available energy.

It is assumed that the customers are not billed the frequency-dependent price. In the auction-based market control of [151,164,167], the customers are also not billed the equilibrium price. Customers offering flexibility can be reimbursed for the offered flexibility, for the used flexibility, or by a yearly, fixed fee. The frequency-dependent price can, therefore, be interpreted as a control signal. This control signal guarantees that the necessary reserves are provided, while the total welfare of all devices remains maximal. The algorithm remains identical when the equilibrium price would be billed to the customer. One of the main criticisms with respect to these types of algorithms is the assumption that consumers are very sophisticated, to the level of being daily energy traders that are aware of their utility functions. When the price is not billed and the devices compose their utility function based on the heuristics described in section 7.2, this assumption is omitted.

7.4 Real-Time Planning of the Cluster Consumption

A load aggregator will try to use the available flexibility to maximize its profits during a whole day. It is, therefore, required to take into account future information when the actual cluster consumption is defined by the auctioneer agent. This is done by a rolling horizon control, as described in [151, 164, 167, 168, 184]. Further extensions are required to these frameworks to guarantee the availability of the contracted reserves.

This work focusses on the real-time decisions made concerning the real-time consumption of the loads and the activation of the contracted reserves. The day-ahead decisions are outside the scope of this work. The contracted primary $R^{1,+/-}_{\mathbf{load},t}$ and secondary $R^{2,+/-}_{\mathbf{load},t}$ reserve capacity and the planned day-ahead consumption P^{DA}_t are therefore assumed to be known, while the real-time consumption levels $P^{\mathbf{Load}}_t$ are optimized. Note that the actual cluster consumption can differ from the planned real-time consumption $P^{\mathbf{Load}}_t$ due to the activation of the contracted reserves.

The determination of a collective consumption plan for a cluster of aggregated loads is extensively discussed in [151, 164, 167, 168]. However, it will require several extensions to incorporate the activation of fast spinning reserves.

The objective of the load aggregator is to maximize his profits for the given period, by making a power consumption plan that respects the device limitations. The load aggregator is active on the real-time imbalance market. When the real-time consumption does not match the planned day-ahead consumption, an imbalance price is used by the TSO to calculate the reimbursement, or penalty, the aggregator receives. Activated reserves are not included in the calculation of the aggregator's imbalance. To increase his profits, the aggregator can consume less than the planned day-ahead consumption during a high positive imbalance price to receive a high reimbursement. The extra energy can be consumed during a low negative imbalance price, which will result in a small penalty. I.e. during an unexpected excess of wind power, the negative imbalance price can become zero. The objective of the aggregator that maximizes his profits on the imbalance market equals :

$$\max_{P^{\mathbf{Load}}_t} \quad \sum_{t=1}^{T} c^{+}_{imb,t} \left[P^{DA}_t - P^{\mathbf{Load}}_t\right]_+ \triangle t - c^{-}_{imb,t} \left[P^{\mathbf{Load}}_t - P^{DA}_t\right]_+ \triangle t \quad (7.8)$$

For a $\in \mathbb{R}$, [a]+ denotes the max[a, 0]

where $c^{-}_{imb,t}$ and $c^{+}_{imb,t}$ are the expected negative and positive real-time imbalance prices. The deviation is the difference between the day-ahead contract P^{DA}_t and real-time power demand $P^{\mathbf{Load}}_t$ at time step t. During each time period, the maximum consumption of the cluster is limited. The auctioneer agent makes an estimation of the minimum (P^{min}_t) and maximum power (P^{max}_t) the cluster of loads can consume each time step. Due to the repetitive behaviour of customers, these parameters can be estimated. The cluster of loads also has a limited amount of energy consumption. These limitations can be described by the flexibility bounds of the cluster E^{max} and E^{min}. E^{max} is defined as the accumulated energy if all loads were to start immediate consumption at maximum power and then idle, while E^{min} is when consumption is postponed by all loads as long as possible. The EVs and domestic water heaters send their individual flexibility bounds to the auctioneer agent [151, 164, 167, 168]. This way the auctioneer has historic information of daily flexibility bounds. The constraints describing the cluster limitations are, therefore:

$$P^{min}_t \leq P^{\mathbf{Load}}_t \leq P^{max}_t \tag{7.9}$$

$$E_{t+1} = E_t + P^{\mathbf{Load}}_t \triangle t \tag{7.10}$$

$$E^{min}_t \leq E_t \leq E^{max}_t \tag{7.11}$$

The previous control formulation, as described in [151, 164, 167, 168], does not incorporate the possible activation of contracted reserves. As was shown in Fig. 7.3, to be able to provide upward reserves, the cluster needs to consume a minimal amount of power, whereas downward reserves require the cluster to not consume the maximal amount of power. Besides that, when one MW is already contracted as a primary reserve capacity, it cannot be procured again as a secondary reserve. The consumption of the cluster $P^{\mathbf{Load}}_t$ is, therefore, bound by:

$$P^{min}_t \leq P^{\mathbf{Load}}_t - R^{1,+}_{\mathbf{load},t} - R^{2,+}_{\mathbf{load},t} \tag{7.12}$$

$$P^{\mathbf{Load}}_t + R^{1,-}_{\mathbf{load},t} + R^{2,-}_{\mathbf{load},t} \leq P^{max}_t \tag{7.13}$$

The amount of primary and secondary reserves that will be activated during the next time step is unknown. The sum of $R^{1,\pm}_{\mathbf{load},t} + R^{2,\pm}_{\mathbf{load},t}$ is, therefore, chosen to be equal to the amount of contracted reserves to guarantee their availability. The aggregated cumulated energy of the cluster depends on the activation of the reserves provided by the cluster and can be represented by two scenarios:

$$E^{+}_{t+1} = E^{+}_t + \left(P^{\mathbf{Load}}_t - R^{1,+}_{\mathbf{load},t} - R^{2,+}_{\mathbf{load},t}\right) \triangle t \tag{7.14}$$

$$E^{-}_{t+1} = E^{-}_t + \left(P^{\mathbf{Load}}_t + R^{1,-}_{\mathbf{load},t} + R^{2,-}_{\mathbf{load},t}\right) \triangle t \tag{7.15}$$

When no reserves are activated, the cumulated energy is noted as E_{t+1}. If all contracted upward reserves would be activated during the day, the cumulated energy would equal E^{+}_{t+1} and when all contracted downward reserves would be activated, the cumulated energy would equal E^{-}_{t+1}. These last two are the worst-case scenarios, whereas E_{t+1} can be considered as the expected scenario. For all possible scenarios, the cumulated energy is limited by the flexibility bounds of the cluster. This can be defined as:

$$E_t^{min} \leq E_t^{+} \tag{7.16}$$

$$E_t^{-} \leq E_t^{max} \tag{7.17}$$

Each quarter hour, the real-time power demand $P_t^{\mathbf{Load}}$ is recalculated to adapt to the new estimates of the cluster flexibility and the new predictions of the imbalance prices. The planning horizon shrinks, until a new clearing of the day-ahead market, as in [151]. Besides uncertainties on the cluster flexibility, the actual power consumption in the previous time step could be lower, or higher, due to the activation of reserves. This rolling horizon approach is presented in Fig. 7.8. Imbalance prices are assumed to be known in this work. To cope with the uncertainties regarding the predictions of the real-time imbalance prices, stochastic [185–187], or robust optimization techniques [185, 188], can be applied. In a stochastic optimization formulation, different possible price scenarios are taken into account, while in a robust optimization formulation, the price uncertainties will be described by uncertainty intervals. Including uncertainty on the real-time imbalance prices is outside the scope of this work.

By applying the heuristic of Fig. 7.2, the planned energy consumption for the actual time slot is distributed over the cluster of loads. As discussed in section 7.3, if secondary reserves are requested $R^{2,\pm}_{\mathbf{load},t}$, these should be added to the planned $P_t^{\mathbf{Load}}$. If primary reserves are contracted, the frequency-dependent price is formed. This control approach is presented in Fig. 7.9. One of the main advantages of this approach is its scalability: the computation of the path planning is independent of the total amount of loads.

7.5 Simulation Results

The proposed primary frequency method is tested on the test grid presented in Fig. 7.10. In this grid, there is a generating unit with a reheat steam turbine and a governor with droop action as defined in [183]. The turbine time constants are T_{RH}, T_{CH} and $F_{HP}T_{RH}$, the governor time constant is T_G, with a gain defined by R. M is double the inertia constant H and D is the load-damping constant. Typical values of these constants can be found in [183]. The droop

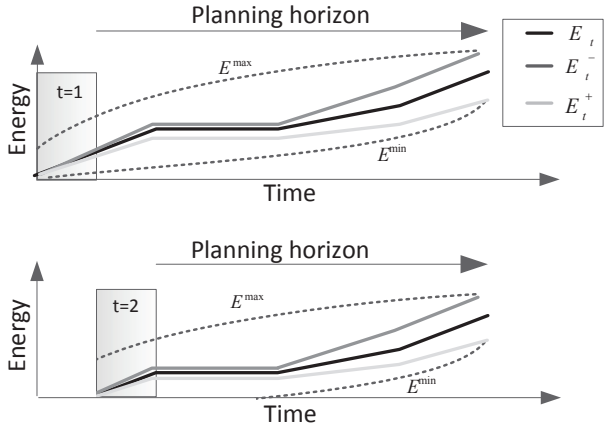

Figure 7.8: Rolling horizon cluster load control.

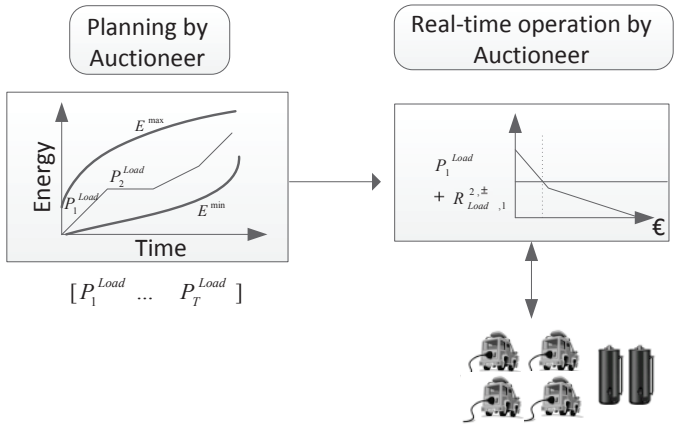

Figure 7.9: Planning the power consumption by the cluster of loads.

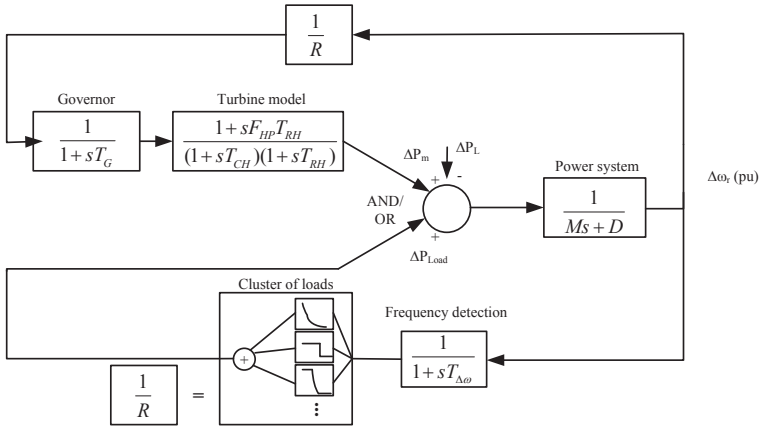

Figure 7.10: Block diagram of the simulated system.

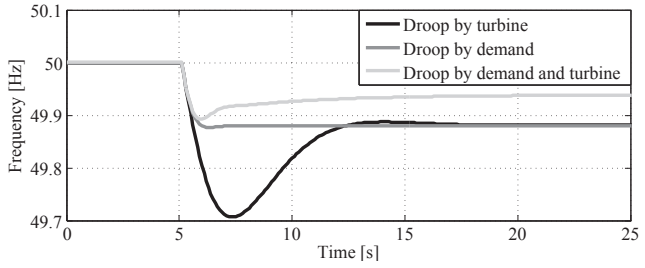

Figure 7.11: Frequency transient when 5% of generation is lost.

action by the reheat turbine can be turned off and replaced by a droop provided by the cluster of loads. Frequency detection by the devices is assumed to have a time constant $T_{\triangle\omega}$ equal to 0.2s [189]. It is assumed that a device can change its consumption level with a time constant lower than $T_{\triangle\omega}$, which is, therefore, not modelled. Note that the aggregator could also send-out a time constant larger than 0.2s to all devices to create a requested, first-order feedback loop. The droop constant of the reheat turbine is identical to the emulated droop constant by the cluster of loads and equals 0.05. Both types of control are compared in Fig. 7.11, where the system response is plotted when 5% of generation is lost. The steady-state frequency is identical, due to the identical droop constant, but the transient response differs. The cluster of loads has a fast response to the disturbance and, therefore, the frequency dip is less severe.

Fig. 7.12 plots the aggregated bid function, the applied price-frequency relationship and the price evolution during this simulation. Reserves were contracted from 49.8 Hz to 50.2 Hz, without a deadzone and an identical droop as the reheat steam turbine. In case the controllable demand is responsible for the primary frequency control, the price quickly increases to adapt the consumption of the controllable demand to the generation. The users have received the price-frequency relationship from the auctioneer agent, so there is no need to communicate this price in real-time. The users know the price, based on their frequency measurement. When both the turbine and the controllable demand take part in the frequency control, it can be seen that the price quickly rises, but starts to decrease after a few seconds. The turbine has a slower response, so it will take a few seconds before the turbine provides its share in the primary frequency control. Due to the fast response of the devices, the frequency drop is reduced. When the controllable demand is not used for frequency reserves, the price is independent of the frequency and remains constant during the frequency drop.

Note from Fig. 7.12 that replacing the only conventional generator responsible for primary frequency control completely by controllable demand would require a large amount of controllable demand. Therefore, the controllable demand will rather just be a part of the total primary reserves, where the fast response of the demand can reduce the frequency drop before slower conventional generators will help to restore the balance between generation and demand.

In a second simulation, the real-time planning of the cluster of loads is evaluated. 5000 EVs and 5000 electric water heaters are aggregated and are controlled by the multi-agent control framework. The maximum charging rate of the EVs is 3.3 kW. Their availability and energy consumption are modelled based on [129]. The electric domestic water heaters have a capacity of 200 l and a maximum power consumption level of 3.3 kW. Consumption data of the electric domestic water heaters was available from the LINEAR project [71]. The EVs make a linear bid to the auction-based market, whereas the heaters make a block bid. Each quarter hour, these bids are updated according to the state of the devices. Upward and downward reserves of 0.5 MW are contracted during the whole day, except from 10 AM to 4 PM. The Belgian imbalance prices of October 1st 2013 are applied, while the assumed, activated reserves are based on the net regulation volume of that day. In Belgium, the negative and positive imbalance prices $c^-_{imb,t}$ and $c^+_{imb,t}$ are often almost identical.

The determination of the collective consumption plan for the cluster of loads during the day is done with the rolling horizon control framework, described in section 7.4. Two consumption controllers are compared in Fig. 7.13: one takes into account the extra constraints (7.12)-(7.17) to guarantee the availability of the contracted reserves, while the other controller equals the one of [151, 164],

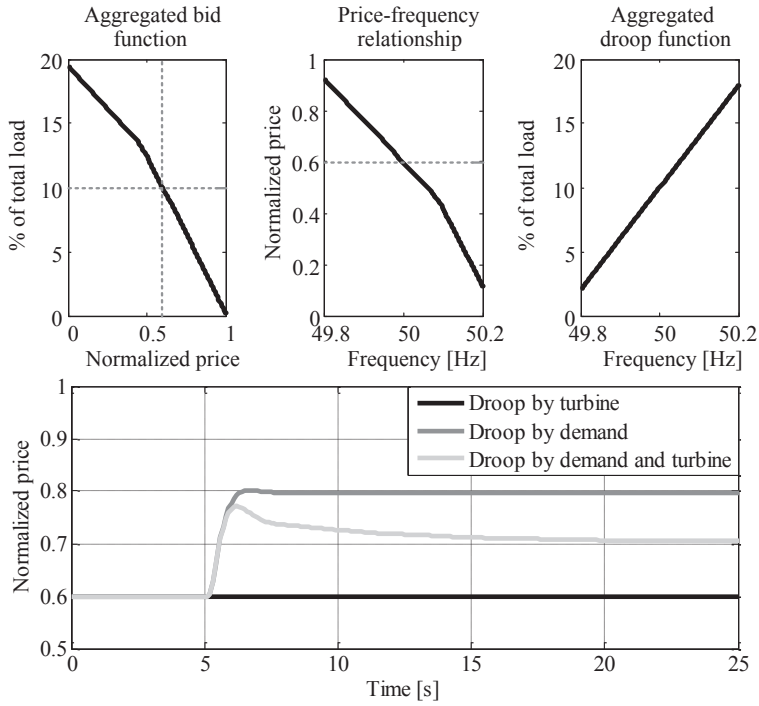

Figure 7.12: The evolution of the price signal to the users when 5% of generation is lost.

where reserve constraints are neglected. To maximize profits, both controllers try to generate a lower consumption than planned during high imbalance prices, while consumption is increased during low imbalance prices. The controller that neglects the reserve constraints can reduce the consumption to lower values, since it does not include a margin to provide upward reserves. Therefore, it often fails to provide the reserves requested by the system operator. When comparing the accumulated energy paths of both control approaches, it is clear that the controller that takes into account the reserve constraints operates less closely to the flexibility bounds of the cluster and is, therefore, able to provide the contracted reserves. The day-ahead planning for both consumption controllers was obtained by the method described in Appendix B, with the day-ahead prices of October 1st 2013.

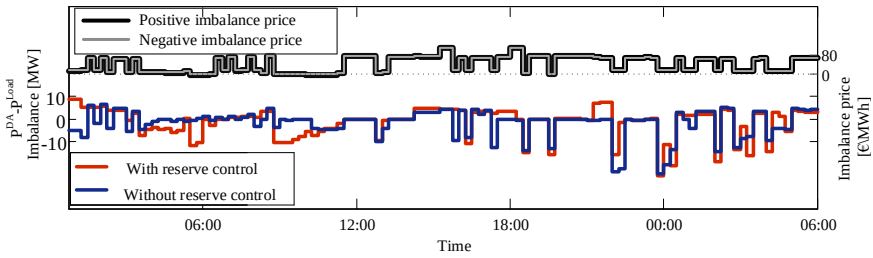

(a) To increase profits, the cluster of loads consumes less than the planned day-ahead profile during a high positive imbalance price and consumes more energy during a low negative imbalance price.

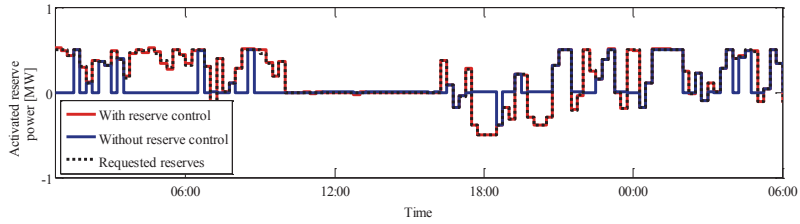

(b) The activated reserves and the tracking of these reserves are plotted. The reserves can often not be provided when they are not taken into account in the optimization formulation.

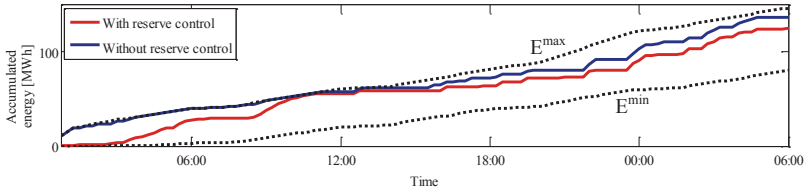

(c) The accumulated energy of the cluster of loads is plotted. The accumulated energy remains further from the flexibility bounds of the cluster of loads when reserves are taken into account. The contracted reserves can then always be provided in future time slots.

Figure 7.13: A simulation of one day of the real-time planning of the cluster of loads with and without reserve control.

7.6 Conclusion

A general, multi-agent framework, based on utility maximization, is proposed for frequency support by dynamic demand. The multi-agent controller consists of two parts. One part is responsible for the real-time operation, while the other part is responsible for a real-time planning of the consumption plan. It was shown that, when the algorithm activates primary and secondary reserves, the customer welfare remains maximal. Devices can identify their value of the received energy by making use of utility functions. With the proposed control framework, the primary and secondary frequency control by a conventional generator can be imitated. A rolling horizon control is applied to define a consumption plan that maximizes the load aggregators profits. The controller takes into account the contracted spinning reserves, to guarantee their availability in the future time periods.

Appendix A
Primary Frequency Support

The primary frequency support has a distributed optimization interpretation. The purpose of the primary load frequency support by dynamic demand is to eliminate the load-generation mismatch in the whole system, while maximizing system utility. This can be formulated as the following optimization problem:

$$\min_{P_h} \; -\sum_{h=1}^{N} U\left(P_h\right) + \lambda_m P_h \tag{7.18}$$

subject to

$$\sum_{h=1}^{N} P_h + P_{inel} = G;$$

where P_{inel} is the total load in the system, except the N devices participating in the frequency support and G is the total generated power. λ_m is the fixed market price for power at 50 Hz. The Lagrangian dual function of this problem is defined as:

$$\Lambda(\lambda_{freq}) = \min_{P_h} \; -\sum_{h=1}^{N} U\left(P_h\right) + \lambda_m P_h + \lambda_{freq}\left(\sum_{h=1}^{N} P_h + P_{inel} - G\right) \tag{7.19}$$

The maximization of the Lagrangian dual function is the dual problem. The dual problem can be solved by a dual ascent procedure [182] to find the optimal

lagrange multiplier λ^*_{freq} of the dual problem, which is the price that would eliminate the supply-demand imbalance. This method, however, requires that each device knows the system transfer function to estimate the supply-demand imbalance [182]. This is avoided in our work. The optimal lagrange multiplier λ^*_{freq} will be found by the frequency-dependent pricing described in section 7.3.3.

The supply-demand imbalance $\left(\sum_{h=1}^{N} P_h + P_{inel} - G\right)$ is a subgradient of the dual problem. If this subgradient is zero, the concave, unconstrained, dual problem is solved.

The frequency deviation $\frac{\Delta\omega^k - \Delta\omega^{k-1}}{\Delta t}$ is a measure of the supply-demand imbalance. When the frequency deviation converges to zero, the supply-demand imbalance is zero. A stable frequency can only be obtained when the supply-demand imbalance is zero, as otherwise an excess, or lack, of energy in the system would increase, or decrease, the speed of the generators. So, a stable frequency implies a supply-demand imbalance of zero and, therefore, the subgradient of the dual problem is zero. Therefore, if the frequency-dependent price of section 7.3.3 results in a stable power system, the frequency deviation will become zero and the concave, unconstrained, dual problem is solved. Customers respond to a price signal, independent of the way the price is obtained, so the price that results in a supply-demand imbalance of zero obtained with the dual ascent method of [182] is identical to the frequency-dependent price that results in a supply-demand imbalance of zero, obtained by the method of Section 7.3.3. I.e. if there is an excess of 1MW generation that needs to be consumed by the cluster of controllable loads, there can be only one price that results in an extra consumption of 1MW by this cluster. This stable frequency-dependent price is the optimal lagrange multiplier λ^*_{freq}.

The main advantage of the pricing method described in Section 7.3.3 is that the devices don't need to have knowledge about the system transfer functions. Besides that, the customers don't need to perform an iterative price update, but the price is directly linked to the measured frequency. Therefore, the required local intelligence reduces. Finally, analysing the stability is easy, as the aggregated demand behaves as a conventional generator.

Appendix B
Day-Ahead Planning

The day-ahead objective of the aggregator is to minimize its costs for providing the necessary energy:

$$\min_{P_t^{DA}} \sum_{t=1}^{T} c_t^{DA} P_t^{DA} \triangle t \tag{7.20}$$

where c_t^{DA} is the expected day-ahead price at time step t. The amount of power that can be consumed each time step P_t^{DA} is limited and can be defined based on historical information of daily flexibility bounds [151, 164, 167, 168]. The cluster limitations are:

$$P_t^{min} \leq P_t^{DA} \leq P_t^{max} \tag{7.21}$$

$$E_{t+1} = E_t + P_t^{DA} \triangle t \tag{7.22}$$

$$E_t^{min} \leq E_t \leq E_t^{max} \tag{7.23}$$

If the aggregator has contracted reserves, these should be included in the cluster limitations.

$$P_t^{min} \leq P_t^{DA} - R_{contr,t}^{1,+} - R_{contr,t}^{2,+} \tag{7.24}$$

$$P_t^{DA} + R_{contr,t}^{1,-} + R_{contr,t}^{2,-} \leq P_t^{max} \tag{7.25}$$

$$E_{t+1}^{+} = E_t^{+} + \left(P_t^{DA} - R_{contr,t}^{1,+} - R_{contr,t}^{2,+}\right) \triangle t \tag{7.26}$$

$$E_{t+1}^{-} = E_t^{-} + \left(P_t^{DA} + R_{contr,t}^{1,-} + R_{contr,t}^{2,-}\right) \triangle t \tag{7.27}$$

$$E_t^{min} \leq E_t^{+} \tag{7.28}$$

$$E_t^{-} \leq E_t^{max} \tag{7.29}$$

Similar to the extra constraints of section 7.4, the aggregator should limit the consumption in order to be able to provide the contracted reserves $R_{contr,t}^{1,2,\pm}$. Also, the aggregated cumulated energy of the cluster, in case all upward or downward reserves would be activated, is limited by the flexibility bounds of the cluster.

The required primary and secondary reserves are often guaranteed by long-term contracts in Europe [190, 191] and are, therefore, not considered to be variables

in this work. The time of the day that reserves are contracted will have an impact on the profit of the aggregator, i.e. the minimum consumption, to be able to provide upward reserves during peak periods, can have a high cost. Future and ongoing work will focus on the day-ahead market decisions and the long-term contracts. The day-ahead planning can be further improved by taking into account the expected percentage of up, or down, regulation of each hour, which can be extracted from historical data [192].

Chapter 8

General Conclusions and Future Work

This chapter presents the main conclusions and contributions of this thesis and emphasizes possible tracks for future research.

8.1 Overview and Conclusions

This dissertation deals with different grid-supporting control strategies by distributed generation and residential demand. The increasing amount of PV generation connected to the distribution grid will change the state of the grid. The energy flows in distribution grids will become bidirectional. Furthermore, EVs are gaining popularity and the charging of EVs can lead to large and undesirable peaks in the electrical consumption. In the Linear project, our research group has carefully analysed the impact of both PVs and EVs on the power quality. It is clear from this previous research that, to ensure an acceptable power quality, measures will have to be taken. Therefore, in this work, we have analysed the properties of unbalanced distribution grids to which PV panels and EVs are connected in detail. This is the basis for developing new strategies to guarantee a successful grid integration.

The increasing amount of distributed generation and the increasing number of electric vehicles is, however, not the only upcoming revolution in the electricity grid. The introduction of an automatic metering infrastructure will further change the operation of the grid. A two-way, digital communication technology

will make it possible to interact with different devices installed in the grid. Each device on the network can be given sensors to gather data. This data will be giving new insights in the operation and control of the network. The number of possible applications that can be deployed, once the two-way communication infrastructure is installed, is growing fast as well. Advanced modelling and control will be part of the main features of the smart grid. Therefore, we have analysed different modelling and control methods that will work with the available data of the new sensors in the network. First of all, we have improved the modelling of low voltage distribution grids, based on grid measurements. After that, different control strategies are presented for both single-phase and three-phase PV units and EVs. These strategies will make use of the two-way communication infrastructure.

The main contributions of the work can be summarized as follows:

- A detailed analysis and an improved modelling of three-phase, four-wire, distribution grids
- Control rules for both single-phase and three-phase PV units and loads have been designed specifically for three-phase, four-wire, distribution grids
- Development of a real-time pricing scheme to mitigate voltage problems in distribution grids
- The extension of a multi-agent auction-based demand response system to provide voltage control and frequency control

The conclusions and contributions of each chapter are summarized below.

In **Chapter 2**, the effect of realistic uncertainties on cable lengths and load models to the outcome of a grid simulation was investigated. In the literature, accurate grid topology data is assumed to be available. However, this data is typically inaccurate, incomplete, or even missing. As an alternative to composing a grid model based on grid topology data, we have shown that it is possible to train an accurate grid model based on historical smart meter data. The errors made by this trained model remain sufficiently small. The model can adapt to different grid loading levels. It also automatically identifies the phase of connection of each customer. Furthermore, the algorithm has been verified in a practical laboratory grid and we have verified that the grid model can be used in a voltage management strategy with real-life conditions.

In **Chapter 3**, a careful analysis has been made of the effect that reactive power has on unbalanced distribution grids. In the literature, different, local control rules for reactive power have been applied to single-phase networks. These rules have been tested for unbalanced, three-phase, four-wire grids. In many parts of

the world (including Australia, Asia, Europe, and Africa), distribution networks are of the three-phase, four-wire type. We showed that the neutral point shifting effect requires special care for active and reactive voltage control in unbalanced networks. To improve the local control rules, we defined a formulation to optimize them. We define a local control rule, that is a function of the produced PV power, by a first order spline. The parameters of all of the splines are regularly retuned by a central convex optimization program. This is the first time that an efficient formulation for the tuning of local control rules has been presented in the literature.

In **Chapter 4**, a phase balancing mechanism is proposed. Balanced, three-phase, four-wire distribution grids can host significantly more distributed generation and electric vehicles. Both off-board three-phase EV chargers and three-phase PV units can be adapted to balance a three-phase, four-wire, distribution grid. Grid conditions will be improved by absorbing power from a phase with a lower loading and injecting this power into the phase with the highest loading. We accurately analysed the maximum amount of possible improvements of component loading, voltage unbalance, grid voltages and grid losses for a specific grid. This benchmark has been compared with a local control rule, which has been defined to facilitate a practical implementation.

In **Chapter 5**, a locational pricing strategy has been presented to mitigate voltage problems caused by a high penetration of PV in distribution networks. An alternative method for the DSO to control the grid voltage is to give a real-time, financial incentive to a customer to adapt its consumption, or to reduce the power injection by PV units. An iterative gradient algorithm is used to define the prices that result in acceptable grid voltages at a minimum cost. The algorithm has been applied to three-phase, four-wire, distribution grids. It was shown that, due to the unbalanced nature of these grids, prices will have to differ between phases to effectively control the grid voltage. We have analysed the effect of reactive voltage control and phase balancing on the necessary incentive the DSO has to give to control the grid voltage. We showed that both reactive voltage control and phase balancing will significantly reduce the necessary incentive and will decrease the network price volatility.

In **Chapter 6**, a multi-agent auction-based demand response system, developed at VITO, was investigated and improved. First of all, a mathematical framework was created to analyse the properties of the algorithm and compare it with other systems. The algorithm was extended with reactive power control and the possibility to take into account distribution grid voltage limits and transformer overloading. Special attention was given to the neutral point shifting effect. We proved that the algorithm has significantly lower requirements for the communication overhead, compared to other implementations. It also reduces the required computational power at the device level, compared to other

implementations.

Finally, in **Chapter 7**, the multi-agent, auction-based demand response algorithm of Chapter 6 was further extended to participate in frequency control, while the low communication overhead remained. As discussed in the literature, residential demand can make a significant and reliable contribution to frequency control. Different systems have been proposed before in the literature. The advantages of our extension to the multi-agent algorithm are numerous compared to previously discussed methods. First of all, a general framework is used to include comfort settings. It is important that the frequency control by residential demand has a minimal impact on customer comfort. Secondly, the primary frequency response of a conventional generator can be imitated. Besides that, our system is able to cope with both primary and secondary frequency control at the same time. Finally, the contracted spinning reserves are guaranteed to be available.

The multi-agent auction-based demand response algorithm that was extended in Chapters 6 and 7 can be combined with the methods described in Chapter 3 and 4. The real-time, locational pricing strategy of Chapter 5 is an alternative method that tries to control loads and distributed generation by locational prices. It can not be combined with the other methods.

8.2 Future Work

An important aspect of scientific research is the validation and valorization of the newly-proposed methods and ideas. Therefore, these are part of the main recommended future activities. Validation is a challenging task. A large grid needs to be available to test the methods in real-life conditions. The different developed control algorithms have been tested whenever possible. However, more tests are needed. To valorize the proposed ideas, a thorough economical analysis is necessary. By means of a close cooperation with system operators, the actual value of the provided grid services will have to be defined. Investment costs and operation costs will also have to be analysed. Algorithms might have to be adapted when taking into account these costs.

Many of the developed algorithms rely on communication. An important aspect of a practical implementation is defining the best-suited communication infrastructure. Central and optimal algorithms become more feasible when communication between different agents is fast, cheap and with a large communication channel capacity. On the other hand, when the communication channel has strict limitations, local control algorithms will be preferred. An

important research track is, therefore, to evaluate different current and future communication standards that might be used in the smart grid.

The communication requirements for the proposed network support algorithms are similar to the requirements for demand response programs. The implementations will use more modern communication technologies, such as broadband communication (via cable, DSL, fiber, etc.), or next-generation cellular communication such as LTE or WiMAX. Such technologies allow for two-way communication and the implementation of more time-sensitive applications [193]. Communication could be passed along to the in-home network, that distributes commands to appliances and devices. An important aspect of the communication technology will be limited and consistent latency. If the delay is high, the performance of the control algorithms will deteriorate, as it takes more time to adapt to changing conditions in the network. The required bandwidth is limited, as the messages that need to be exchanged are small.

Several aspects of the described control strategies in the different chapters can be explored. Further recommendations follow from the conclusions of the different chapters:

- The grid identification method, described in **Chapter 2**, can be further extended. The method described in this chapter assumes that a complete data set of smart meter data is available for every household. In reality, smart meter data of some customers can be missing for short periods of time. Missing data arises in almost all serious statistical analyses and, therefore, different techniques have been developed to cope with this issue [194]. The process of replacing missing data with substituted values is called data imputation.
  To compute a grid model, the system operator needs to collect all of the historic information on each household. This data can reveal their daily routines, which can be valuable information for third parties. Some customers might not agree with this information sharing. Distributed algorithms can be applied to resolve this issue. By an iterative exchange of messages, they can train the model without having access to the historic load profile data. Further research could consist of selecting the best distributed algorithm for this purpose.
  Finally, the method described in Chapter 2 was tested in real life, in a small laboratory grid with 6 households. Further research should include a test in real life, in a large distribution grid with at least 50 households.
- An algorithm that optimizes local control functions of PV inverters was presented in **Chapter 3**. It can be investigated how often the local control parameters have to be adapted. I.e. local control parameters can be tuned for a whole week to avoid overvoltage. The amount of communication is

decreased, in expense of reduced performance. The algorithm was limited to local control rules that define their output, based on the produced active power. A local control function that depends on the measured voltage magnitude is one of the most popular local control rules. Optimizing these local control rules would be an interesting research direction.

- **Chapter 4** describes the use of a balancing inverter to transfer power from one phase to another. The most important track of future research is developing a prototype and testing it under different circumstances. New control algorithms will have to be implemented, with special care for the DC-bus voltage control. This prototype should then be tested in real life conditions, like in the Vito HomeLab. The optimal location of a balancing inverter should be analysed. A rule of thumb can be defined for the system operator, to easily define the best location, without having to simulate each grid. Finally, an economical evaluation will have to be made. The system operator will have to reimburse the customers that install a balancing inverter, or charger, for the increased cost of the installation. Defining the exact compensation method is a challenging task. The system operator will have to analyse the exact benefits of this system, compared to classic methods, such as grid reinforcement.

- The locational pricing strategy of **Chapter 5** gives incentives for flexible loads and PV units to adapt their consumption. The flexible loads were assumed to have a continuous behavior. However, some flexible loads, like white good appliances, can only be turned on or off. This might create difficulties to converge to a final, fixed price. Further research should analyse the behavior of these white good appliances under the proposed pricing scheme and adapt the price update rule, if necessary, to guarantee convergence of the network price.

- The multi-agent algorithm of **Chapter 6** takes into account network limits in a single-aggregator setting. Only one load aggregator controls the different devices. An interesting future research track is to analyse how this method can be extended to cope with multiple aggregators that are active in the same distribution network. To reduce the communication overhead of the implementation and improve the response time to variations in the grid, an event-driven implementation can be analysed.

- In **Chapter 7**, a method is described to activate primary and secondary frequency reserves with active demand. The algorithm ensures that the contracted reserves can be provided. The algorithm is limited to the intra-day decisions. An important aspect, in practice, would be the contracting of these reserves. Future research should optimize the contracted amount of reserves, at each moment, provided by dynamic demand.

The developed algorithm can also be extended to provide virtual inertia in a controlled manner with residential demand response. The amount of rotational inertia in the grid is expected to decrease. This inertia limits and dampens the grid frequency variations. The power electronic interface of EVs can quickly respond to frequency deviations, providing a form of virtual inertia. The developed algorithm can be used to exactly mimic the inertia of a big, synchronous generator with a fleet of EVs and can guarantee the availability of this virtual inertia.

Bibliography

[1] G. Pepermans, J. Driesen, D. Haeseldonckx, R. Belmans, and W. D'haeseleer, "Distributed generation: definition, benefits and issues," *Energy Policy*, vol. 33, no. 6, pp. 787 – 798, 2005. [Online]. Available: http://www.sciencedirect.com/science/article/pii/S0301421503003069

[2] Elia, "Voorspellingen en gerealiseerde productie windvermogen/PV-zonnevermogen," Tech. Rep., Nov. 2014. [Online]. Available: http://www.elia.be/nl/grid-data/productie/

[3] VREG, "Evolutie van het aantal zonnepanelen en hun vermogen," Tech. Rep., Nov. 2014. [Online]. Available: http://www.vreg.be/sites/default/files/uploads/evolutie_aantal_panelen_en_vermogen.pdf

[4] J. Lopes, F. Soares, and P. Almeida, "Integration of electric vehicles in the electric power system," *Proc. of the IEEE*, vol. 99, no. 1, pp. 168 –183, jan. 2011.

[5] N. Leemput, J. Van Roy, F. Geth, P. Tant, B. Claessens, and J. Driesen, "Comparative analysis of coordination strategies for electric vehicles," in *Innovative Smart Grid Technologies (ISGT Europe), Manchester*, Dec 2011, pp. 1–8.

[6] J. Carrasco, L. Franquelo, J. Bialasiewicz, E. Galvan, R. Guisado, M. Prats, J. Leon, and N. Moreno-Alfonso, "Power-electronic systems for the grid integration of renewable energy sources: A survey," *IEEE Trans. on Ind. Electronics*, vol. 53, no. 4, pp. 1002–1016, Jun 2006.

[7] H. Gharavi and R. Ghafurian, "Smart grid: The electric energy system of the future," *Proc. of the IEEE*, vol. 99, no. 1, pp. 917–921, Jun. 2011.

[8] P. Jahangiri and D. Aliprantis, "Distributed volt/var control by PV inverters," *IEEE Trans. on Power Syst.*, vol. 28, no. 3, pp. 3429–3439, Aug 2013.

[9] E. Caamano, J. Thornycroft, H. D. Moor, S. Cobben, M. Jantsch, T. Erge, H. Laukamp, D. Suna, and B. Gaiddon, "Wp4.1 state-of-the-art on dispersed PV power generation: Publications review on the impacts of PV distributed generation and electricity networks," PV upscale project, Tech. Rep., 2007.

[10] G. Mokhtari, A. Ghosh, G. Nourbakhsh, and G. Ledwich, "Smart robust resources control in LV network to deal with voltage rise issue," *IEEE Trans. on Sust. Energy*, vol. 4, no. 4, pp. 1043–1050, Oct. 2013.

[11] F. Shahnia, P. Wolfs, and A. Ghosh, "Voltage unbalance reduction in low voltage feeders by dynamic switching of residential customers among three phases," *IEEE Trans. Smart Grid*, vol. 5, no. 3, pp. 1318–1327, May 2014.

[12] L. Degroote, B. Renders, B. Meersman, and L. Vandevelde, "Neutral-point shifting and voltage unbalance due to single-phase DG units in low voltage distribution networks," in *PowerTech, 2009 IEEE Bucharest.* IEEE, 2009, pp. 1–8.

[13] F. Shahnia, R. Majumder, A. Ghosh, G. Ledwich, and F. Zare, "Sensitivity analysis of voltage imbalance in distribution networks with rooftop PVs," in *Proc. IEEE Power and Energy Society General Meeting*, 2010, pp. 1–8.

[14] C. Gonzalez, J. Geuns, S. Weckx, T. Wijnhoven, P. Vingerhoets, T. De Rybel, and J. Driesen, "LV distribution network feeders in Belgium and power quality issues due to increasing PV penetration levels," in *3rd IEEE PES Innovative Smart Grid Technologies Conf.*, Berlin, Germany, Oct 14-17 2012.

[15] F. Shahnia, A. Ghosh, G. Ledwich, and F. Zare, "Voltage unbalance sensitivity analysis of plug-in electric vehicles in distribution networks," in *Universities Power Engineering Conf. (AUPEC), 2011 21st Australasian*, Sept 2011, pp. 1–6.

[16] NEN-EN50160, "Voltage characteristics of electricity supplied by public electricity networks," 2010.

[17] K. Brekke, "European energy regulators' view on en 50160 and highlights of the 4th ceer benchmarking report on quality of electricity supply," in *Electricity Distribution - Part 2, 2009. CIRED 2009. The 20th International Conference and Exhibition on*, Jun 2009, pp. 1–30.

[18] S. Weckx, C. Gonzalez de Miguel, T. De Rybel, and J. Driesen, "LS-SVM-based on-load tap changer control for distribution networks with rooftop PVs," in *Innovative Smart Grid Technologies (ISGT Europe), Copenhagen*, Oct 2013, pp. 1–5.

[19] J.-H. Choi and J.-C. Kim, "Advanced voltage regulation method of power distribution systems interconnected with dispersed storage and generation systems," *IEEE Trans. on Power Del.*, vol. 16, no. 2, pp. 329–334, Apr 2001.

[20] P. Ramaswamy and G. Deconinck, "Smart grid reconfiguration using simple genetic algorithm and NSGA-II," in *Innovative Smart Grid Technologies (ISGT Europe), Berlin*, Oct 2012, pp. 1–8.

[21] P. C. Ramaswamy, "Reconfiguration of electricity distribution grids with distributed energy resources," Ph.D. dissertation, KULeuven, Leuven, 2014. [Online]. Available: https://lirias.kuleuven.be/handle/123456789/468940

[22] R. Tonkoski, L. A. Lopes, and T. H. El-Fouly, "Coordinated active power curtailment of grid connected PV inverters for overvoltage prevention," *IEEE Trans. Sust. Energy*, vol. 2, no. 2, pp. 139–147, 2011.

[23] F. Geth, N. Leemput, J. Van Roy, J. Buscher, R. Ponnette, and J. Driesen, "Voltage droop charging of electric vehicles in a residential distribution feeder," in *Innovative Smart Grid Technologies (ISGT Europe), Berlin*, Oct 2012, pp. 1–8.

[24] R. Tonkoski, L. Lopes, and T. El-Fouly, "Droop-based active power curtailment for overvoltage prevention in grid connected PV inverters," in *Industrial Electronics (ISIE), 2010 IEEE International Symposium on*, July 2010, pp. 2388–2393.

[25] K. Turitsyn, P. Sulc, S. Backhaus, and M. Chertkov, "Options for control of reactive power by distributed photovoltaic generators," *Proc. of the IEEE*, vol. 99, no. 6, pp. 1063–1073, 2011.

[26] E. Demirok, P. Casado Gonzalez, K. H. Frederiksen, D. Sera, P. Rodriguez, and R. Teodorescu, "Local reactive power control methods for overvoltage prevention of distributed solar inverters in low-voltage grids," *IEEE J. Photovolt.*, vol. 1, no. 2, pp. 174–182, Oct. 2011.

[27] E. Dall'Anese, S. Dhople, and G. Giannakis, "Optimal dispatch of photovoltaic inverters in residential distribution systems," *IEEE Trans. on Sust. Energy*, vol. 5, no. 2, pp. 487–497, April 2014.

[28] F. Geth, "Battery energy storage systems and distribution grid support," Ph.D. dissertation, KULeuven, Leuven, 2014. [Online]. Available: https://lirias.kuleuven.be/handle/123456789/457524

[29] M. Albadi and E. El-Saadany, "Demand response in electricity markets: An overview," in *Power Engineering Society General Meeting, 2007. IEEE*, Jun 2007, pp. 1–5.

[30] Elia, "What is an ARP?" Tech. Rep., Jan. 2014. [Online]. Available: http://www.elia.be/en/products-and-services/balance/process

[31] Y. Rebours, D. Kirschen, M. Trotignon, and S. Rossignol, "A survey of frequency and voltage control ancillary services part i: Technical features," *IEEE Trans. on Power Syst.*, vol. 22, no. 1, pp. 350–357, Feb 2007.

[32] Elia, "Evolution of ancillary services needs to balance the belgian control area towards 2018," Tech. Rep., May 2013. [Online]. Available: http://www.elia.be/~/media/files/Elia/Grid-data/Balancing/Reserves-study-2018.pdf

[33] K. De Vos, A. G. Petoussis, J. Driesen, and R. Belmans, "Revision of reserve requirements following wind power integration in island power systems," *Renewable Energy*, vol. 50, pp. 268–279, 2013.

[34] H. Holttinen, "Impact of hourly wind power variations on the system operation in the Nordic countries," *Wind Energy*, vol. 8, no. 2, pp. 197–218, 2005. [Online]. Available: http://dx.doi.org/10.1002/we.143

[35] P. A. Østergaard, "Geographic aggregation and wind power output variance in Denmark," *Energy*, vol. 33, no. 9, pp. 1453 – 1460, 2008. [Online]. Available: http://www.sciencedirect.com/science/article/pii/S0360544208001187

[36] A. Molina-Garcia, F. Bouffard, and D. Kirschen, "Decentralized demand-side contribution to primary frequency control," *IEEE Trans. on Power Syst.*, vol. 26, no. 1, pp. 411 –419, Feb. 2011.

[37] Eurelectric, "Ancillary services - full report," 2004.

[38] F. Tamp and P. Ciufo, "A sensitivity analysis toolkit for the simplification of mv distribution network voltage management," *IEEE Trans. on Smart Grid*, vol. 5, no. 2, pp. 559–568, March 2014.

[39] M. Baran and I. El-Markabi, "A multiagent-based dispatching scheme for distributed generators for voltage support on distribution feeders," *IEEE Trans. Power Syst.*, vol. 22, no. 1, pp. 52–59, Feb 2007.

[40] G. Mokhtari, G. Nourbakhsh, and A. Ghosh, "Smart coordination of energy storage units (ESUs) for voltage and loading management in distribution networks," *IEEE Trans. Power Syst.*, vol. 28, no. 4, pp. 4812–4820, Nov 2013.

[41] P. Richardson, D. Flynn, and A. Keane, "Optimal charging of electric vehicles in low-voltage distribution systems," *IEEE Trans. Power Syst.*, vol. 27, no. 1, pp. 268–279, 2012.

[42] M. Nick, R. Cherkaoui, and M. Paolone, "Optimal allocation of dispersed energy storage systems in active distribution networks for energy balance and grid support," *IEEE Trans. Power Syst.*, vol. 29, no. 5, pp. 2300 – 2310, 2014.

[43] F. Marra, G. Yang, C. Traeholt, E. Larsen, J. Ostergaard, B. Blazic, and W. Deprez, "EV charging facilities and their application in LV feeders with photovoltaics," *IEEE Trans. Smart Grid*, vol. 4, no. 3, pp. 1533–1540, Sept 2013.

[44] A. Keane and M. O'Malley, "Optimal allocation of embedded generation on distribution networks," *IEEE Trans. Power Syst.*, vol. 20, no. 3, pp. 1640–1646, Aug 2005.

[45] D. Popovic, J. Greatbanks, M. Begovic, and A. Pregelj, "Placement of distributed generators and reclosers for distribution network security and reliability," *Int. J. of Electrical Power and Energy Systems*, vol. 27, no. 5?6, pp. 398 – 408, 2005.

[46] G. Valverde and T. Van Cutsem, "Model predictive control of voltages in active distribution networks," *IEEE Trans. Smart Grid*, vol. 4, no. 4, pp. 2152–2161, Dec 2013.

[47] F. Milano and O. Hersent, "Optimal load management with inclusion of electric vehicles and distributed energy resources," *IEEE Trans. on Smart Grid*, vol. 5, no. 2, pp. 662–672, March 2014.

[48] L. Yu, D. Czarkowski, and F. de Leon, "Optimal distributed voltage regulation for secondary networks with DGs," *IEEE Trans. on Smart Grid*, vol. 3, no. 2, pp. 959–967, Jun 2012.

[49] P. Richardson, D. Flynn, and A. Keane, "Local versus centralized charging strategies for electric vehicles in low voltage distribution systems," *IEEE Trans. Smart Grid*, vol. 3, no. 2, pp. 1020 –1028, Jun 2012.

[50] S. Weckx, C. Gonzalez de Miguel, and J. Driesen, "Combined central and local active and reactive power control of PV inverters," *IEEE Trans. Sust. Energy*, vol. 5, no. 3, pp. 776–784, July 2014.

[51] Q. Zhou and J. Bialek, "Generation curtailment to manage voltage constraints in distribution networks," *Generation, Transmission Distribution, IET*, vol. 1, no. 3, pp. 492–498, May 2007.

[52] A. Borghetti, M. Bosetti, S. Grillo, S. Massucco, C. Nucci, M. Paolone, and F. Silvestro, "Short-term scheduling and control of active distribution systems with high penetration of renewable resources," *Systems Journal, IEEE*, vol. 4, no. 3, pp. 313–322, Sept 2010.

[53] P. Pachanapan, O. Anaya-Lara, A. Dysko, and K. Lo, "Adaptive zone identification for voltage level control in distribution networks with DG," *IEEE Trans. on Smart Grid*, vol. 3, no. 4, pp. 1594–1602, Dec 2012.

[54] S. Weckx, J. Driesen, and R. D'hulst, "Optimal real-time pricing for unbalanced distribution grids with network constraints," in *Power and Energy Society General Meeting (PES), 2013 IEEE*, July 2013, pp. 1–5.

[55] A. Samadi, R. Eriksson, L. Soder, B. Rawn, and J. Boemer, "Coordinated active power-dependent voltage regulation in distribution grids with PV systems," *IEEE Trans. Power Del.*, vol. 29, no. 3, pp. 1454–1464, Jun 2014.

[56] M. A. Kashem and G. Ledwich, "Distributed generation as voltage support for single wire earth return systems," *IEEE Trans. Power Del.*, vol. 19, no. 3, pp. 1002–1011, July 2004.

[57] B. Robbins, C. Hadjicostis, and A. Dominguez-Garcia, "A two-stage distributed architecture for voltage control in power distribution systems," *IEEE Trans. Power Syst.*, vol. 28, no. 2, pp. 1470–1482, May 2013.

[58] V. Calderaro, G. Conio, V. Galdi, G. Massa, and A. Piccolo, "Optimal decentralized voltage control for distribution systems with inverter-based distributed generators," *IEEE Trans. Power Syst.*, vol. 29, no. 1, pp. 230–241, Jan 2014.

[59] Q. Zhou and J. Bialek, "Simplified calculation of voltage and loss sensitivity factors in distribution networks," in *Proc. of the 16th Power Systems Computation Conference (PSCC2008), Glasgow, Scotland*, 2008.

[60] D. Khatod, V. Pant, and J. Sharma, "A novel approach for sensitivity calculations in the radial distribution system," *IEEE Trans. on Power Delivery*, vol. 21, no. 4, pp. 2048–2057, Oct 2006.

[61] C. Cheng and D. Shirmohammadi, "A three-phase power flow method for real-time distribution system analysis," *IEEE Trans. on Power Syst.*, vol. 10, no. 2, pp. 671 –679, may 1995.

[62] K. Christakou, J. LeBoudec, M. Paolone, and D.-C. Tomozei, "Efficient computation of sensitivity coefficients of node voltages and line currents in unbalanced radial electrical distribution networks," *IEEE Trans. on Smart Grid*, vol. 4, no. 2, pp. 741–750, Jun 2013.

[63] I. Dzafic, R. Jabr, E. Halilovic, and B. Pal, "A sensitivity approach to model local voltage controllers in distribution networks," *IEEE Trans. Power Syst.*, vol. 29, no. 3, pp. 1419–1428, May 2014.

[64] M. Brenna, E. De Berardinis, L. Delli Carpini, F. Foiadelli, P. Paulon, P. Petroni, G. Sapienza, G. Scrosati, and D. Zaninelli, "Automatic distributed voltage control algorithm in smart grids applications," *IEEE Trans. on Smart Grid*, vol. 4, no. 2, pp. 877–885, Jun 2013.

[65] J. Marti, H. Ahmadi, and L. Bashualdo, "Linear power-flow formulation based on a voltage-dependent load model," *IEEE Trans. on Power Del.*, vol. 28, no. 3, pp. 1682–1690, July 2013.

[66] L. Marron, X. Osorio, A. Llano, A. Arzuaga, and A. Sendin, "Low voltage feeder identification for smart grids with standard narrowband PLC smart meters," in *Power Line Communications and Its Applications (ISPLC), 2013 17th IEEE International Symposium on*, March 2013, pp. 120–125.

[67] H. Pezeshki and P. Wolfs, "Consumer phase identification in a three phase unbalanced LV distribution network," in *Innovative Smart Grid Technologies (ISGT Europe), Berlin*, Oct 2012, pp. 1–7.

[68] V. Arya, D. Seetharam, S. Kalyanaraman, K. Dontas, C. Pavlovski, S. Hoy, and J. R. Kalagnanam, "Phase identification in smart grids," in *Proc. IEEE Int Smart Grid Communications (SmartGridComm) Conf*, 2011, pp. 25–30.

[69] M. Dilek, "Integrated design of electrical distribution systems: Phase balancing and phase prediction case studies," Ph.D. dissertation, Blacksburg Virginia, 2001.

[70] S. Bolognani and L. Schenato, "Identification of power distribution network topology via voltage correlation analysis," *Proc. IEEE Conf. on Decision and Control*, 2013.

[71] E. Peeters, C. Develder, J. Das, J. Driesen, and R. Belmans, "Linear: towards a breakthrough of smart grids in Flanders," in *Proc. 2nd Int. Conf. Innovation for Sustainable Production*, vol. 3, Bruges, Belgium, 18–21 Apr. 2010, pp. 3–6.

[72] *Kabels Voor Ondergrondse Aanleg, met Synthetische Isolatie en Versterkte Mantel (Type 1kV)*, NBN Std. C 33-322, 1975 Std.

[73] W. Labeeuw and G. Deconinck, "Residential electrical load model based on mixture model clustering and markov models," *IEEE Trans. Ind. Inform.*, vol. 9, no. 3, pp. 1561–1569, 2013.

[74] H. L. Willis, *Power Distribution Planning Reference Book*. Abingdon: Dekker, 2004.

[75] S. Weckx, C. Gonzalez de Miguel, J. Tant, T. De Rybel, and J. Driesen, "Parameter identification of unknown radial grids for theft detection." in *Innovative Smart Grid Technologies (ISGT Europe), Berlin*, Oct 2012, pp. 1–6.

[76] S. Boyd and L. Vandenberghe, *Convex Optimization*. Cambridge University Press, Mar. 2004.

[77] MATLAB, *(R2013a)*. The MathWorks Inc., 2013.

[78] Caird, "Meter phase identification," US patent application Patent 20 100 164 473, 2010.

[79] S. Weckx, R. D'Hulst, and J. Driesen, "Optimal frequency support by dynamic demand." in *PowerTech, 2013 IEEE Grenoble*, 2013, pp. 1–6.

[80] K. De Craemer and G. Deconinck, "Balancing trade-offs in coordinated PHEV charging with continuous market-based control," *Innovative Smart Grid Technologies (ISGT Europe), Berlin*, pp. 1–8, Oct 2012.

[81] M. D. Galus, S. Koch, and G. Andersson, "Provision of load frequency control by phevs, controllable loads, and a cogeneration unit," *IEEE Trans. on Ind. Electron.*, vol. 58, no. 10, pp. 4568–4582, 2011.

[82] T. Stetz, F. Marten, and M. Braun, "Improved low voltage grid-integration of photovoltaic systems in Germany," *IEEE Trans. Sust. Energy*, vol. 4, no. 2, pp. 534–542, 2013.

[83] P. Vovos, A. Kiprakis, A. Wallace, and G. Harrison, "Centralized and distributed voltage control: Impact on distributed generation penetration," *IEEE Trans. Power Syst.*, vol. 22, no. 1, pp. 476–483, 2007.

[84] M. Braun, T. Stetz, R. Bründlinger, C. Mayr, K. Ogimoto, H. Hatta, H. Kobayashi, B. Kroposki, B. Mather, M. Coddington, K. Lynn, G. Graditi, A. Woyte, and I. MacGill, "Is the distribution grid ready to accept large-scale photovoltaic deployment? state of the art, progress, and future prospects," *Progress in Photovoltaics: Research and Applications*, vol. 20, no. 6, pp. 681–697, 2012.

[85] K. Tanaka, M. Oshiro, S. Toma, A. Yona, T. Senjyu, T. Funabashi, and C. Kim, "Decentralised control of voltage in distribution systems by distributed generators," *Generation, Transmission Distribution, IET*, vol. 4, no. 11, pp. 1251–1260, 2010.

[86] Y. He, M. Petit, and P. Dessante, "Optimization of the steady voltage profile in distribution systems by coordinating the controls of distributed generations," in *Innovative Smart Grid Technologies (ISGT Europe), Berlin*, 2012, pp. 1–7.

[87] A. Gabash and P. Li, "Active-reactive optimal power flow for low-voltage networks with photovoltaic distributed generation," in *Energy Conf. and Exhibition, 2012 IEEE International*, Florence, Italy, 2012, pp. 381–386.

[88] S. Bolognani and S. Zampieri, "A distributed control strategy for reactive power compensation in smart microgrids," *IEEE Trans. on Automatic Control*, vol. 58, no. 11, pp. 2818–2833, Nov. 2013.

[89] P. Sulc, S. Backhaus, and M. Chertkov, "Optimal distributed control of reactive power via the alternating direction method of multipliers," *IEEE Trans. on Energy Conversion*, vol. 29, no. 4, pp. 968–977, Dec 2014.

[90] A. Cagnano, F. Torelli, F. Alfonzetti, and E. D. Tuglie, "Can PV plants provide a reactive power ancillary service? a treat offered by an on-line controller," *Renewable Energy*, vol. 36, no. 3, pp. 1047 – 1052, 2011.

[91] E. Demirok, D. Sera, R. Teodorescu, P. Rodriguez, and U. Borup, "Evaluation of the voltage support strategies for the low voltage grid connected PV generators," in *Energy Conversion Congress and Exposition (ECCE), 2010 IEEE*, Atlanta, GA, 2010, pp. 710–717.

[92] Y. Chistyakov, E. Kholodova, K. Netreba, A. Szabo, and M. Metzger, "Combined central and local control of reactive power in electrical grids with distributed generation," in *Energy Conf. and Exhibition, 2012 IEEE International*. Florence, Italy: IEEE, 2012, pp. 325–330.

[93] K. De Brabandere, B. Bolsens, J. Van den Keybus, A. Woyte, J. Driesen, and R. Belmans, "A voltage and frequency droop control method for parallel inverters," *IEEE Trans. Power Elec.*, vol. 22, no. 4, pp. 1107–1115, 2007.

[94] J. Tant, F. Geth, D. Six, P. Tant, and J. Driesen, "Multiobjective battery storage to improve PV integration in residential distribution grids," *IEEE Trans. Sust. Energy*, vol. 4, no. 1, pp. 182 –191, jan. 2013.

[95] International Energy Agency, photovoltaic power systems programme, "Photovoltaic and solar forecasting: State of the art," International Energy Agency, Tech. Rep., 2013.

[96] S. Perez, R.and Kivalov, J. Schlemmer, K. Hemker, D. Renné, and T. Hoff, "Validation of short and medium term operational solar radiation forecasts in the US," *Solar Energy*, vol. 84, no. 12, pp. 2161–2172, 2010.

[97] V. Lonij, V. Jayadevan, A. Brooks, J. Rodriguez, K. Koch, M. Leuthold, and A. Cronin, "Forecasts of PV power output using power measurements of 80 residential PV installs," in *Photovoltaic Specialists Conf. , 2012 38th IEEE*. Austin, TX: IEEE, 2012, pp. 003 300–003 305.

[98] M. Schmidt, A. Panosyan, E. Barthlein, K. O'Brien, and O. Mayer, "Method of generating sets of PV plant power time series for grid simulation purposes," in *Innovative Smart Grid Technologies (ISGT Europe), Berlin*, 2012, pp. 1–7.

[99] M. Elnozahy and M. Salama, "A comprehensive study of the impacts of PHEVs on residential distribution networks," *IEEE Trans. Sust. Energy*, vol. 5, no. 1, pp. 332–342, Jan 2014.

[100] M. Gray and W. Morsi, "Power quality assessment in distribution systems embedded with plug-in hybrid and battery electric vehicles," *IEEE Trans. Power Syst.*, vol. 30, no. 2, pp. 663–671, 2014.

[101] R. Yan and T. Saha, "Investigation of voltage sensitivities to photovoltaic power fluctuations in unbalanced distribution networks," in *Power and Energy Society General Meeting, 2012 IEEE*, July 2012, pp. 1–7.

[102] H. Pezeshki, P. Wolfs, and G. Ledwich, "Impact of high PV penetration on distribution transformer insulation life," *IEEE Trans. Power Del.*, vol. 29, no. 3, pp. 1212–1220, Jun 2014.

[103] S. Weckx, C. Gonzalez de Miguel, P. Vingerhoets, and J. Driesen, "Phase switching and phase balancing to cope with a massive photovoltaic penetration," in *Electricity Distribution (CIRED 2013), 22nd Int. Conf. and Exhibition on*. IET, 2013, pp. 1–4.

[104] W. M. Siti, A. Jimoh, and D. Nicolae, "Distribution network phase load balancing as a combinatorial optimization problem using fuzzy logic and newton raphson," *Electric Power Systems Research*, vol. 81, no. 5, pp. 1079 – 1087, 2011. [Online]. Available: http://www.sciencedirect.com/science/article/pii/S0378779610003299

[105] P.-T. Cheng, C.-A. Chen, T.-L. Lee, and S.-Y. Kuo, "A cooperative imbalance compensation method for distributed-generation interface converters," *IEEE Trans. Ind. Applications,*, vol. 45, no. 2, pp. 805 – 815, march-april 2009.

[106] F. Wang, J. Duarte, and M. Hendrix, "Control of grid-interfacing inverters with integrated voltage unbalance correction," in *IEEE Power Electronics Specialists Conf. PESC*, jun 2008, pp. 310 –316.

[107] B. Meersman, B. Renders, L. Degroote, T. Vandoorn, and L. Vandevelde, "Three-phase inverter-connected DG-units and voltage unbalance," *Electric Power Systems Research*, vol. 81, no. 4, pp. 899 – 906, 2011.

[108] H. Patel and V. Agarwal, "PV based distributed generation with compensation feature under unbalanced and non-linear load conditions for a 3-phase, 4-wire system," in *2006. ICIT 2006. IEEE Int. Conf. Ind. Technology, on*, dec. 2006, pp. 322 –327.

[109] H. Beltran, Z. Chen, E. Belenguer, N. Aparicio, S. SeguiChilet, and F. Gimeno-Sales, "Photovoltaic inverters used as active filters for improvement of LV distribution networks," in *Electric Utility Deregulation and Restructuring and Power Technologies, 2008. DRPT 2008. 3rd Int. Conf. on*, 2008, pp. 2749–2756.

[110] R. Caldon, M. Coppo, and R. Turri, "Distributed voltage control strategy for LV networks with inverter-interfaced generators," *Electric Power Systems Research*, vol. 107, no. 0, pp. 85 – 92, 2014.

[111] M. Falahi, H.-M. Chou, M. Ehsani, L. Xie, and K. Butler-Purry, "Potential power quality benefits of electric vehicles," *IEEE Trans. Sust. Energy*, vol. 4, no. 4, pp. 1016–1023, Oct 2013.

[112] S. Weckx, R. D'Hulst, B. Claessens, and J. Driesen, "Multiagent charging of electric vehicles respecting distribution transformer loading and voltage limits," *IEEE Trans. Smart Grid*, vol. 5, no. 6, pp. 2857–2867, 2014.

[113] J. Van Roy, N. Leemput, F. Geth, R. Salenbien, J. Buscher, and J. Driesen, "Apartment building electricity system impact of operational electric vehicle charging strategies," *IEEE Trans. Sust. Energy*, vol. 5, no. 1, pp. 264–272, Jan 2014.

[114] F. Marra, G. Yang, Y. Fawzy, C. Traeholt, E. Larsen, R. Garcia-Valle, and M. Jensen, "Improvement of local voltage in feeders with photovoltaic using electric vehicles," *IEEE Trans. Power Syst.*, vol. 28, no. 3, pp. 3515–3516, Aug 2013.

[115] J. de Hoog, T. Alpcan, M. Brazil, D. Thomas, and I. Mareels, "Optimal charging of electric vehicles taking distribution network constraints into account," *IEEE Trans. Power Syst.*, vol. 30, no. 1, pp. 365 – 375, 2014.

[116] A. O'Connell, D. Flynn, and A. Keane, "Rolling multi-period optimization to control electric vehicle charging in distribution networks," *IEEE Trans. Power Syst.*, vol. 29, no. 1, pp. 340–348, Jan 2014.

[117] M. Singh, I. Kar, and P. Kumar, "Influence of EV on grid power quality and optimizing the charging schedule to mitigate voltage imbalance and reduce power loss," in *Power Electronics and Motion Control Conf. (EPE/PEMC), 2010 14th Int.*, Sept 2010, pp. T2–196–T2–203.

[118] K. Clement-Nyns, E. Haesen, and J. Driesen, "The impact of charging plug-in hybrid electric vehicles on a residential distribution grid," *IEEE Trans. Power Syst.*, vol. 25, no. 1, pp. 371–380, Feb 2010.

[119] X. Su, M. Masoum, and P. Wolfs, "Optimal PV inverter reactive power control and real power curtailment to improve performance of unbalanced four-wire LV distribution networks," *IEEE Trans. Sust. Energy*, vol. 5, no. 3, pp. 967–977, July 2014.

[120] A. Bonfiglio, M. Brignone, F. Delfino, and R. Procopio, "Optimal control and operation of grid-connected photovoltaic production units for voltage support in medium-voltage networks," *IEEE Trans. Sust. Energy*, vol. 5, no. 1, pp. 254–263, Jan 2014.

[121] Y. Ueda, K. Kurokawa, T. Tanabe, K. Kitamura, and H. Sugihara, "Analysis results of output power loss due to the grid voltage rise in grid-connected photovoltaic power generation systems," *IEEE Trans. on Ind. Electronics*, vol. 55, no. 7, pp. 2744–2751, July 2008.

[122] E. Demirok, D. Sera, R. Teodorescu, P. Rodriguez, and U. Borup, "Clustered PV inverters in LV networks: An overview of impacts and comparison of voltage control strategies," in *Electrical Power Energy Conf. (EPEC), 2009 IEEE*, oct. 2009, pp. 1 –6.

[123] N. Leemput, F. Geth, J. Van Roy, A. Delnooz, J. Buscher, and J. Driesen, "Impact of electric vehicle on-board single-phase charging strategies on a Flemish residential grid," *IEEE Trans. Smart Grid*, vol. 5, no. 4, pp. 1815–1822, July 2014.

[124] P. Ferreira, P. M. S. Carvalho, L. A. F. M. Ferreira, and M. Ilic, "Distributed energy resources integration challenges in low-voltage networks: Voltage control limitations and risk of cascading," *IEEE Trans. Sust. Energy*, vol. 4, no. 1, pp. 82–88, Jan 2013.

[125] S. Hashemi, J. Ostergaard, and G. Yang, "A scenario-based approach for energy storage capacity determination in LV grids with high PV penetration," *IEEE Trans. Smart Grid*, vol. 5, no. 3, pp. 1514–1522, May 2014.

[126] B. Rotthier, T. Van Maerhem, P. Blockx, P. Van den Bossche, and J. Cappelle, "Home charging of electric vehicles in Belgium," in *Electric*

Vehicle Symposium and Exhibition (EVS27), 2013 World, Nov 2013, pp. 1–6.

[127] Synergrid, "Specifieke technische voorschriften voor decentrale productie-installaties die in parallel werken met het distributienet, Synergrid regulation c10/11," Federatie van de netbeheerders elektriciteit en aardgas in België, Tech. Rep., 2012.

[128] S. Weckx, C. G. de Miguel, and J. Driesen, "Reducing grid losses and voltage unbalance with PV inverters," in *Power and Energy Society General Meeting, 2014 IEEE*, July 2014, pp. 1–5.

[129] J. Van Roy, N. Leemput, S. De Breucker, F. Geth, P. Tant, and J. Driesen, "An Availability Analysis and Energy Consumption Model for a Flemish Fleet of Electric Vehicles," in *European Electric Vehicle Congr. (EEVC)*, Brussels, Belgium, Oct 26-28, 2011.

[130] E. Sortomme, M. M. Hindi, S. D. J. MacPherson, and S. S. Venkata, "Coordinated charging of plug-in hybrid electric vehicles to minimize distribution system losses," *IEEE Trans. Smart Grid*, vol. 2, no. 1, pp. 198–205, 2011.

[131] Z. Ma, D. S. Callaway, and I. A. Hiskens, "Decentralized charging control of large populations of plug-in electric vehicles," *IEEE Trans. Control Syst. Technol.*, vol. 21, no. 99, pp. 67 – 78, 2013.

[132] L. Jian, H. Xue, G. Xu, X. Zhu, D. Zhao, and Z. Shao, "Regulated charging of plug-in hybrid electric vehicles for minimizing load variance in household smart microgrid," *IEEE Trans. Ind. Electr.*, vol. 60, no. 8, pp. 3218–3226, Aug 2013.

[133] L. Gan, U. Topcu, and S. Low, "Optimal decentralized protocol for electric vehicle charging," *IEEE Trans. Power Syst.*, vol. 28, no. 2, pp. 940–951, May 2013.

[134] "IBM ILOG CPLEX Optimizer," http://www-01.ibm.com/software/integration/optimization/cplex-optimizer/, 2014.

[135] W. Tang, S. Bi, and Y. Zhang, "Online coordinated charging decision algorithm for electric vehicles without future information," *IEEE Trans. Smart Grid*, vol. 5, no. 6, pp. 2810–2824, Nov 2014.

[136] M. Kraning, E. Chu, J. Lavaei, and S. Boyd, "Dynamic network energy management via proximal message passing," *Foundations and Trends in Optimization*, vol. 1, no. 2, pp. 73–126, 2014.

[137] A. von Jouanne and B. Banerjee, "Assessment of voltage unbalance," *IEEE Trans. Power Del.*, vol. 16, no. 4, pp. 782–790, Oct 2001.

[138] D. Jenicek, W. Inam, and M. Ilic, "Locational dependence of maximum installable PV capacity in LV networks while maintaining voltage limits," in *North American Power Symposium (NAPS), 2011*, Aug 2011, pp. 1–5.

[139] P. Samadi, A. Mohsenian-Rad, R. Schober, V. W. S. Wong, and J. Jatskevich, "Optimal real-time pricing algorithm based on utility maximization for smart grid," in *Proc. First IEEE Int Smart Grid Communications (SmartGridComm) Conf*, 2010, pp. 415–420.

[140] N. U. Hassan, M. A. Pasha, C. Yuen, S. Huang, and X. Wang, "Impact of scheduling flexibility on demand profile flatness and user inconvenience in residential smart grid system," *Energies*, vol. 6, no. 12, pp. 6608–6635, 2013. [Online]. Available: http://www.mdpi.com/1996-1073/6/12/6608

[141] B. Gao, W. Zhang, Y. Tang, M. Hu, M. Zhu, and H. Zhan, "Game-theoretic energy management for residential users with dischargeable plug-in electric vehicles," *Energies*, vol. 7, no. 11, pp. 7499–7518, 2014. [Online]. Available: http://www.mdpi.com/1996-1073/7/11/7499

[142] B. Ko, N. P. Utomo, G. Jang, J. Kim, and J. Cho, "Optimal scheduling for the complementary energy storage system operation based on smart metering data in the DC distribution system," *Energies*, vol. 6, no. 12, pp. 6569–6585, 2013. [Online]. Available: http://www.mdpi.com/1996-1073/6/12/6569

[143] S. Weckx, R. D'Hulst, and J. Driesen, "Voltage sensitivity analysis of a laboratory distribution grid with incomplete data," *IEEE Trans. on Smart Grid*, vol. 6, no. 3, pp. 1271 – 1280, 2015.

[144] M. Fahrioglu and F. Alvarado, "Using utility information to calibrate customer demand management behavior models," *IEEE Trans. on Power Syst.*, vol. 16, no. 2, pp. 317–322, 2001.

[145] I. Sharma, K. Bhattacharya, and C. Canizares, "Smart distribution system operations with price-responsive and controllable loads," *IEEE Trans. on Smart Grid*, vol. 6, no. 2, pp. 795 – 807, 2014.

[146] J.-Y. Joo and M. Ilic, "Multi-layered optimization of demand resources using lagrange dual decomposition," *IEEE Trans on Smart Grid*, vol. 4, no. 4, pp. 2081–2088, Dec 2013.

[147] E. DallAnese, S. Dhople, B. Johnson, and G. Giannakis, "Decentralized optimal dispatch of photovoltaic inverters in residential distribution

systems," *IEEE Trans. on Energy Conversion,*, vol. 29, no. 4, pp. 957–967, Dec 2014.

[148] D. P. Bertsekas and D. P. Bertsekas, *Nonlinear Programming*, 2nd ed. Athena Scientific, Sep. 1999.

[149] N. Gatsis and G. Giannakis, "Residential load control: Distributed scheduling and convergence with lost ami messages," *IEEE Trans. Smart Grid*, vol. 3, no. 2, pp. 770–786, Jun 2012.

[150] Z. Ma, D. Callaway, and I. Hiskens, "Optimal charging control for plug-in electric vehicles," in *Control and Optimization Methods for Electric Smart Grids*, ser. Power Electronics and Power Systems, A. Chakrabortty and M. D. Ilić, Eds. Springer New York, 2012, vol. 3, pp. 259–273. [Online]. Available: http://dx.doi.org/10.1007/978-1-4614-1605-0_13

[151] S. Vandael, B. Claessens, M. Hommelberg, T. Holvoet, and G. Deconinck, "A scalable three-step approach for demand side management of plug-in hybrid vehicles," *IEEE Trans. on Smart Grid*, vol. 4, no. 2, pp. 720–728, Jun 2013.

[152] Z. Fan, "A distributed demand response algorithm and its application to PHEV charging in smart grids," *IEEE Trans. Smart Grid*, vol. 3, no. 3, pp. 1280–1290, Sept 2012.

[153] E. DallAnese, H. Zhu, and G. Giannakis, "Distributed optimal power flow for smart microgrids," *IEEE Trans. Smart Grid*, vol. 4, no. 3, pp. 1464–1475, Sept 2013.

[154] C.-K. Wen, J.-C. Chen, J.-H. Teng, and P. Ting, "Decentralized plug-in electric vehicle charging selection algorithm in power systems," *IEEE Trans. Smart Grid*, vol. 3, no. 4, pp. 1779–1789, 2012.

[155] E. Karfopoulos and N. Hatziargyriou, "A multi-agent system for controlled charging of a large population of electric vehicles," *IEEE Trans. Power Syst.*, vol. 28, no. 2, pp. 1196–1204, May 2013.

[156] S. D. Ramchurn, P. Vytelingum, A. Rogers, and N. Jennings, "Agent-based control for decentralised demand side management in the smart grid," in *The 10th Int. Conf. on Autonomous Agents and Multiagent Systems - Volume 1*, ser. AAMAS '11, Richland, SC, 2011, pp. 5–12.

[157] B. Roossien, A. van den Noort, R. Kamphuis, F. Bliek, M. Eijgelaar, and J. de Wit, "Balancing wind power fluctuations with a domestic virtual power plant in Europe's first smart grid," in *PowerTech, 2011 IEEE Trondheim*, 2011, pp. 1–5.

[158] P. Papadopoulos, N. Jenkins, L. Cipcigan, I. Grau, and E. Zabala, "Coordination of the charging of electric vehicles using a multi-agent system," *IEEE Trans. Smart Grid*, vol. 4, no. 4, pp. 1802–1809, Dec 2013.

[159] K. Kok, C. Warmer, and I. Kamphuis, "Powermatcher: multiagent control in the electricity infrastructure," in *Proc. of the 4th Int. joint Conf. on Autonomous agents and multiagent systems*. ACM, 2005, pp. 75–82.

[160] K. Kok, C. Warmer, and R. Kamphuis, "The powermatcher: Multiagent control of electricity demand and supply," *IEEE Intell. Syst.*, vol. 21, no. 2, pp. 89–90, 2006.

[161] K. Kok, B. Roossien, P. MacDougall, O. van Pruissen, G. Venekamp, R. Kamphuis, J. Laarakkers, and C. Warmer, "Dynamic pricing by scalable energy management systems ; field experiences and simulation results using powermatcher," in *Power and Energy Society General Meeting, 2012 IEEE*, July 2012, pp. 1 –8.

[162] R. Ambrosio, N. Halim, Z. Liu, D. Pendarakis, and M. G. Yao, "Method and system for efficient energy distribution in electrical grids using sensor and actuator networks," US Patent US 20 090 228 324, March 04, 2008.

[163] K. Kok, M. J. J. Scheepers, and I. G. Kamphuis, "Intelligence in electricity networks for embedding renewables and distributed generation," ser. Intelligent Systems, Control and Automation: Science and Engineering, 2010, vol. 42.

[164] K. De Craemer, S. Vandael, B. Claessens, and G. Deconinck, "An event-driven dual coordination mechanism for demand side management of PHEVs," *IEEE Trans. on Smart Grid*, vol. 5, no. 2, pp. 751–760, March 2014.

[165] F. Bliek, A. van den Noort, B. Roossien, R. Kamphuis, J. de Wit, J. van Der Velde, and M. Eijgelaar, "Powermatching city, a living lab smart grid demonstration," in *Innovative Smart Grid Technologies Conf. Europe, Gothenburg*. IEEE, 2010, pp. 1–8.

[166] P. Samadi, H. Mohsenian-Rad, R. Schober, and V. Wong, "Advanced demand side management for the future smart grid using mechanism design," *IEEE Trans. Smart Grid*, vol. 3, no. 3, pp. 1170–1180, 2012.

[167] F. Ruelens, S. Vandael, W. Leterme, B. Claessens, M. Hommelberg, T. Holvoet, and R. Belmans, "Demand side management of electric vehicles with uncertainty on arrival and departure times," in *Innovative Smart Grid Technologies (ISGT Europe), Berlin*, 2012, pp. 1–8.

[168] B. Claessens, S. Vandael, F. Ruelens, and M. Hommelberg, "Self-learning demand side management for a heterogeneous cluster of devices with binary control actions," in *Innovative Smart Grid Technologies (ISGT Europe), Berlin*, 2012, pp. 1–8.

[169] P. Tarasak, "Optimal real-time pricing under load uncertainty based on utility maximization for smart grid," in *Proc. IEEE Int. Smart Grid Communications Conf.*, 2011, pp. 321–326.

[170] M. D. Galus, R. Waraich, F. Noembrini, K. Steurs, G. Georges, K. Boulouchos, K. Axhausen, and G. Andersson, "Integrating power systems, transport systems and vehicle technology for electric mobility impact assessment and efficient control," *IEEE Trans. Smart Grid*, vol. 3, no. 2, pp. 934–949, 2012.

[171] I. Gurobi Optimization, "Gurobi optimizer reference manual," 2014. [Online]. Available: http://www.gurobi.com

[172] D. P. Bertsekas and J. N. Tsitsiklis, *Parallel and distributed computation: numerical methods*. Upper Saddle River, NJ, USA: Prentice-Hall, Inc., 1989.

[173] J. Short, D. Infield, and L. Freris, "Stabilization of grid frequency through dynamic demand control," *IEEE Trans. on Power Syst.*, vol. 22, no. 3, pp. 1284 –1293, aug. 2007.

[174] J. Kondoh, N. Lu, and D. Hammerstrom, "An evaluation of the water heater load potential for providing regulation service," *IEEE Trans. on Power Syst.*, vol. 26, no. 3, pp. 1309 –1316, aug. 2011.

[175] Z. Xu, J. Ostergaard, M. Togeby, and C. Marcus-Moller, "Design and modelling of thermostatically controlled loads as frequency controlled reserve," in *Power Engineering Society General Meeting, 2007. IEEE*, Jun 2007, pp. 1 –6.

[176] H. Liu, Z. Hu, Y. Song, and J. Lin, "Decentralized vehicle-to-grid control for primary frequency regulation considering charging demands," *IEEE Trans. on Power Syst.*, vol. 28, no. 3, pp. 3480–3489, Aug 2013.

[177] P. Almeida, J. Lopes, F. Soares, and L. Seca, "Electric vehicles participating in frequency control: Operating islanded systems with large penetration of renewable power sources," in *PowerTech, 2011 IEEE Trondheim*, Jun 2011, pp. 1 –6.

[178] B. Biegel, L. Hansen, P. Andersen, and J. Stoustrup, "Primary control by on/off demand-side devices," *IEEE Trans. on Smart Grid*, vol. 4, no. 4, pp. 2061–2071, 2013.

[179] K. Vanthournout, R. D'hulst, D. Geysen, and G. Jacobs, "A smart domestic hot water buffer," *IEEE Trans. on Smart Grid*, vol. 3, no. 4, pp. 2121 –2127, dec. 2012.

[180] M. Hommelberg, B. van der Velde, C. Warmer, I. Kamphuis, and J. Kok, "A novel architecture for real-time operation of multi-agent based coordination of demand and supply," in *Proc. IEEE Power and Energy Society General Meeting - Conversion and Delivery of Electrical Energy in the 21st Century*, 2008, pp. 1–5.

[181] D. P. Bertsekas, *Constrained Optimization and Lagrange Multiplier Methods (Optimization and Neural Computation Series)*, 1st ed. Athena Scientific, 1996.

[182] C. Zhao, U. Topcu, and S. Low, "Optimal load control via frequency measurement and neighborhood area communication," *IEEE Trans. on Power Syst.*, vol. 28, no. 4, pp. 3576 – 3587, 2013.

[183] P. Kundur, *Power System Stability and Control*, New York, 1994.

[184] J. Mathieu, M. Kamgarpour, J. Lygeros, and D. Callaway, "Energy arbitrage with thermostatically controlled loads," in *Control Conference (ECC), 2013 European*, 2013, pp. 2519–2526.

[185] Z. Chen, L. Wu, and Y. Fu, "Real-time price-based demand response management for residential appliances via stochastic optimization and robust optimization," *IEEE Trans. on Smart Grid*, vol. 3, no. 4, pp. 1822–1831, Dec 2012.

[186] A. Shapiro, D. Dentcheva, and A. Ruszczynski, *Lectures on stochastic programming : modeling and theory*, ser. MPS-SIAM series on optimization. Society for Industrial and Applied Mathematics, 2009.

[187] F. Ruelens, S. Weckx, W. Leterme, B. Claessens, S. Vandael, and R. Belmans, "Stochastic portfolio management of an electric vehicles aggregator," in *Innovative Smart Grid Technologies (ISGT Europe), Copenhagen*, 2013, pp. 1–8.

[188] A. Conejo, J. Morales, and L. Baringo, "Real-time demand response model," *IEEE Trans. on Smart Grid*, vol. 1, no. 3, pp. 236–242, Dec 2010.

[189] K. De Brabandere, T. Loix, K. Engelen, B. Bolsens, J. Van Den Keybus, J. Driesen, and R. Belmans, "Design and operation of a phase-locked loop with kalman estimator-based filter for single-phase applications," in *IEEE Industrial Electronics, IECON 2006 - 32nd Annual Conference on*, Nov 2006, pp. 525–530.

[190] K. De Vos, "Sizing and allocation of operating reserves following wind power integration," Ph.D. dissertation, KULeuven, Leuven, 2013. [Online]. Available: http://www.esat.kuleuven.be/electa/publications/fulltexts/pub_2446.pdf

[191] Y. Rebours, D. Kirschen, M. Trotignon, and S. Rossignol, "A survey of frequency and voltage control ancillary services part ii: Economic features," *IEEE Trans. on Power Syst.*, vol. 22, no. 1, pp. 358–366, Feb 2007.

[192] E. Sortomme and M. El-Sharkawi, "Optimal charging strategies for unidirectional vehicle-to-grid," *IEEE Trans. on Smart Grid*, vol. 2, no. 1, pp. 131–138, March 2011.

[193] Department of energy, "Communications requirements of smart grid technologies," Department of energy, Tech. Rep., 2010.

[194] R. J. A. Little and D. B. Rubin, *Statistical Analysis with Missing Data*. New York, NY, USA: John Wiley & Sons, Inc., 1986.

Short curriculum

Sam Weckx

Born February 25, 1986 in Leuven (Belgium)

1999-2004	Secondary school Science-Mathematics (8h) Voorzienigheid Diest
2004–2007	Bachelor of Engineering KU Leuven Graduated Magna Cum Laude
2007-2009	Master of Engineering: Energy KU Leuven Graduated Magna Cum Laude
2009–2010	Master of Engineering: Mechatronics and Robotics KU Leuven Graduated Magna Cum Laude
2010-2015	Phd Student with FWO-VITO research grant KU Leuven and VITO

List of publications

Reviewed Journals

Published

1. **Weckx, S.**, Driesen, J. (2015). Load Balancing with EV chargers and PV inverters in Unbalanced Distribution Grids. IEEE Transactions on Sustainable Energy, 2015, vol.6, no.2, pp.635-643, April 2015

2. González de Miguel, C., **Weckx, S.**, De Rybel, T., Driesen, J. (2015). Dynamic Thermal Modeling of a Voltage Divider Capacitive Coupling. IEEE Transactions on Power Delivery, 2015, accepted for publication

3. **Weckx, S.**, D'hulst, R., Driesen, J. (2015). Voltage Sensitivity Analysis of a Laboratory Distribution Grid With Incomplete Data. IEEE Transactions on Smart Grid, 2014, vol.6, no.3, pp.1271-1280, May 2015

4. **Weckx, S.**, D'hulst, R., Driesen, J. (2015). Primary and secondary frequency support by a multi-agent demand control system. IEEE Transactions on Power Systems, 2014, vol.30, no.3, pp.1394-1404, May 2015

5. **Weckx, S.**, D'hulst, R., Driesen, J. (2015). Locational pricing to mitigate voltage problems caused by a high PV penetration. Energies 2015, 8, 4607-4628

6. **Weckx, S.**, D'hulst, R., Claessens, B., Driesen, J. (2014). Multi-agent charging of electric vehicles respecting distribution transformer loading and voltage limits. IEEE Transactions on Smart Grid, 2014 , vol.5, no.6, pp.2857-2867, Nov. 2014

7. **Weckx, S.**, González de Miguel, C., Driesen, J. (2014). Combined Central and Local Active and Reactive Power Control of PV Inverters. IEEE Transactions on Sustainable Energy, 2014, vol.5, no.3, pp.776-784, July 2014

Submitted

8. **Weckx, S.**, Driesen, J. (2015). Optimal Local Reactive Voltage Control by PV Inverters. Submitted to Renewable Energy, Special Issue on Optimization Methods in Renewable Energy Systems Design

Patents

1. **Weckx, S.**, Driesen, J., D'hulst, R., Claessens, B. (2013) Method and system for distributing and/or controlling an energy flow taking into account constraints relating to the electricity network. WO 2014057133 A2

International Conferences

1. **Weckx, S.**, González de Miguel, C., Driesen, J. (2014). Reducing Grid Losses and Voltage Unbalance with PV inverters, Power Engineering Society General Meeting (PESGM) Washington, 27-31 July 2014.

2. Ruelens, F., **Weckx, S.**, Leterme, W., Vandael, S., Claessens, B., Belmans, R. (2013). Stochastic Portfolio Management of an Electric Vehicles Aggregator. Innovative Smart Grid Technologies (ISGT) Copenhagen, 6-9 October 2013.

3. **Weckx, S.**, González de Miguel, C., Vingerhoets, P., Driesen, J. (2013). Phase switching and phase balancing to cope with a massive photovoltaic penetration, CIRED Stockholm, 10-13 June 2013.

4. **Weckx, S.**, D'hulst, R., Driesen, J. (2013). Optimal Real-Time Pricing for Unbalanced Distribution Grids with Network Constraints. Power Engineering Society General Meeting (PESGM) Vancouver, 21-25 July 2013.

5. **Weckx, S.**, D'hulst, R., Driesen, J. (2013). Optimal frequency support by dynamic demand. PowerTech Grenoble, 16-20 June 2013.

6. **Weckx, S.**, González de Miguel, C., De Rybel, T., Driesen, J. (2013). LS-SVM-based On-Load Tap Changer Control for Distribution Networks with Rooftop PV's. Innovative Smart Grid Technologies (ISGT) Copenhagen, 6-9 October 2013.

7. **Weckx, S.**, D'hulst, R., Driesen, J. (2013). Distributed Residential Load Control of Binary behaving loads. PowerTech Grenoble, 16-20 June 2013.

8. González de Miguel, C., **Weckx, S.**, Efkarpidis, N., Vingerhoets, P., De Rybel, T., Driesen, J. (2013). Constrained PV Penetration Level in LV Distribution Networks Based on the Voltage Operational Margin, CIRED Stockholm, 10-13 June 2013.

9. Tant, J., Zwysen, J., Engelen, K., Leemput, N., Van Roy, J., **Weckx, S.**, Driesen, J. (2012). Power Electronics for Electric Vehicles: a Student Laboratory Platform. 13th IEEE Workshop on Control and Modeling for Power Electronics (COMPEL), Kyoto, Japan, 10-13 June 2012

10. **Weckx, S.**, GonzalezDeMiguel, C., Tant, J., De Rybel, T., Driesen, J. (2012). Parameter Identification of Unknown Radial Grids for Theft Detection. Innovative Smart Grid Technologies (ISGT) Berlin, 15-17 October 2012 IEEE.

11. Gonzalez, C., Geuns, J., **Weckx, S.**, Wijnhoven, T., Vingerhoets, P., De Rybel, T., Driesen, J. (2012). LV Distribution Network Feeders in Belgium and Power Quality Issues due to Increasing PV Penetration Levels. 2012 Innovative Smart Grid Technologies (ISGT) Berlin, 15-17 October 2012 IEEE.

FACULTY OF ENGINEERING SCIENCE
DEPARTMENT OF ELECTRICAL ENGINEERING (ESAT)
DIVISION OF ELECTRICAL ENERGY AND COMPUTER ARCHITECTURES (ELECTA)
Kasteelpark Arenberg 10 box 2445
B-3001 Heverlee
sam.weckx@esat.kuleuven.be
http://www.esat.kuleuven.be/electa/